Universidad Loyola Andalucía

Role of cerium as a chemical vector for the design of new generation of ammonia synthesis catalysts

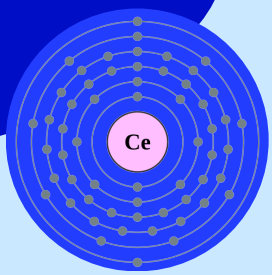

DOCTORAL THESIS

Ego amissus pugna sed autere bellum
Acta est fabula

Author: Javier Arroyo Caire
Directors: Manuel Antonio Díaz Pérez
Juan Carlos Serrano Ruiz
Tutor: Carlos Ortiz Domínguez

International degree

Sevilla, 2025

UNIVERSIDAD LOYOLA ANDALUCÍA

DOCTORAL THESIS

“Role of cerium as a chemical vector for the design of new generation of ammonia synthesis catalysts”

PhD. In Systems & Sustainable Engineering

PhD. Student:	Javier Arroyo Caire
Directors:	Juan Carlos Serrano Ruiz Manuel Antonio Díaz Pérez
Tutor:	Carlos Ortiz Domínguez
International degree	

Sevilla, 2025

“In the middle of difficulty lies opportunity.”
Albert Einstein

A Carmen y Emiliano, mis abuelos.

Agradecimientos-Acknowledgments

A mi familia, a mi padre, a Isabel y a mi Miguelito, por demostrar lealtad y apoyo incondicional en esta larga travesía que ha durado casi una década. A mi madre.

A Manu y Juan Carlos, mis directores de tesis, colegas y compañeros de aventuras. Nunca encontraré palabras de agradecimiento lo suficientemente buenas para vosotros, por haberme sacado de las sombras, por ayudarme a recordar mi propio valor como investigador, por no haberos bajado jamás del carro. Vuestras manos en mi espalda me hacen seguir adelante. Que esta Tesis sea uno más de muchos éxitos compartidos.

Agradecimientos a los profesionales que he conocido en la Universidad Loyola, sin duda un nicho de conocimiento y amistad, a partes iguales, especialmente a mis compis, Ana, Valentina y Álex, por compartir inquietudes comunes y hacer menos amargos los momentos difíciles. Gracias a Reyes, por ponerle una sonrisa a todos los momentos de la vida.

Gracias a Anabel, por haberme empujado a reconstruir mi mundo cuando de él solo quedaban los cimientos, por armarme de paciencia y de templanza, por tus consejos de incalculable valor, por compartir conmigo pasado y presente. Nada de esto habría sido posible sin ti.

Agradecimientos a los compañeros del departamento de Química Inorgánica de la Universidad de Alicante, por habernos ayudado tanto en nuestra sólida y robusta colaboración, especialmente a Stiven, por ser mi ángel de la guarda durante buena parte de mi etapa predoctoral.

Gracias a Chris, por compartir a diario tu mundo conmigo y por entrar en el mío, sin límites, por deslumbrarme con tu torrente de luz, por enseñarme que cada momento cuenta. Como dijo Frida Kahlo, “si yo pudiera darte una cosa en la vida, me gustaría darte la capacidad de verte a ti mismo a través de mis ojos”.

Gracias a mis amig@s, en especial a Marc y Jose Manuel, por disfrutar conmigo mis éxitos y soportar el peso de mis fracasos, por haber estado y estar siempre, sin condiciones, sin barreras. Compartir pequeños momentos (casi) a diario con vosotros es una parte fundamental de mi estilo de vida.

Mi agradecimiento a mis antiguos compañeros de la Universidad de Sevilla, por haberme ayudado a entender que la investigación es mi vocación, en especial a Alberto

Gómez Barea, por darme la oportunidad de demostrarme a mí mismo que tengo la capacidad de conseguir lo que quiera.

Gracias también a l@s que estuvieron y ya no forman parte de mi vida, porque mis vivencias con vosotr@s también me han llevado hasta aquí.

Gracias a Albert, por haber sido importante para mí durante una gran parte del tiempo que he invertido en desarrollar esta tesis doctoral.

Particular thanks to the professional researchers, technicians and other staff at MDX, TITech. Your kind availability and teachings allowed me to grow not only as a better researcher, particularly in the thermocatalytic ammonia synthesis field, but they also showed me that the right way in this field comes from modesty.

Abstract

The industrial production of ammonia has been carried out by the Haber−Bosch process for more than a century. However, a small-scale decentralized process is on high demand, either for the use of ammonia as raw material in fertilizers industry or for its growing interest as an energy vector for hydrogen storage. Particularly, the rising interest of green ammonia (i.e., ammonia produced from renewables), has motivated a massive research effort during the last two decades concerning new materials which lead to circumvent the main handicap of the iron-based catalysts used in the Haber−Bosch process: the current requirements of high temperatures and pressures that hinder the coupling of ammonia reaction systems with renewable resources (mainly, water electrolysis).

As discussed in the Chapter 1 from the Section II of this document, there is a wide variety of materials suitable for boosting the traditional ammonia synthesis process, thus leading to a successful operation at mild conditions. However, most of these catalysts are on an incipient research state or present some drawbacks (e.g., complex synthesis methods) which hinder their scalability. Thus, the search of more suitable, attainable and stable catalysts is required for an effective transition towards a green ammonia thermocatalytic synthesis scenario.

This doctoral Thesis is focused on the role of cerium (Ce) as a support for 3rd generation ammonia synthesis materials, since its versatile properties allow this metal to be a chemical platform for the design of efficient catalysts.

In the Chapter 1 of this Thesis, a review of the state-of-the-art is done, in which the historical evolution of the most relevant 1st, 2nd and 3rd generation catalysts for ammonia synthesis is presented. Furthermore, the fundamentals of this reaction are unveiled with a particular focus on the metal-support interactions. The results from this work led to the rational design of the catalysts presented in the following Chapters.

In the Chapter 2, the experimental results of the activity of $CeNi_x$ alloys are shown. This work, carried out in the MDX research Center for Element Strategy, International Research Frontiers Initiative, Tokyo Institute of Technology, Japan, highlighted the versatility of cerium by the good performance of the $CeNi_2$ alloy, whose fundamental key relies on the formation of a CeN surface layer over the original alloy, acting as a second active center for the N_2 dissociation and activation steps. Despite the use of a non-noble metal like Ni, an activation energy as low as 55.3 kJ mol^{-1} was achieved for $CeNi_2$ bulk particles.

In the Chapter 3, an experimental work of catalysts made of Ru/CeO_2 and Ru/CeO_2-Al_2O_3 is presented. It was demonstrated that a very simple impregnation-calcination method led to the synthesis of a high surface cerium oxide support for Ruthenium (Ru), creating a catalyst with low crystallinity and good electronic promotion between metal and support, derived from the formation of surface oxygen vacancies, typical from the reduction of cerium oxide ($Ce_4^+ \rightarrow Ce_3^+$). Further enhancement in the kinetic mechanism can be found by the structural promotion of alumina. Activation energies as low as 44.8 kJ mol^{-1} were obtained.

In the Chapter 4, the activity of Ru/CeO_2-La_2O_3 catalysts is shown. In this case, it was demonstrated that the activity of the original Ru/CeO_2 catalyst can be enhanced by the addition of La to the oxide lattice, since the crystal structure of ceria can be disrupted by the formation of Ce-La solid solutions. As a result, there is a decrease in the crystallinity of the oxydes and a higher number of structural defects is obtained. Thus, it was observed that a superior generation of surface oxygen defects boosts the electron promotion of the support towards the metal. The optimum catalyst was made of a 50% of Ce in molar bases and its apparent activation energy was as low as 34.1 kJ mol^{-1}.

The results presented in the present Thesis demonstrate that cerium can be a key element for the design of catalysts for green ammonia thermocatalytic synthesis, either in the form of cerium nitride in metallic alloy complexes with Ni or in the form of ceria as a support for Ru. Furthermore, the performance of the latter can be further enhanced by structural promotion with Al_2O_3 or by functional promotion by enhanced formation of oxygen vacancies using La_2O_3, which resulted in a better electron transfer towards Ru.

Certainly, the versatility of cerium and its wide margin to design better performing catalysts can play a key role in the transition of ammonia synthesis towards the industrial application as both green hydrogen storage energy carrier and raw material for decentralized small plants of green fertilizers.

Index

Index of tables

Manuscript. Introduction and Chapter 4

Compendium of publications

Chapter 1

Chapter 2

Chapter 3

Index of figures

Manuscript. Introduction and Chapter 4

Compendium of publications

Chapter 1

Chapter 2

Chapter 3

I. Section 1: Introduction, objectives and structure of the Thesis

1. Introduction

Ammonia (NH_3) is one of the most relevant chemicals worldwide, since it serves as a feedstock for the production of fertilizers and chemicals[1]. 190 MMT/year of NH_3 are produced worldwide which, owing to the high energy requirements of the process, are responsible for 1-2% of the global anthropogenic CO_2 emissions[2,3]. During the last decades, NH_3 is being considered as one of the best potential candidates as a green hydrogen (H_2) storage material. The NH_3 molecule has a H_2 storage capacity as high as 17.7 wt%. Its interest relies on the reversibility of the NH_3 synthesis reaction, presented in Eq. 1, which leads to the potential use of NH_3 as a carbon-free H_2 carrier. Considering that the vapor pressure of NH_3 is ca. 1 MPa at room temperature, NH_3 can easily be stored and transported in liquid form, thus the use of NH_3 as a H_2 carrier could solve one of the most relevant handicaps for the establishment of the H_2 infrastructure: its transportation and storage.

$$N_2+3H_2 \leftrightarrow 2NH_3 \qquad \Delta H_R^0=-91.9 \text{ kJ mol}_{N_2}^{-1} \qquad \text{Eq. 1}$$

The kinetics of this chemical reaction is limited by the dissociation of nitrogen (N_2), since the cleavage of the strong triple N≡N (945 kJ mol^{-1}) bond is typically a slow step[4,5]. On the other hand, the NH_3 reaction is moderately exothermic. Therefore, the industrial production of this commodity represents a chemical engineering challenge, considering that the reaction is limited by kinetics at low temperatures and by thermodynamic at high temperatures.

The equilibrium NH_3 mole fraction (yield) as a function of pressure is presented in Figure 1 , at different temperatures. At room temperature, an equilibrium NH_3 yield above 90% can be achieved, even at atmospheric pressure, although, at such low temperature, the reaction is kinetically disfavoured. However, as the temperature increases, the equilibrium yield readily decreases. Therefore, if temperatures higher than 400-500 ºC are required for kinetic reasons, the operation pressure must be higher than 7-27 MPa to dampen the temperature effect, resulting in a typical low NH_3 yield of 20%.

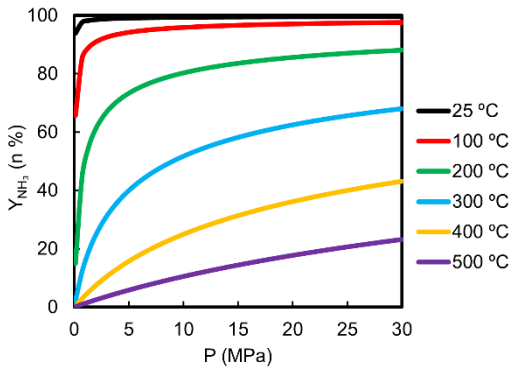

Figure 1. Equilibrium NH_3 mole fraction (yield) as a function of pressure, at different temperatures

The industrial production of NH_3 has mostly been carried out by the Haber−Bosch process since 1913 and almost exclusively since the 1940s[6,7]. Currently, most of the H_2 used for the reaction is obtained by steam reforming of methane. Therefore, natural gas is commonly used as a raw material. The Haber−Bosch process (Figure 2), is divided into two sections: the natural gas steam reforming and the NH_3 thermocatalytic reaction system. The catalyst inside the fixed bed NH_3 reactor (showed in the scheme as KMR) consists of iron (Fe), multipromoted with K_2O, Al_2O_3 and CaO (1st generation catalyst)[8]. This catalyst is active within a temperature range of 400-500 ºC. Since an NH_3 concentration of ca. 20% is required, high pressures ranging from 10 to 30 MPa are necessary for both kinetic and thermodynamic reasons. Under such conditions, only large, centralized plants are feasible from both industrial and economic points of view[9]. Furthermore, very robust plants with a large reactants recirculation system are demanded to ensure a good production efficiency. In global, the Haber−Bosch process consumes a 5% of the natural gas and 1-2% of the energy worldwide.

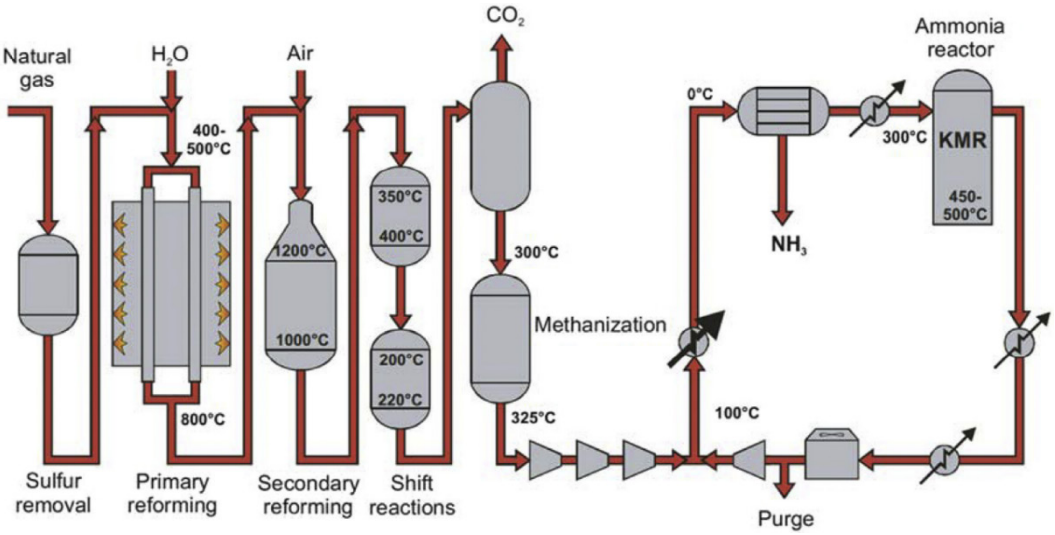

Figure 2. Scheme of the Haber−Bosch process. Reproduced with permission[10]. Copyright 2021, Elsevier Inc.

As aforementioned, the use of NH_3 as both raw material for the production of fertilizers and as a green H_2 carrier is on high demand[3,11]. However, a real implementation of this concept relies on the production of NH_3 at milder operation conditions and driven by renewables. Hence, there are still some challenges to overcome in order to scale-down the Haber−Bosch process and create feasible green NH_3 plants. First, the use of renewable technologies for the production of H_2, mainly water electrolysis, must be carried out at much lower pressures (ca 1-2 MPa) than the Haber−Bosch reactor, thus the coupling between both technologies is still unfeasible[3,12]. In addition, the use of renewable energy sources, such as solar or wind power, requires the installation of decentralized plants, to overcome the seasonal and intermittent supply derived from these technologies. Furthermore, the closest technological solution up to date, the so-called electrolysis-based Haber−Bosch process (eHB) represents an additional challenge, related to the electrification of the NH_3 net[13]. Second, the KMR catalyst, which is the core of the Haber−Bosch process, is only active at severe operation conditions, which hinders a real and effective implementation of green NH_3 production.

In order to solve this technological challenge, new catalysts must be developed in order to promote a reasonable NH_3 synthesis performance at milder conditions. The first attempt to reach such an ambitious goal was carried out using Ru-based catalysts, which started being developed at the end of the 20th century[14,15]. The dissociation of N_2 is faster on Ru-based catalysts than on the Fe-based ones, since the formers present the so-called B5 sites, which act as an active site for N_2 cleavage[16,17]. These 2nd generation catalysts were commercialized in 1998 for the Kellogg Advanced Ammonia Process (KAAP), in the form of Ru supported on high surface area graphitic carbon (HSAG), doubly promoted with Cs and Ba, achieving NH_3 yields of 40-50% at mild temperatures of 370-400 ºC and pressures of 5-10 MPa[18,19]. In these materials, the NH_3 desorption limitations, typically observed for the Fe-based catalysts, can be circumvented[20,21]. However, there are some drawbacks related to this 2nd generation catalysts: firstly, methanation of the HSAG carbon hinders the catalyst stability, which is much higher for 1st generation catalysts[22]. Secondly, the performance of 2nd generation Ru catalysts at high pressures is limited by H_2 poisoning i.e., H_2 adatoms trend to keep adsorbed on the active B5 sites during the H_2 dissociation process[23–25]. Thus, an increase in the operation pressure is associated with an increase in the H_2 partial pressure. Since H_2 reaction orders are typically negative because of the H_2 poisoning effect, the global NH_3 synthesis activity is more limited as the pressure increases. Thirdly, the lower abundance of Ru and

its higher cost as compared to Fe increases the initial investment and, hence, the regeneration of the material represents a critical step at industrial scales[26,27].

Depending on the catalyst to be used, the NH_3 synthesis kinetic mechanism can be driven by one of two possible pathways: dissociative and/or associative mechanism[28], whose elementary steps are shown in Table 1.

Table 1. Dissociative and associative mechanisms for ammonia synthesis[28]

	Dissociative Mechanism	**Associative Mechanism**
(1)	N_2 (g) + * → N_2*	N_2 (g) + * → N_2*
(2)	N_2* + * → 2N*	H_2 (g) + * → H_2*
(3)	N* + H* → NH* + *	H_2* → 2H*
(4)	NH* + H* → NH_2* + *	N_2* + 2H* → N_2H*
(5)	NH_2* + H* → NH_3* + *	N_2H* + H* → N_2H_2*
(6)	NH_3* → NH_3 (g) + *	N_2H_2* + H* → N_2H_3*
(7)	H_2 (g) + * → H_2*	N_2H_3* + H* → N_2H_4*
(8)	H_2* → 2H*	N_2H_4* → 2NH_2*
(9)		NH_2* + H* → NH_3*
(10)		NH_3* → NH_3 (g) + *

All the 1st and 2nd generation catalysts, as well as most of the catalysts developed in the last three decades, are driven by the dissociative mechanism[29]. As shown in Table 1, this mechanism consists of three global steps, namely, N_2 dissociation and activation (1-2), the formation of NH_x species and NH_3 desorption (3-6) and H_2 dissociation and activation (7-8). As aforementioned, it is accepted by the scientific community that the N_2 dissociation step is the rate determining step (RDS) for both 1st and 2nd generation catalysts[30,31]. Thus, the best performing metals have been theoretically predicted considering that the NH_3 synthesis activity is related to the N_2 dissociation efficiency with the performance of this step depending on the binding strength of the N_2 molecule. On the one hand, too high N_2 binding energies result in low catalytic activities due to a limited desorption of NH_3 from the metal surface[21,32,33]. On the other hand, if the adsorption of N_2 on the metal is too weak, the N_2 dissociation step is too slow and the NH_3 synthesis becomes inefficient. Overall, the Sabatier principle predicts as optimum catalysts those that exhibit intermediate strengths for the binding of N_2 and NH_3. Therefore, Ru, Os and Fe are predicted as the best single transition metals (TMs) according to the volcano plots showed in Figure 3. These predictions were deduced from the statement of the scaling relation i.e., it was observed that there is a linear relation between the N_2 adsorption energy and the N_2 dissociation energy barrier.

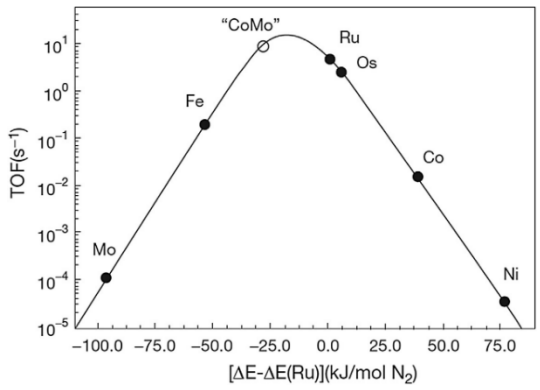

Figure 3. Turnover frequencies (TOFs) of different TMs for NH_3 synthesis as a function of the N_2 adsorption energy. Reproduced with permission[10]. Copyright 2021, Elsevier Inc.

Unlike the dissociative mechanism, in the associative pathway the N_2 molecule is not dissociated, being adsorbed molecularly and activated on the catalyst (Table 1, step 1). Thus, H* adatoms generated from the H_2 dissociation (Table 1, steps 2-3) react with the anchored N_2* species to form intermediate N_2H_x species (Table 1, steps 4-7) and then NH_3 is formed and desorbed (Table 1, steps 8-10). In the associative pathway, instead of dissociation, the N_2 molecule is prone to react over the N≡N triple bond by either distal or alternate hydrogenation. This mechanism is driven by the particular action of specific alternative active sites, commonly known as secondary active centres, which are typical for catalysts based on hydrides, nitrides and single-atom catalysts (SACs)[29].

The increasing interest of NH_3 as a green H_2 carrier along with the continuous growth of population (which is intimately related to an increase in the production of fertilizers) has motivated the research community to find a suitable alternative to the Haber−Bosch process with emphasis on the scale-down of the process. The enhancement of NH_3 separation using sorbents[3,12] and the search of novel catalytic materials and processes to produce NH_3 more efficiently at mild conditions have been the focus of new investigations[10,34,35]. There are many alternative processes to thermocatalytic NH_3 synthesis in a research stage well-described in comprehensive reviews. A general overview of the most relevant processes is provided below and a scheme is shown in Figure 4:

1. **Electrochemical-driven NH_3 synthesis.** This technology is based on a REDOX reaction assisted by electricity in two separated cells: on the one hand, H_2 (or directly H_2O) is oxidized in the anode. Thus, protons are generated and carried in the electrochemical medium. On the other hand, N_2 reduction to NH_3 takes place in the cathode, where the electrons produced in the anode are transported via an

external circuit[36]. The main advantage of this process is the possibility to carry water electrolysis and NH_3 synthesis in a single unit, which is particularly attractive for an efficient coupling of the NH_3 production with renewable technologies[37]. However, many challenges must be overcome to consider electrochemical NH_3 synthesis as an alternative to the Haber−Bosch process, namely the low Faradaic efficiencies at low temperatures and the competing hydrogen evolution reaction (HER) which proceeds at a similar range of potentials[38].

2. **Non-thermal catalytic plasma.** Plasma is based on the generation of an ionized gas containing electrons and excited species, which can activate the N_2 molecule independently from the catalytic reaction. This leads to the breaking of the scaling reaction typical from 1st and 2nd generation catalysts for thermocatalytic synthesis, with plasma acting as a second active centre and the catalyst working for H_2 dissociation and the hydrogenation of N* activated species independently. Non-thermal plasma offers two advantages over the traditional process: on the one hand, the system can work at lower temperatures, an aspect that hinders the N_2 dissociation in the thermocatalytic process. On the other hand, the catalyst needs to have good hydrogenation properties rather than an optimum N_2 binding energy, thus non-noble metals such as Ni or Co can be used with good performance in plasma-driven NH_3 synthesis. Nevertheless, current plasma energy efficiencies must be improved in order to consider non-thermal plasma as a potential technology for small-scale NH_3 production.

3. **Photochemical NH_3 synthesis.** The photochemical route is based on the action of a semiconductor, which acts as an intermediate charge vector i.e., photo-generated and bare electrons can be produced driven by the action of solar light[39]. Then, these electrons can be used to reduce and hydrogenate the N_2 molecule and produce NH_3. This step is similar to that attributed to the electrocatalytic process. Indeed, there is a mixed approach in a research stage with higher energy efficiency than the pure photochemical process: the photochemically assisted electrocatalytic synthesis[40,41]. In this case, the electronic charge generated by the interaction of the semiconductor with light is divided into two distinct electrochemical cells. This avoids the oxidation of NH_3 after synthesis in single photochemical cells, thus increasing the global efficiency. Despite this process is a promising alternative for room temperature NH_3 synthesis, its low solar energy

efficiency and embryonic stage of development hinder its application at higher scale[42,43].

4. **Chemical looping.** This process relies on carrying out the elementary steps from NH_3 synthesis independently, thus optimum conditions can be used for each stage, with successful operation at ambient pressure. Chemical looping takes place by means of reaction intermediates, in which N_2 or H_2 are fixed in the first step and then converted to NH_3 in the second step, following an associative mechanism[44–46]. The N_2 fixation step, which is the key step, is typically achieved by the nitridation of either pure metal (e.g., Mn, Co, Mo, Ca, etc.) or metal hydrides (LiH, BaH_2, etc.) and the nitrides are subsequently hydrogenated to form NH_3. This behaviour is similar to that observed with some catalysts investigated for the thermocatalytic process, such as rare earth nitrides or LiH[47], in which some elementary steps are prone to take place independently by the formation of either reaction intermediates or hydrogen/nitrogen surface vacancies. The coupling of chemical looping NH_3 synthesis with electrochemical processes is a promising technology that requires further research to overcome energy efficiency issues[48,49].

5. **Mechanocatalytic NH_3 synthesis.** The formation of NH_3 at room temperature and atmospheric pressure has very recently been reported in mechanocatalytic systems i.e., ball mills filled with stainless steel balls and an Fe-based catalyst[50,51]. This technique is based on the generation of hot spots during the milling process, over which reaction intermediates can be formed and eventually produce NH_3. Despite it has been proved that NH_3 can be produced continuously for periods of ca. 100 h, it is known that the catalyst is prone to experiment structural and chemical changes, which leads to extended transient periods of 10-20 h and the NH_3 production rates remain very low. Nevertheless, even considering the embryonic stage of mechanocatalytic synthesis, the high energy efficiency of the milling process together with the positive initial results (i.e., the possibility to generate NH_3 at the mildest conditions ever reported with the use of an Fe catalyst), make this technology very promising.

Besides some demonstration NH_3 production plants based on electrocatalytic processes, none of the technologies described above are mature enough to be applied at industrial scale, even considering that a strong progress is being made by the scientific community. Regarding thermocatalytic NH_3 synthesis, an exponential increase in the number of scientific publications during the last two decades has been noticed[52]. The

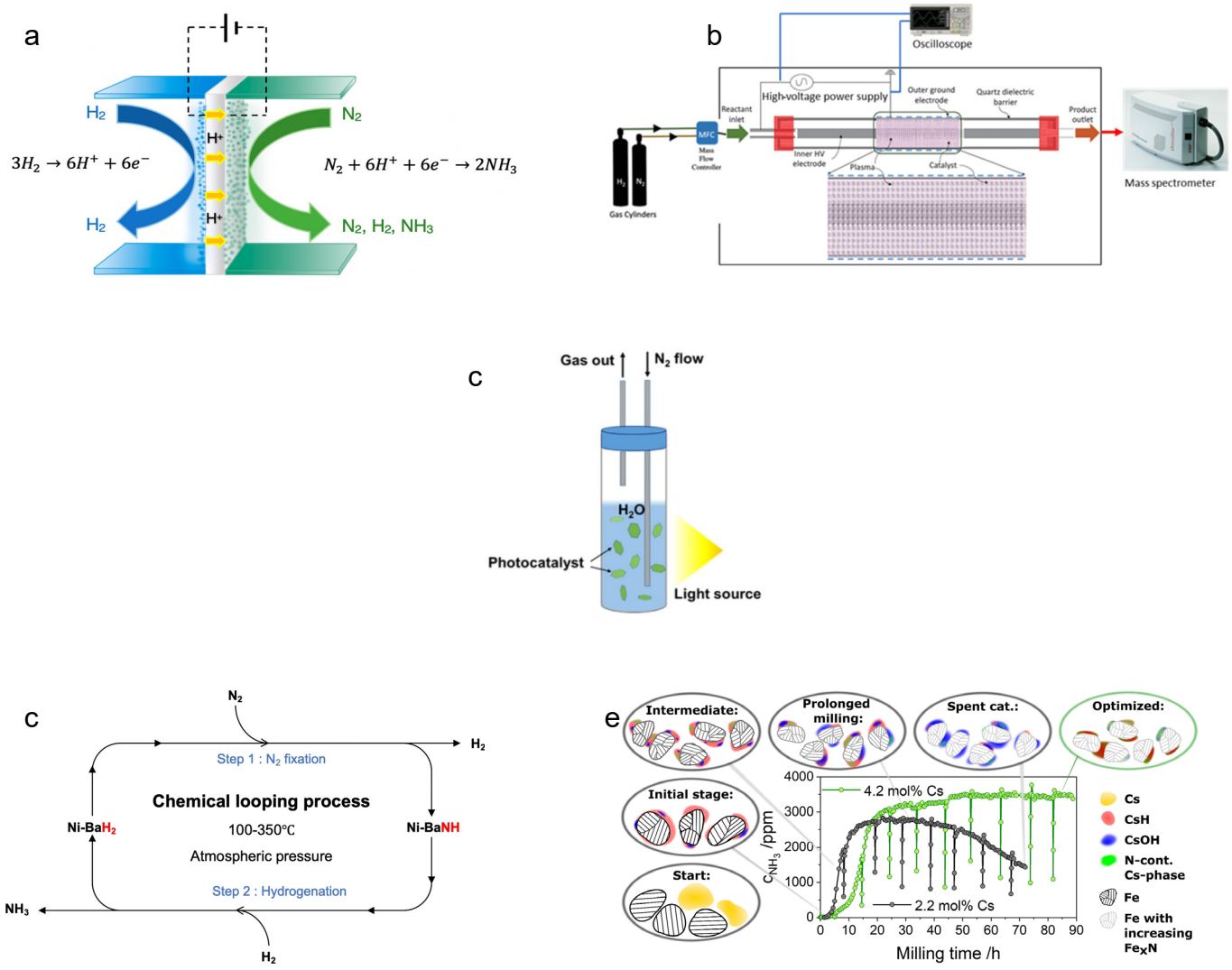

Figure 4. Scheme of alternative technologies to thermocatalytic NH_3 synthesis: (a) electrochemical-driven NH_3 synthesis[93]; (b) non-thermal catalytic plasma[94]; (c) photochemical NH_3 synthesis. Reproduced with permission[95]. Copyright 2019, Elsevier Inc.; (d) chemical looping. Reproduced with permission[93]. Copyright 2021,Springer Nature; (e) mechanocatalytic NH_3 synthesis[51]

objective of the research community is to find new formulas to make feasible the coupling of NH_3 synthesis with renewables at low scales. Particularly, catalysts with low activation energies, are desirable for this application.

The first novel catalyst discovered was made of Ru supported on the so called C12A7:e^-, a mix of calcium (Ca) and Al oxides which can behave as an inorganic electride[53,54]. This material showed an outstanding electron donation capacity (e.g., low work function and high electron density) together with a reversible hydrogen storage capacity via hydrogen spillover, which made it an excellent support for Ru. As a result, a positive H_2 reaction order and a positive pressure effect were noticed and an apparent activation energy around 50 kJ mol^{-1} was found. The N_2 dissociation energy barrier for this catalyst was estimated to be ca. 29 kJ mol^{-1} by DFT calculations as a consequence

of the high electron injection from the support to the TM, much lower than that attributed to 1st and 2nd generation catalysts. Therefore, N_2 cleavage was no longer considered the RDS for Ru/ C12A7:e^-, which tends to switch towards the formation of NH_x species[23]. The insights on the kinetics of this catalyst were so relevant since two of the most relevant handicaps from the 1st and 2nd generation catalysts were circumvented, namely the H_2 poisoning and a slow and limiting N_2 dissociation step. This is the basis for the 3rd generation NH_3 synthesis catalysts that have attracted the attention of the scientific community during the last two decades[55].

Thus, most of the research efforts have been focused on the synthesis of 3rd generation supports for Ru in order to optimize the N_2 dissociation step, as well as on understanding the kinetics of the formation of NH_x species. There are several comprehensive reviews in which these materials are classified as a function of their chemical nature and provide useful information about their performance, kinetic mechanisms and most important properties[14,15,52,56,57]. Recent progress in this field that can be found in the State of the Art are covered in the Chapter 1 of this Thesis.

An optimum utilization of Ru in these 3rd generation catalysts is crucial considering its high cost and low abundance. High NH_3 yields per mole of Ru, known as the turnover frequencies (TOFs), are required. As aforementioned, the research focus relies on the design of 3rd generation novel supports. Most of these supports, particularly the electrides and surface electride materials, are based on a strong electron donation to promote the N_2 dissociation on the Ru surface, following the dissociative mechanism shown in Table 1[58]. However, as aforementioned, there is an alternative pathway: the N_2 molecule can be anchored and hydrogenated to form NH_3 via associative mechanism by means of the generation of lattice nitrogen or hydrogen vacancies, typical from supports such as nitrides, hydrides and other complex materials[29,59,60].

There is an alternative approach to the design of high TOF Ru-based catalysts, based on the utilization of non-noble and more abundant metals, such as Ni or Co. There are limited positive results in this field, since these exhibit poorer N_2 dissociation capacity than Ru (Figure 3). Therefore, in order to make this TMs suitable as NH_3 synthesis materials, the use of functional supports which act as second active centres is required to carry out the N_2 dissociation. There are two original works following this path: on the one hand, the utilization of LiH as support for many TMs demonstrated that the N_2 molecule can be anchored in H^* lattice defects on the support, where it is directly hydrogenated into NH_3 via an associative mechanism[47]. This is due to the formation of

intermediate LiNH species, which leads to the breaking of the scaling relations described above. Apparent activation energies in the 46-64 kJ mol^{-1} range were reported for several TM/LiH catalysts. The scheme of the kinetic mechanism for LiH-based catalysts is shown in Figure 5a. On the other hand, the formation of surface nitride N* defects also act as second active centres for N_2 cleavage in the case of metal nitrides, following an associative mechanism[61]. Since there is a competition between N_2 and H_2 for the occupation of these active sites, a non-noble TM with a good H_2 dissociation capacity can lead to the obtention of a global good performing catalyst. This is the case of Ni/CeN, whose scheme as NH_3 synthesis catalyst is shown in Figure 5b. The key aspect for the good performance of CeN as a second active centre for N_2 dissociation is the low nitrogen vacancy formation energy (E_{NV} = 1.3 eV).

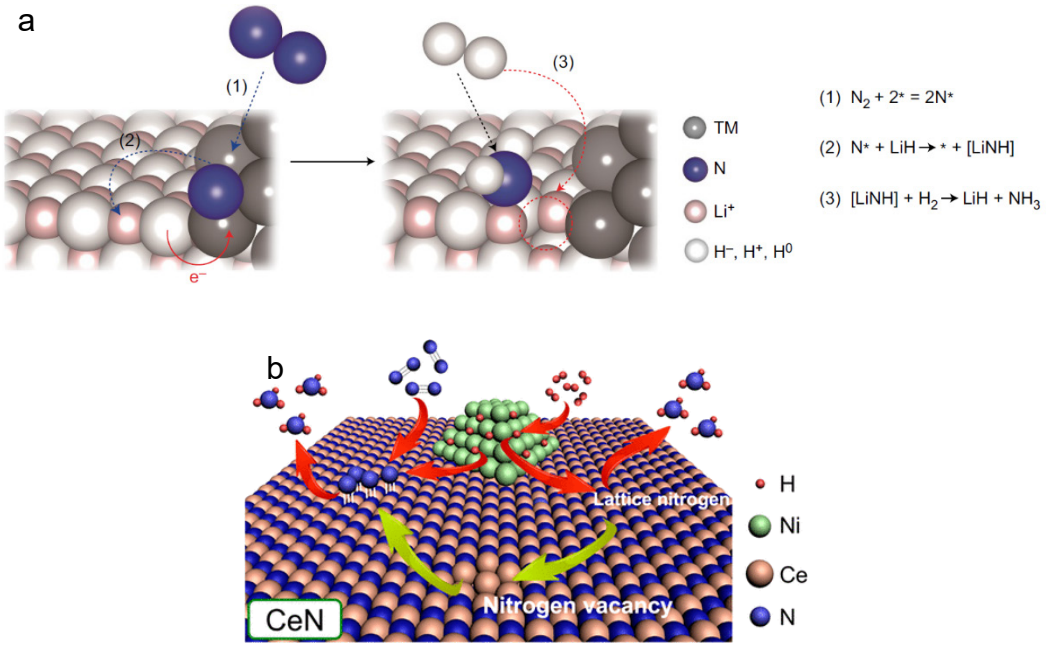

Figure 5. Schematic description of the kinetic mechanism of catalysts driven by the action of second active centres: (a) TM/LiH. Reproduced with permission[95]. Copyright 2016, Springer Nature; (b) Ni/CeN[61]

Even though the performances and kinetic mechanisms of these non-noble TM based catalysts are as efficient as some of the best 3rd generation Ru-based catalysts, mainly supported on surface electrides, the synthesis methods for the obtention of these materials are usually based on several complex steps such as solid-state reactions[47,62], or arc electric furnace synthesis[63]. Moreover, the air and moisture stability of nitrides, hydrides and their derivates is typically poor and their oxidation is considered irreversible in most cases[64]. These aspects strongly hinder the application of these catalysts,

particularly if aforementioned scale-down is required for the transition to an efficient green NH_3 production.

The most recent efforts have been focused on the synthesis of intermetallics SACs. Ternary intermetallics are synthesized from elementary metals, which are combined to form specific formulas[65–68]. These materials cannot only be used as supports for Ru but also as compact catalysts containing Ru. As an example of ternary intermetallics, LaRuSi showed an outstanding performance of 1.76 mmol g^{-1} h^{-1}, at 400 ºC and 0.1 MPa, with an apparent activation energy of 40.4 kJ mol^{-1}, even though the specific surface area of this catalyst was as low as 1-2 m^2 g^{-1}. Nevertheless, the surface of this catalyst can be treated by chemical etching with ethylene diamine tetraacetic acid (EDTA) in order to maximize the concentration of Ru active sites on the surface[64], with a considerable increase in the NH_3 synthesis performance. Furthermore, the air stability of this catalyst was demonstrated to be excellent. In later studies, the kinetic mechanism of this outstanding catalyst was unveiled: first of all, since La and Ru atoms are in close contact, the electron transfer between La and Ru is strong. Furthermore, the formation of lattice hydride species was reported, thus the H^* sites act as a second active centre for N_2 dissociation. Lately, the formation of a bowl active site i.e., four La atoms on the surface and one Si atom in the subsurface, leads to a boosted N_2 dissociation step. In addition, the Si atom shows a variable valence state, with a versatile electron charge, which accounts for an efficient NH_x species formation via electrostatic repulsion[69].

It has been demonstrated that the optimum size for Ru nanoparticles is 1.8-2.5 nm[70,71], since the active B5 sites concentration is maximum in this particle size range. Nevertheless, recent studies unveiled that the kinetic behaviour of Ru catalysts when the particle size is decreased up to sub-nanometric scale differs from traditional 2nd generation mechanism: instead of dissociated, N_2 molecules can be anchored into the active sites from Ru SACs and afterwards converted into NH_3 via distal hydrogenation[72,73]. This is similar to the action of second active centres attributed to intermetallics, hydrides and nitrides, following an associative pathway. Despite the preliminary results in this field are promising, there are some challenges that hinder SACs applications: first of all, as in the rest of associative-driven catalysts, the competition between both N_2 and H_2 to occupy the single atom active sites is a barrier for an efficient global mechanism, thus these catalysts can potentially suffer from H_2 poisoning[74]. Secondly, the single atoms sites are designed from a structural support with specific templates i.e., the number of single atom sites available for the metal is limited and the

metal loading is usually low[72,75–78]. In addition, metal tends to agglomerate during the reaction process, partially losing the active sites, thus the synthesis methods must be successfully optimized[79].

Even though the research studies are starting to focus on the use of non-noble materials, the NH_3 synthesis paradox still remains unravelled: while the scientific community understands that the application of new materials is necessary to use NH_3 as the intermediate molecule to a real transition into a green H_2 scenario in the near future and, as a result, a large variety of catalysts has been developed at lab-scale since the last two decades, the 1st generation Haber−Bosch process cannot be outfaced yet. In order to effectively move towards a greener scenario, well-known, abundant, available and stable catalysts are required and, in spite of the considerable efforts carried out in terms of catalysts design, these 3rd generation materials are still far from this objective.

In this sense, a promising strategy relies on the promotion of Ru with rare earth (RE)-based materials such as cerium (Ce)[68]. These elements possess several interesting properties, such as the facile reducibility of Ce (from Ce^{4+} to Ce^{3+}), the generation of strong metal-support interactions (SMSI) when Ru is loaded on the surface of RE oxides, the formation of highly dispersed catalysts and the versatility i.e., they can perform as NH_3 synthesis in different chemical forms (oxides, perovskites, nitrides, hydrides and intermetallics)[56]. RE materials have been successfully used as 2nd and 3rd generation NH_3 synthesis catalysts at lab scale, mainly as supports. Ce is the most abundant and cheaper rare earth element. After reduction of Ce^{4+} into Ce^{3+}, the oxide preserves the original crystalline matrix and, as a consequence, oxygen vacancies are formed in the reduction process[80]. Bare electrons are caged in these oxygen vacancies, as shown in the Eq. 2:

$$Ce^{4+} + e^- \rightarrow Ce^{3+} \qquad \text{Eq. 2}$$

The electron donation from these oxygen vacancies towards Ru leads to an outstanding improvement of the performance of Ru/CeO_2 catalysts over conventional 2nd generation materials[81,82]. However, commercial ceria (CeO_2) typically shows low surface area and poor metal dispersion, thus NH_3 synthesis performances are not usually considered efficient enough[68]. Moreover, the electron transfer from ceria to Ru is limited and H_2 adatoms tend to engage into the active sites, so Ru/CeO_2 can suffer from H_2 poisoning. Research on ceria-based supports is quite extensive and several approaches have been carried out in order to demonstrate that it is a real alternative to 1st and 2nd generation catalysts. Considering that the low surface area is a well-known limitation of CeO_2, most of these studies have focused on understanding of the morphological and

structural properties of this material as NH_3 synthesis support. It was demonstrated that SMSI is induced on the Ru-Ce interaction sites, thus morphological aspects are quite relevant[83,84]. In addition, some novel approaches have been given in order to improve the ceria natural structure. As an example, Ru/CeO_2 with a modified support structure of a yolk-shape sphere was prepared and, as a result, the particle size of CeO_2 was adjusted, leading to the tunning of the SMSI[85]. The schematic representation of the performance of this catalyst is shown in Figure 6. Furthermore, it is accepted that the CeO_2 structure can be altered by the addition of secondary elements, thus the generation of surface oxygen vacancies can be increased[86]. It has been demonstrated that the oxygen vacancies active sites from the original Ru/CeO_2 catalyst can be improved by the addition of Zr,[87] La[88] or Sn[89]. Most of these studies highlight the impact of the reduction temperature, with a trade-off between the generation of surface defects and the high temperature sintering.

It was demonstrated that Ce hydrides and oxyhydrides outperformed CeO_2 as supports for Ru. As long as CeH_3 owns the original reversible reducibility attributed to Ce, in this case, the formation of hydrogen vacancies allows the simultaneous mobility of H^- and electrons, improving the tolerance to H_2 poisoning and significantly enhancing the performance of CeO_2 supports[90]. A hybrid dissociative-associative mechanism is the key aspect of these catalysts: while the back electron donation from the H^- vacancies to Ru via dissociative mechanism is prone to be given at the TM-support interface sites, an additional associative cleavage of N_2 on the H^- lattice defects takes place, providing an excellent performance to this hydride as support. Furthermore, oxyhydrides generated from a mixed solid solution of CeO_2 and CeH_3 outperform the oxide and hydride-based materials[91]. The additional performance is attributed to the increase in the H^- mobility given by the knock-off effect (i.e., the combination of grouping of tetrahedral structures of O^{2-} and H^- with the electrostatic repulsion between these anions)[92]. $Ru/CeH_{1.5}O_{0.75}$ showed an NH_3 synthesis activity of ca. 1.7 mmol g^{-1} h^{-1}, at 260 ºC, 0.1 MPa and a weight hourly space velocity (WHSV) of 36000 mL g^{-1} h^{-1}.

On the other hand, it has also been demonstrated that some rare earth nitrides are able to produce NH_3 by themselves, without any TM loading on the surface[61]. This is due to the formation of defects on the nitride surface layer (N_V), in which N_2 can be anchored and hydrogenated via an associative mechanism. However, both N_2 and H_2 molecules trend to occupy the N_V active sites, thus the global rates are usually low. The performance of this nitride second active centre breaks the barrier to N_2 dissociation which limits the use of non-noble metals as NH_3 synthesis catalysts. Additionally, Ni/CeN

exhibited an excellent NH_3 synthesis performance, with an apparent activation energy as low as 50.6 kJ mol^{-1}. In this case, even though Ni is unable to participate in the N_2 cleavage, it is an excellent H_2 dissociation metal i.e., it acts as a second active centre for the donation of dissociated H_2 species to the N_2 activated species.

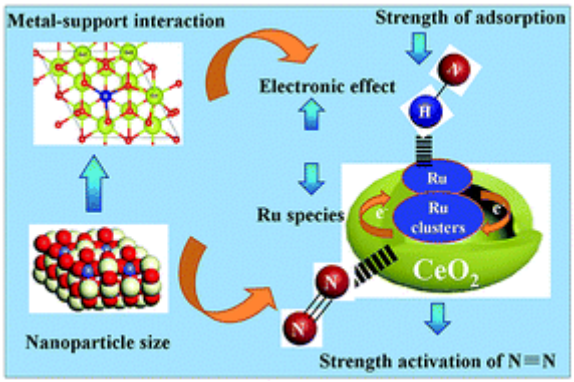

Figure 6. Schematic description of the kinetic mechanism of modified Ru/CeO_2 with carbon templates. Reproduced with permision[85]. Copyright 2019, Royal Society of Chemistry.

As aforementioned, intermetallics are being currently considered as an alternative to traditional materials for NH_3 synthesis. The majority of the most promising formulas necessarily work by the presence of RE elements. Not only (RE)(TM)Si trimetallics, but also bimetallics typically used as H_2 storage materials, such as $LaNi_5$, demonstrated a high NH_3 synthesis performance[63]. At the NH_3 synthesis conditions, the $LaNi_5$ morphology gets modified into a core-shell structure, with the formation of a LaN surface layer, while Ni tends to be enclosed in the core. Similarly to the RE nitrides, N_2 is anchored on the LaN surface layer, while H_2 is additionally dissociated in the core made of Ni via H_2 spillover through the nitride layer. As a result, nanoparticles (NPs) of $LaNi_5$ showed an NH_3 synthesis performance of 4.5 mmol g^{-1} h^{-1} at 400 ºC and 0.1 MPa and an apparent activation energy of 53.8 kJ mol^{-1}.

As a summary, RE elements possess a versatile chemical nature, with excellent electronic properties and are prone to promote the NH_3 synthesis in several forms, not only as supports for Ru in the form of oxides and hydrides, but also as supports for non-noble metals in the form of nitrides (exhibiting some activity even with the absence of metal loading) and in the form of intermetallics. It must be noted that most of the RE-based materials used as NH_3 synthesis catalysts are made of La (Ru/LaH_xO_y, $LaNi_5$, LaRuSi). However, Ce is more abundant and shows better properties for NH_3 production than La, such as a lower N_V formation energy. Therefore, gaining further insights on the

behaviour of Ce as a chemical platform for the design of 3rd generation NH_3 synthesis catalysts would be greatly interesting.

2. Objectives

The general objective of this Thesis is to gain insights into the thermocatalytic NH_3 synthesis and to produce suitable catalysts, with a particular focus on the specific role of Ce in different chemical forms. Besides, this general objective is comprised of four specific objectives:

1. Deep understanding on the NH_3 synthesis fundamentals and the intrinsic insights that define this chemical reaction i.e., thermodynamic limitations, kinetic mechanisms and key aspects, as well as the current state-of-the-art in the development of catalysts. This specific objective is covered in the Chapter 1 of this Thesis.
2. Design of efficient non-noble metal-based Ce catalysts. This specific objective is covered in the Chapter 2 of this Thesis.
3. Synthesis of air and moisture stable CeO_2 supports for Ru, made by simple impregnation methods, with the approach of producing scalable and efficient catalysts. This specific objective is covered in the Chapter 3.
4. Optimization of the performance of Ru/CeO_2 by the addition of La into the crystalline net of ceria, which further enhances the metal-support interactions. This specific objective is covered in the Chapter 4.

3. Structure. Compendium of publications

This thesis is structured in four Chapters. The first three Chapters correspond to published works in scientific journals, establishing the compendium of publications of this work. The Chapter 4 is developed apart in the main text of this Thesis.

A brief description of all the Chapters is given as follows:

1. **Chapter 1: A Conceptual Approach for the Design of New Catalysts for Ammonia Synthesis: A Metal–Support Interactions Review.**

   A review of the State of the Art is conducted in this Chapter. A historical evolution of the progress in the development of NH_3 synthesis catalyst is presented, with a particular emphasis on the specific action of the different supports. Furthermore, the fundamentals of the NH_3 synthesis reaction are introduced, thus the reader can have a good background on the most relevant kinetic aspects attributed to this reaction: scaling relation, elementary steps of both

dissociative and associative kinetic mechanisms, N_2 dissociation and activation, H_2 poisoning, electron transfer, etc.

2. **Chapter 2: $CeNi_x$ Alloys as Catalysts for Ammonia Synthesis: Insights on Ni-CeN Surface Layer Formation and Its Impact.**

This Chapter is the result of an international research stay in the *MDX research Center for Element Strategy, International Research Frontiers Initiative, Tokyo Institute of Technology, Japan*, under the supervision of prof. Kitano. $CeNi_x$ alloys, which are well-known as H_2 storage materials, are tested as NH_3 synthesis catalysts. Two formulas are analysed: $CeNi_2$ and $CeNi_5$. These catalysts are prepared following an arc melting of pure Ce and Ni elements in stoichiometric proportions. It is demonstrated that the formation of a CeN crystalline layer on the catalyst surface is responsible of the superior activity of $CeNi_2$ over $CeNi_5$ (the CeN surface layer is not formed for the latter). For the transformed $CeNi_2$, an activation energy of 55.3 kJ mol^{-1} is achieved, similar to some of the best Ru-based NH_3 synthesis catalysts. This is due to the action of the nitrogen vacancies on the CeN surface layer, which act as a second active center for a boosted N_2 dissociation.

3. **Chapter 3: Efficient CeO_2 and CeO_2-Al_2O_3 supports for Ru as 3rd generation ammonia synthesis catalysts: enhanced kinetic mechanism over commercial Ru/CeO_2.**

The expertise acquired during the stay in Japan was applied in the research line of thermocatalytic NH_3 synthesis at Loyola facilities, resulting in the experimental reaction systems described in Chapters 3 and 4.

After demonstrating the good performance of Ce as a second active center for the N_2 dissociation in the form of CeN in the Chapter 2, a different approach is explored in the Chapter 3. In this case, Ce is used in the form of CeO_2 as support for Ru. A simple impregnation-calcination method carries the synthesis of a Ru/CeO_2 catalyst that outstands a catalyst made of a commercial ceria, with a higher specific surface area and low crystallinity, leading to an increase in the formation of surface oxygen vacancies. Therefore, the SMSI are enhanced via electron donation towards Ru. As a result, an activation energy as low as 46.1 kJ mol^{-1} is achieved. The addition of basic alumina to the support matrix further enhances the kinetic mechanism, showing an activation energy of 44.8 kJ mol^{-1} with a 50 wt% of alumina. This is due to an increase in the global specific surface area. The performance at 400 ºC and 0.1 MPa of this catalyst is slightly lower than

that attributed to Ru/CeO_2, which is reasonable considering that half of the active support is substituted by a cheaper non-functional material, such as Al_2O_3.

4. **Chapter 4: Ru/CeO_2-La_2O_3 catalysts for ammonia synthesis: on the search of an optimum Ce/La ratio.**

Ongoing with the positive results from Chapter 3, it has been previously reported that the addition of La promotes the formation of defects on the crystalline structure of CeO_2, thus increasing the generation of oxygen vacancies. This leads to an increase of the SMSI by an enhanced electron promotion. The interest of this Chapter comes from the lack of analysis of the optimum Ce/La ratio.

In this Chapter, it is verified that a 50% molar basis of Ce onto the Ce-La mixed oxide matrix support provides an optimum kinetic scheme, showing an NH_3 reaction rate of 2.7 mmol g^{-1} h^{-1} at 400 ºC and 0.1 MPa and an activation energy as low as 34.1 kJ mol^{-1}. This is the best Ru/CeO_2-La_2O_3 catalyst and one of the best global catalysts ever reported in terms of NH_3 synthesis performance, even considering that the synthesis method is as simple as an impregnation and coprecipitation-calcination process. The outstanding performance of this catalyst over Ru/CeO_2 comes from the disrupt of the crystalline structure by the addition of La into the support matrix. As a result, the formation of surface oxygen species i.e., oxygen vacancies, is much higher for the Ru/CeO_2-La_2O_3 catalyst than that attributed to Ru/CeO_2. Below a 50 n% of Ce into the mixed oxide support, the crystalline structure gets shattered and tends to transform into the La_2O_3 matrix, which explains the optimum observed for a 50% loading.

II. Section 2: publications

1. Chapter 1: A Conceptual Approach for the Design of New Catalysts for Ammonia Synthesis: A Metal–Support Interactions Review

Title: A Conceptual Approach for the Design of New Catalysts for Ammonia Synthesis: A Metal–Support Interactions Review.

Authors: Javier Arroyo−Caire, Manuel Antonio Diaz−Perez, Mayra Anabel Lara−Angulo and Juan Carlos Serrano−Ruiz.

Reference: *Nanomaterials* 2023, 13, 2914. https://doi.org/10.3390/nano13222914.

Published date: 8 November 2023.

Impact factor: JIF 4.4 (JCR, 2023).

Position: CHEMISTRY, MULTIDISCIPLINARY 70/231 (Q2).

nanomaterials

MDPI

Review

A Conceptual Approach for the Design of New Catalysts for Ammonia Synthesis: A Metal—Support Interactions Review

Javier Arroyo-Caire, Manuel Antonio Diaz-Perez, Mayra Anabel Lara-Angulo and Juan Carlos Serrano-Ruiz *

Materials and Sustainability Group, Department of Engineering, Universidad Loyola Andalucía, Avda. de las Universidades s/n, Dos Hermanas, 41704 Seville, Spain; jarroyo@uloyola.es (J.A.-C.); madiaz@uloyola.es (M.A.D.-P.); malangulo@uloyola.es (M.A.L.-A.)
* Correspondence: jcserrano@uloyola.es; Tel.: +34-955-641-600 (ext. 2579)

Abstract: The growing interest in green ammonia production has spurred the development of new catalysts with the potential to carry out the Haber–Bosch process under mild pressure and temperature conditions. While there is a wide experimental background on new catalysts involving transition metals, supports and additives, the fundamentals behind ammonia synthesis performance on these catalysts remained partially unsolved. Here, we review the most important works developed to date and analyze the traditional catalysts for ammonia synthesis, as well as the influence of the electron transfer properties of the so-called 3rd-generation catalysts. Finally, the importance of metal–support interactions is highlighted as an effective pathway for the design of new materials with potential to carry out ammonia synthesis at low temperatures and pressures.

Keywords: green ammonia; mild conditions; electron transfer; 3rd-generation catalysts

Citation: Arroyo-Caire, J.; Diaz-Perez, M.A.; Lara-Angulo, M.A.; Serrano-Ruiz, J.C. A Conceptual Approach for the Design of New Catalysts for Ammonia Synthesis: A Metal—Support Interactions Review. *Nanomaterials* **2023**, *13*, 2914. https://doi.org/10.3390/nano13222914

Academic Editor: George Z. Kyzas

Received: 26 September 2023
Revised: 2 November 2023
Accepted: 6 November 2023
Published: 8 November 2023

1. Introduction

Ammonia is one of the most widely consumed chemicals worldwide. The high annual ammonia production (ca. 190 MMt·year^{-1} in 2020 [1]), along with the growing demand for nitrogen-containing fertilizers [2], represents an environmental challenge since the synthesis of this commodity is currently carried out by the conventional Haber–Bosch process, one of the most energy-consuming industrial processes (ca. 200–400 bar of pressure and 400–600 °C of temperature), responsible for approximately 1.2% of global anthropogenic CO_2 emissions [3].

In addition, like most industrial processes nowadays, the hydrogen used for ammonia synthesis (see Equation (1)) is mainly obtained from non-renewable sources (e.g., natural gas reforming), which eventually results in a considerable environmental impact.

$$N_2 + 3H_2 \rightarrow 2NH_3 \quad (1)$$

In order to make this industrial system economically feasible, the Haber–Bosch process is carried out in large central facilities which, in reality, contain two large industrial plants in one (a steam methane reforming plant and an ammonia synthesis plant). Considering the growing concern around Greenhouse Gas (GHG) emissions, there is a pressing need to increase the sustainability of the process by coupling ammonia synthesis with renewable hydrogen production via wind- or photovoltaic (PV)-driven water electrolysis. However, effective coupling of both technologies requires ammonia synthesis to be carried out under significantly milder pressure and temperature conditions than those used in the Haber–Bosch process. The use of lower temperatures and pressures in the synthesis reactor paves the way for designing smaller non-centralized ammonia plants, which could act as local fertilizer producers [4]. This green ammonia concept represents a shift from traditional high-scale centralized production to low-scale distributed generation [3].

Apart from its main use as a raw material for fertilizers (approximately 80% of the total ammonia produced [3]), ammonia has recently demonstrated a potential use as a hydrogen carrier in virtue of its high hydrogen content (ca. 18 wt%) [1,3,5,6]. Moreover, ammonia is much easier and also cheaper to transport than hydrogen, based on its low vapor pressure (≃10 bar). Actually, ammonia has a well-established international supply chain and could become a suitable and effective pathway to transport hydrogen. Thus, ammonia could be considered as a potential and attractive carbon-neutral feedstock for the near future energy applications.

Based on the rising importance of ammonia production under mild conditions, the feasibility of new methods such as chemical looping [7–9], photocatalysis [10,11], photothermal catalysis [12], plasma [13,14], electrochemical-assisted synthesis [15,16] and other methods at the embryonic stage of development, such as mechanocatalytic synthesis [17], is being analyzed. However, although important advances, all these technologies are still at the very early stage of investigation and additional studies are required to demonstrate their efficiency and scalability in realistic industrial conditions [5,18].

Regarding these promising technologies, they have some advantages but also many challenges to compete effectively with more mature thermocatalytic ammonia synthesis [18]: plasma synthesis can be carried out under mild conditions and can afford transients typical from renewables. However, ammonia synthesis rates are still low, and it is a high energy-consuming process. Electrochemical synthesis also enables operating under mild conditions and reduces CO_2 emissions by the use of H_2O as a hydrogen source, but it has some drawbacks, such as the competition of both nitrogen and hydrogen to be adsorbed on the TM and low ammonia selectivity. In addition, photocatalytic synthesis also enables ammonia synthesis under mild conditions, but dinitrogen promotion and activation performance targets are not good enough yet. Therefore, it seems that thermocatalytic ammonia synthesis is the most advantageous and developed technology to date, with a high future potential, since there are many research possibilities to improve the current technology.

On the other hand, the design of novel materials for ammonia thermocatalytic synthesis has experimented important progress in recent years, especially since the elucidation of the positive synergy between the metal functionality (usually ruthenium) and a wide variety of promoters and supports. In recent decades, different materials have been investigated with the aim to optimize the design of suitable catalysts [5,18,19].

Investigation of these materials is motivated by the potential environmental advantages of improving the ammonia synthesis activity of current industrial catalysts by several orders of magnitude, which relies on a reduction in energy consumption in the current Haber–Bosch ammonia plants. As aforementioned, decreasing temperature and pressure can potentially result in a decrease in CO_2 emissions since less energy is required to obtain ammonia. Additionally, the possibility of coupling ammonia synthesis carried out by novel catalysts with renewable energies would increase the environmental attractiveness of the process even more, since the necessary hydrogen could be obtained from water electrolysis, making ammonia synthesis a carbon-neutral process [5].

Based on the recent and fast development of new strategies for the design of new materials with high activity for ammonia synthesis under mild conditions and on the complexity of the phenomenology associated with each kind of catalyst, this review provides: (i) a general view of the progress made through the different generations of catalysts, (ii) a comprehensive explanation of the different mechanisms involved in the thermocatalytic ammonia synthesis reaction and (iii) the future outlook and perspectives for the development of new materials. Unlike several works published to date [18,20–25], the aim of this review is to unveil the fundamentals of electron transfer and metal–support interactions, since these concepts are key aspects for the development of the so-called 3rd-generation catalysts for ammonia synthesis. In fact, since the discovery of the C12A7:e^- electride, investigations into metal–support interactions led to a drastic change in the paradigm of catalyst development [26]. As demonstrated in this review, the promotion of the electron

transfer between the support and TM can be used as a reasonable criterion for the design of efficient ammonia synthesis materials.

2. Thermocatalytic Ammonia Synthesis

2.1. Historical Evolution of Catalysts for Ammonia Synthesis

The Haber–Bosch process is the predominant route for ammonia production worldwide [3]. The ammonia synthesis reaction (Equation (1)) is limited by the high stability of the N_2 molecule (N≡N bond energy of 945 kJ·mol^{-1}), which is one of the strongest known chemical bonds and requires precise forces to work at high temperatures (400–600 °C) to increase the reaction rate. Since this reaction is exothermic (−92 kJ·mol^{-1}), it is necessary to operate at high pressures (200–400 bar) to overcome the thermodynamic limitations derived from working at those temperatures [27]. The industrial process has been operating since the early 20th century on the so-called 1st-generation catalysts based on iron oxides [21]. Industrially, the most commonly used catalysts are those derived from magnetite (Fe_3O_4). However, iron oxides by themselves do not exhibit significant activity so these materials are generally supported on Al_2O_3 and promoted by other components such as K_2O, CaO or MgO [20,21,28,29]. The ammonia synthesis reaction over Fe is sensitive to the structure rather than to electronic interactions, with Fe(111) being the most active facet [30]. Although 1st-generation promoted iron-based catalysts are widely used (mostly due to their low price), they present low intrinsic activities, thereby being forced to operate at high temperatures to achieve industrially acceptable activities. Operation at high temperatures harms equilibrium conversion, thereby needing to operate at elevated pressures and increasing the complexity of the industrial process. The classical Haber–Bosch process is therefore non-compatible with renewable hydrogen production processes (e.g., water electrolysis), which normally operate under milder operation conditions.

At the end of the 20th century, a new class of catalysts based on ruthenium over carbon were developed in an attempt to reduce synthesis pressures and temperatures [20,21]. The discovery and optimization of these 2nd-generation catalysts (i.e., ruthenium over carbon normally promoted with Cs or Ba) led to a new industrial process for the production of ammonia called the Kellogg Advanced Ammonia Process (KAAP), in which it is possible to obtain yields of 40–50%, at lower temperatures (370–400 °C) and pressures (50–100 bar) as compared to the conventional Haber–Bosch process using iron oxides as the catalyst [22].

Moreover, Ru-based catalysts have been demonstrated to be highly effective towards ammonia synthesis, and more active than the conventional Fe-based catalysts [31]. However, ruthenium is a low abundant noble metal which hinders its industrial use due to its high cost. Therefore, since the release and development of the KAAP process, several strategies for the design of new catalyst based on Ru have been evaluated in order to increase the activity and stability of these kind of catalysts, with the objective of minimizing the amount of noble metal in the catalyst.

As in the case of iron-based catalysts, generally, the dissociative adsorption of N_2 is the Rate Determining Step (RDS) on ruthenium catalysts, as it will be explained in more detail in the Section 2.3. The high activity of Ru-based catalysts for ammonia synthesis, in comparison with other transition metals (from now, TMs), is normally associated with the active B5 site (i.e., a configuration of three ruthenium atoms in a layer with two further ruthenium atoms in the layer just above), which works as an active center for N_2 cleavage [22,31]. The concentration of B5 sites on the catalysts is dependent on their particle size, so several studies have been focused on the rational design of nanomaterials (i.e., reducing the size of the particles to a nano scale) in order to promote the amount of B5 sites on the catalysts. It was demonstrated that catalysts with a size ranging from 1.8 to 2.5 nm exhibit the highest amount of this specific kind of active sites, so different synthesis procedures have been checked to decrease the size of the particles, which is generally higher [32]. Furthermore, from a structural point of view, as it is common in heterogeneous catalysis, a high specific surface and a proper porosity is desirable, and this is also generally obtained by decreasing the particle size.

However, even considering a reduction on the size of the particles and the presence of a noble metal, a sole Ru over carbon catalyst commonly exhibits poor ammonia synthesis activity [33] and ruthenium-based materials are thus commonly promoted by the addition of some extra compounds: alkali and alkaline earth promoters have been demonstrated to be very effective at achieving high activities towards ammonia production [22]. Among them, cesium and barium are the most widely used, although their beneficial effects are attributed to different phenomena. As an example, the addition of different amounts of cesium to a ruthenium over ceria (Ru/CeO_2) catalyst, as well as the impact of the synthesis route, were recently explored [34]. It was concluded that both the concentration of the cesium promoter and the procedure followed for the preparation of the catalyst could influence the performance of the material for the ammonia synthesis reaction. From these results, it was observed that the optimal behavior in terms of ammonia production and Turnover Frequencies (TOF) was obtained by adding the cesium to the support before ruthenium impregnation, with an optimal load of Ru of 2% wt. and a Cs/Ce rate of 0.35. It was suggested that larger amounts of promoter could block the Ru active sites, decreasing the activity as a result. The beneficial effect encountered once the correct concentration of cesium was used was attributed to the electron-donating effect of cesium as well as an improvement on the resistance of the so-made catalyst to hydrogen poisoning that commonly affect the ruthenium-based catalysts (see Section 2.3 for more details). The interaction of cesium and the support can change the electronic properties of the catalyst, increasing its performance due to the synergetic effect of ruthenium and cesium. The electronic promotion encountered with the addition of cesium was also previously reported by several authors and it is well accepted that the low electro negativity of alkali and alkaline materials promotes the mentioned beneficial electronic effect [33].

Similarly, the addition of barium to different ruthenium-supported catalysts has been demonstrated to significantly increase the activity for ammonia production [33,35–37]. The presence of barium on the catalyst seems to also influence the electronic properties of the material in some extent due principally to the presence of Ba^0 [38]. However, it was suggested that barium promotion comes from changes in the catalyst structure, by increasing the highly active B5 sites [22].

It is interesting to note that despite the enhancement obtained by the addition of cesium being much higher than that encountered when barium acts as a promoter [33], it has been demonstrated that cesium degrades more rapidly than barium on a ruthenium supported over yttria-stabilized zirconia catalyst [35], thus increasing the industrial attractiveness of the latter. Therefore, it is clear that the activity is not the only effect to be considered for a successful scalability of thermocatalytic ammonia synthesis technology.

Based on the different effects observed with Cs or Ba (i.e., electronic and structural, respectively), the synergy between these two promoters was also investigated on a ruthenium over carbon catalyst [39]. It was claimed that a Ru catalyst promoted by Cs and Ba exhibited higher activities than those promoted by a sole species (Cs or Ba). This is pretty interesting since it demonstrates that for a successful design of a catalyst for ammonia synthesis under mild conditions, every single beneficial effect should be considered to maximize its activity.

The promotion effect of other alkali elements, like potassium and sodium, has also been analyzed [38,40], although their beneficial effect over ruthenium catalysts is lower than that obtained with cesium or barium. In fact, it is well accepted that the effectiveness of the promoters increases inversely with the electronegativity of the element used [41]. Nonetheless, despite the beneficial effect observed with K or Na, it is not as high as that obtained with Cs or Ba, the addition of both Na and K to Ru-based catalysts results in a remarkable promotion of ammonia synthesis [38,40] and it is worth to consider these elements as promising promoters since they are much more abundant on earth than cesium and barium, which could facilitate their spread into the industrial scale. It was recently demonstrated [42] that ammonia synthesis activities are higher when potassium is added to Ru/MgO and Ru/CeO_2 catalysts. Thus, an enhancement of more than double when

4% wt. of K is added to the Ru/CeO_2 catalyst was reported, and a threefold increase for K-Ru/MgO catalyst as compared to the unpromoted Ru/CeO_2 and Ru/MgO.

It is also interesting to note that the role of promoters is intimately associated with the nature of the support and the effect can vary significantly [22]. For instance, although the addition of small quantities of Cs (as low as a relation of Cs/Ru = 1) to a Ru/MgO catalyst could significantly increase the activity, a relation much higher (Cs/Ru = 10) did not result in a substantial enhancement when Al_2O_3 is used as support. In the case of alumina acting as support, it is suggested that the promoter interacts with the acid sites of the Al_2O_3, not covering the Ru surface, which results in a "deactivation" of the beneficial effect of the Cs [22].

Nowadays, a Ru-based catalyst promoted by Cs which uses high surface graphite carbon (HSGC) as support is commonly used at the industrial scale in the KAAP process [22]. However, at the same time, a wide range of materials are still being investigated intensively as potential supports, seeking a high activity and stability towards ammonia synthesis under mild conditions. Since the development of the KAAP process, 2nd-generation Ru-based catalysts have been further researched, with a special emphasis on the support morphology and its properties [22].

In this context, some common oxides, like MgO, ZrO_2, CeO_2, and Al_2O_3, which are among the most commonly used heterogeneous catalyst supports, have been proposed as a possible way to enhance ammonia synthesis activity and stability. Among them, it has been demonstrated that those oxides with a certain degree of basicity can help to increase the catalytic performance for ammonia synthesis [34,43]. In fact, as aforementioned, some authors claim that acid sites (as those in Al_2O_3) can strongly interact with ammonia once produced, limiting its desorption and finally decreasing the overall activity as a result [22], although they could promote the activation of the dinitrogen. The importance of the basicity on the ammonia synthesis activity was also highlighted by Miyahara et al. [43] using Ru-based catalysts supported on lanthanoids oxides.

Authors encountered a positive relation between the basicity of the catalyst and the TOF, demonstrating that the ammonia production rate increases when light lanthanoid oxides (e.g., Ru/Pr_2O_3, Ru/CeO_2, Ru/LaO_3) were used as supports, which means that the enhancement on the ammonia synthesis activity was intimately related with the catalysts with the highest basic site concentration.

On the other hand, the effect of oxygen vacancies of the support has also been identified as an important parameter to consider for the ammonia synthesis activity [44,45]. It has been demonstrated by several works that a high amount of oxygen vacancies can promote the nitrogen adsorption and its activation in photochemical applications [46–48]. Based on this idea, the effect of oxygen vacancies was studied, analyzing ceria-based supports with different morphologies for a thermocatalytic ammonia synthesis [44]. The higher activity of CeO_2 nanorods over the CeO_2 nanocubes under the same operating conditions (400 °C, 1 MPa) was attributed to the presence of a high concentration of oxygen vacancies, along with a low crystallinity (which favors the presence of Ru^{4+} ions, instead of metallic Ru particles).

Moreover, the importance of the oxygen vacancies for the ammonia synthesis reaction has been further investigated [45]. The effect of doping a Ru over CeO_2 catalyst with samarium (Sm) (Ru/Sm_2O_3-CeO_2) was studied and it was demonstrated that the addition of Sm^{3+} (up to 7% wt.) to ceria increases the concentration of oxygen vacancies, which greatly increased the ammonia synthesis activity as compared to that catalyst with no Sm. The enhancement observed once Sm was used was related to the improvement of the reducibility properties of Ru and ceria, which could ensure a more efficient breakdown of the nitrogen triple bond by the donation of the electrons from the partially reduced ceria to the Ru metal particle, along with the increase in the hydrogen desorption capacity, which can prevent hydrogen poisoning and thus promote the nitrogen adsorption.

As previously demonstrated in several works, an enhancement into the electronic properties of the catalyst improves the nitrogen dissociation into atoms before reacting with hydrogen to form ammonia. Inspired by this idea, researchers focused their attention into some materials with high ability of donating electrons with the aim of increasing the activity of ammonia production under mild operating conditions. Thus, inorganic electrides, ionic materials in which the electrons serve as anions [49], were considered as a promising support for the active metal.

In this context, there are several electrides that have demonstrated a good performance acting as support for the ruthenium in the ammonia synthesis reaction as compared to 2nd-generation catalysts [26,50–52]. Among them, it is remarkable the work developed with the electride $[Ca_{24}Al_{28}O_{64}]^{4+}(e^-)_4$ (so called C12A7:e^-) [26,53]. The material obtained hydrothermally and latterly reduced at 1173 K (HT-C12A7:e^-) functions as a high efficiency catalyst for ammonia synthesis at atmospheric pressure and 615 K, with activities higher than the majority of conventional catalysts used. Further works demonstrated not only the well-known beneficial effect by the donation of electrons, but also the crucial role of the hydride ion mobility (caused by the reversible hydrogen storage capacity of the C12A7:e^-), which significantly increases the resistance to hydrogen poisoning [50,54]. In addition, and also important to note, it was demonstrated that the RDS was the formation of N-H_x species, since the apparent activation energy of Ru/HT-C12A7:e^- is lower than that corresponding to nitrogen dissociation step, in contrast to conventional catalysts.

On account of the importance of the electron mobility, a wide variety of supports have been tested during the last decade, with the objective of shifting the RDS from nitrogen dissociation towards the formation of NH_x species, most of them enhancing metal–support interactions via promoting electron donation between support and TM, since this strategy leads to globally better-performing materials. The majority of these supports, which constitute the basis of the 3rd-generation catalysts for ammonia synthesis, have the particular feature of permitting a continuous flow and high mobility of electrons by their capacity of location inside the structural cages of the material. Apart from the electride materials aforementioned, there are other types of supports, such as nitrides, amides and hydrides, whose performance for low-temperature NH_3 production have been studied.

On the one hand, the presence of nitrogen vacancies in nitride-derived materials, such as CeN or LaN, activates the adsorption of both N_2 and H_2, promoting the catalytic performance even for metals that, in principle, exhibit a low activity towards ammonia production like Ni. Moreover, pure CeN nanoparticles are able to generate NH_3 at 400 °C (250 $\mu mol \cdot g^{-1} \cdot h^{-1}$ and 1450 $\mu mol \cdot g^{-1} \cdot h^{-1}$ at 0.1 MPa and 0.9 MPa, respectively) which probes that presence of nitrogen vacancies (N_V) derived from the nitride species over the catalyst surface is able to activate both the hydrogen and the nitrogen even with no TM [55–57], since it works as a second active center for both nitrogen dissociation and hydrogen activation. On the other hand, alkaline earth amide materials are also proposed as effective supports for Ru (also for Co) [58]. In fact, Ru over Ba-doped $Ca(NH_2)_2$ have been demonstrated to be much more active for low-temperature NH_3 synthesis than such as benchmark catalyst as Cs-Ru/MgO (100-fold higher at 260 °C). Ru/Ba-$Ca(NH_2)_2$, which exhibits a core–shell configuration and a mesoporous structure with a large surface area, is able to suppress hydrogen poisoning and highly activate N_2 dissociation (in this case, the rate-limiting step is the formation of N-H_x species rather than N_2 cleavage) [37].

Further, the utilization of hydrides as support (details of hydride uses are discussed later in Section 2.2) has been demonstrated to be an effective strategy to enhance the formation of NH_3 under mild conditions. These kinds of materials, which are able to function as an electron and hydrogen donors, have been demonstrated to exhibit an excellent performance for ammonia production under mild conditions. Hydrides are also very versatile since they can be used as supports for many different TMs [59], which is one of the hardest handicaps of 2nd-generation ammonia synthesis catalysts. Furthermore, the internal structure of alkaline hydrides can be modified by the addition of some elements,

like fluorine, to increase the performance of the catalyst [60], which can enable conducting the ammonia synthesis reaction at temperatures as low as 100 °C.

A recent alternative to nitrides, hydrides, electrides and rare earth-based oxides can be found in the use of intermetallic compounds, whose understanding is of outstanding interest since they have promising properties in the field of catalyst design for many different applications and particularly for ammonia synthesis [24,61–63]. Intermetallic materials can be used indistinctly as supports for Ru or as a compact catalyst where the TM is located in the intermetallic matrix. On the one hand, when they are used as supports for Ru, intermetallics exhibit strong metal–support interactions (SMSI): work functions as low as 2.7, 3.2 and 3.2 eV were measured for LaCoSi, LaFeSi and LaMnSi, respectively, which are lower than those of pure La (3.5 eV), thus showing a surface electride-like behavior, which not only leads to a strong metal–support electron transfer, but also to an enhanced thermal stability of Ru. In addition, interactions between Ru and the TM from the support matrix (Co, Fe or Mn) also play an important role in the Ru dispersion and particle size, and in the global kinetic mechanism as well, given that the presence of a second active center is reported for these catalysts: while N_2 dissociation takes place on Ru sites, hydrogenation of N^* dissociated atoms to form NH_x species occurs over La surfaces [64]. On the other hand, single-phase LaRuSi intermetallic material was reported as an efficient catalyst for ammonia synthesis [65], since stronger chemical bonds between Ru and La are assumed to improve the electron transfer [63], whose activity is attributed to a dual behavior as an electride material, similarly to aforementioned intermetallic supports [24,61–63], as well as the reversible exchange between lattice hydride ions and anionic electrons that takes place [65], leading to an activation energy as low as 40.4 kJ·mol^{-1}. Further investigations concluded that (La,Ce,Pr)RuSi intermetallics show an excellent stability to air and moisture [66], with no relevant changes in ammonia synthesis rate after half a year of exposure to ambient air during the storage of the material. Moreover, a successful strategy to enhance those non-loaded intermetallic catalysts based on chemical etching was reported [66]. This process is based on the partial selective removal of the rare earth element over the surface, which leads to an increase in the number of Ru sites on the catalyst surface, as well as an increase in the surface area [66], leading to a 3-fold increase in the ammonia synthesis rate of LaRuSi after 5 h treatment with EDTA-2Na 5 mM. An additional simulation work based on first-principles calculations revealed that a key aspect to explain the high performance of LaRuSi is the presence of a bowl active site, composed by four surface La and one subsurface Si atoms, in which N_2 dissociation is driven by electrostatic and orbital interactions [67]. Furthermore, a highly versatile electron charge for the Si atom located in the bowl Si atom ensures an efficient NH_x species desorption by electrostatic repulsion, where the required energy for NH_x species formation is assumed to be independent of the N_2 adsorption energy, which accounts for an additional approach to circumvent the traditional relation between these two energies [68].

Most recent works on the thermocatalytic ammonia synthesis field are focused on enhancing the performance of materials by two different strategies: on the one hand, the use and understanding of rare earth-derived novel materials is on high demand, since they show different action mechanisms as ammonia synthesis supports, with a very versatile chemical nature [63,69,70]. It is to underline that catalysts based on ruthenium over lanthanum or cerium oxyhydrides [Ru/(Ce-La)$H_{3-2x}O_x$] prepared by solid-state reactions between pure hydride and oxide components show much superior ammonia synthesis activity and stability than their corresponding pure oxide and hydride precursors [71], with a maximum rate for x = 0.25 in case of lanthanum oxyhydrides and x = 0.75 for cerium oxyhydrides. The superior performance of these compounds is attributed to enhanced nitridation resistance over pure lanthanoid hydride species due to better hydrogen ion stabilization in the oxygen lattice, thus ensuring improved electron donation towards Ru.

On the other hand, modification and reorganizing of internal structures of catalysts combine for a rising approach for design of novel materials: first of all, regarding the ruthenium oxyhydrides aforementioned [71], very recent findings suggest that hydrogen diffusivity in the support can be unexpectedly increased by lowering the "x" value, i.e., lowering the available the number of sites for hydrogen diffusion, since knock-off mechanism takes place, which accounts for repulsive Coulombic interactions between H- ions inside the support matrix that are more significant than the generation of active vacancy sites [72]. This finding can lead to improved hydrogen activation and ammonia synthesis performance. Secondly, there are promising results involving the addition of dopant species inside the support matrix, as reported in the experimental study of CaFH solid solution as a stable support for Ru [60]. In this work, it was demonstrated that the addition of fluorine (F^-) to CaH_2 highly enhances the original hydride performance at low temperatures and pressures: the strategy of introducing F^- anions into a CaH_2 matrix led to an increase on the electron donation of the original material. The electron repulsion between H^- and F^- and the weakening of the Ca-H bond (Ca-F ionic bond is stronger than Ca-H one) enables reducing the temperature required for the H_2 migration, i.e., the work function of the support is reduced from 2.7 eV (CaH_2) to 2.2 eV (CaFH). As a result, the doping with F^- generated unprecedently high ammonia synthesis rates, with some measurable activity even at temperatures as low as 50 °C and a pressure of 1 bar (~50 μmol g^{-1} h^{-1}) and an activation energy of 20 kJ·mol^{-1} in the range 50–150 °C, which is approximately a half of that observed on other novel 3rd-generation catalysts [20]. As a third example, nano-powdered $LaNi_5$ as a compact alloy showed a superior performance than any other Ni-based catalyst and even comparable to some Ru-based materials [73]. The high activity of this material is attributed to the self-reorganization of the original homogeneous $LaNi_5$ matrix into a core–shell structure with a surface layer made of LaN under ammonia synthesis reaction conditions, which acts as a second active center for N_2 dissociation, while both LaN surface layer and Ni encapsulated in the core act as hydrogen activators, leading to an ammonia synthesis rate as high as 4500 μmol g^{-1} h^{-1} at 400 °C and 0.1 MPa. Finally, a very recent experimental study of a barium-doped Co/La_2O_3 catalyst revealed that TOF was increased more than 12 fold, under the same experimental conditions, as the reduction temperature of the catalyst was increased from 500 to 700 °C [74]. This enhancement was ascribed to the encapsulation of Co by a nano-fraction of $BaO\text{-}La_2O_3$ over the catalyst surface, whose formation process was enabled by the low melting point of the Ba precursor $Ba(OH)_2$, which could melt and migrate together with La_2O_3 towards the Co surface, thus creating a self-organized core–shell structure made by a core of Co and a low-crystalline layer of $BaO\text{-}La_2O_3$ containing voids, enabling reactant gases to break through it. The formation of this layer further enhances the metal–support electron transfer, leading to an improved ammonia synthesis performance.

To summarize, the evolution of the most relevant catalysts mentioned in this section is shown in the Table 1.

The ammonia synthesis reaction features are described in the Section 2.2, with a particular accent on the 3rd-generation catalysts.

2.2. Ammonia Synthesis Reaction Fundamentals

Theoretical investigations based on microkinetics with the application of the Sabatier principle [75] showed that there is a limit for the catalytic performance among the 3d and 4d TMs, given by the linear relation that exists between the activation energy for N_2 dissociation and the N≡N binding energy: the so-called scaling relation, i.e., there is a fixed TOF, which measures the ammonia synthesis rate for a specific TM, given by the scaling relation [76]. These studies resulted into the volcano plot showed in the Figure 1a, which predicts Fe, Ru and CoMo bimetallics as the most suitable TMs for ammonia synthesis catalysts.

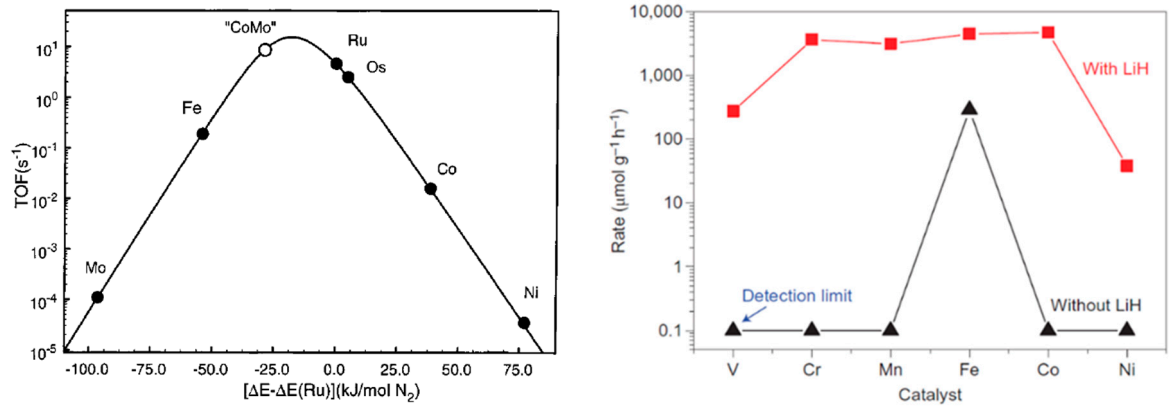

(**a**) (**b**)

Figure 1. Ammonia synthesis performance for different TMs. (**a**) Volcano plot derived from microkinetic studies by the application of the Sabatier principle. Reproduced with permission [68]. Copyright 2001, American Chemical Society, and (**b**) qualitative comparison of the performance of the TMs with and without the LiH supporting effect. Reproduced with permission [59]. Copyright 2017, Springer Nature.

However, the discovery of the stable electride C12A7:e^- demonstrated that the scaling relations can be broken by the addition of a second alternative active center to the material, apart from the TM [59], which is typically associated with the support. As mentioned in the Section 2.1, from this moment, the 3rd-generation catalysts arose, showing unprecedent high catalytic activities, derived from metal–support interactions [20]. Indeed, the most remarkable finding from these 3rd-generation catalysts is the positive circumvent of the scaling relation, which was a limitation for 2nd-generation catalysts. This phenomenon is represented in the Figure 1b [59], where the ammonia synthesis rate is shown when some TMs are supported on LiH (red line) and without LiH (black line), in contrast with the volcano plots derived from the application of the Sabatier principle (Figure 1a) [68]. As can be observed, a qualitative comparison shows that some TMs traditionally unsuitable for ammonia synthesis based on their low binding energy to dissociate N_2 can be used due to the promotional effect of the second active center originated by the presence of the support action.

As a result of the growing interest in the field of the metal–support interactions associated with the 3rd-generation catalysts, great efforts are being made by several groups in order to unravel the reaction mechanism and to understand the implication of the promotional effects.

2.3. Ammonia Synthesis Reaction Mechanism

The reaction mechanisms for the 3rd generation of catalysts have been analyzed [23,77]: two commonly accepted routes for ammonia synthesis have been suggested, as shown in the Table 2: the dissociative route, in which N_2 molecule is cleaved by the electronic promotion effect, i.e., the electron transfer from the TM to the π^* antibonding orbitals of N_2; and the associative route, in which the N_2 dissociation step is circumvented.

In the dissociative mechanism, the electrons encaged (*) in the support (in the form of bare electrons, H^- or other form, depending on the support nature) are transferred to the TM, thus increasing the electron density, which leads to an enhancement of the dissociation of N_2 (1–2). Moreover, the dissociation of H_2 takes place on the TM surfaces and the H^* adatoms spill over into the support (7–8). Then, the activated N* and H* species react to form ammonia (3–6).

In the associative mechanism, in contrast, N_2 direct dissociation is bypassed and molecular dinitrogen is directly hydrogenated by dissociated hydrogen to form ammonia (4–10).

Apart from the action of metal nitrides and other specific materials involving the associative mechanism, the dissociative route seems to be the predominant pathway for most 3rd-generation catalysts studied [21]. As aforementioned, the N_2 activation and

cleavage (1–2) is the RDS. Though operating at high temperatures and pressures was typically the way to boost ammonia synthesis, the use of electronic promoters has been the route to improve the RDS performance in terms of operating under mild conditions [20,21].

Regarding the ammonia synthesis mechanism, high experimental effort has been put towards determining the influence of the metal–support interactions in some catalysts and their electronic promotion, including the roles of H and N layers for hydrides and nitrides, respectively. In addition to the influence of the particular N and H layers on the associative pathway, the global scheme is similar for different supports and corresponds to the dissociative mechanism. In the Figure 2, a scheme for the ammonia synthesis mechanism is shown for catalysts with different configurations: in the case of Ru/C12A7:e^- (electride, Figure 2a) [26] and TM/LiH (Hydride, Figure 2c) [59], the reaction is prone to follow a dissociative adsorption pathway for N_2, whose cleavage is enhanced by the electronic promotion from the support, in the form of bare electrons (C12A7:e^-) or H^- (TM/LiH), respectively. This electronic promotion is explained in detail in the Section 2.4. However, for the Ni/CeN catalyst (nitride, Figure 2b) [56], N_2 reacts following an associative mechanism through its interaction with the N* layer of the support, which reacts with the dissociated H* to form ammonia. In addition, there are some complex materials, such as the TM/$BaCeO_{3-x}N_yH_z$ (rare earth perovskites oxy-nitride hydrides, Figure 2d), which make the two possible routes feasible [78].

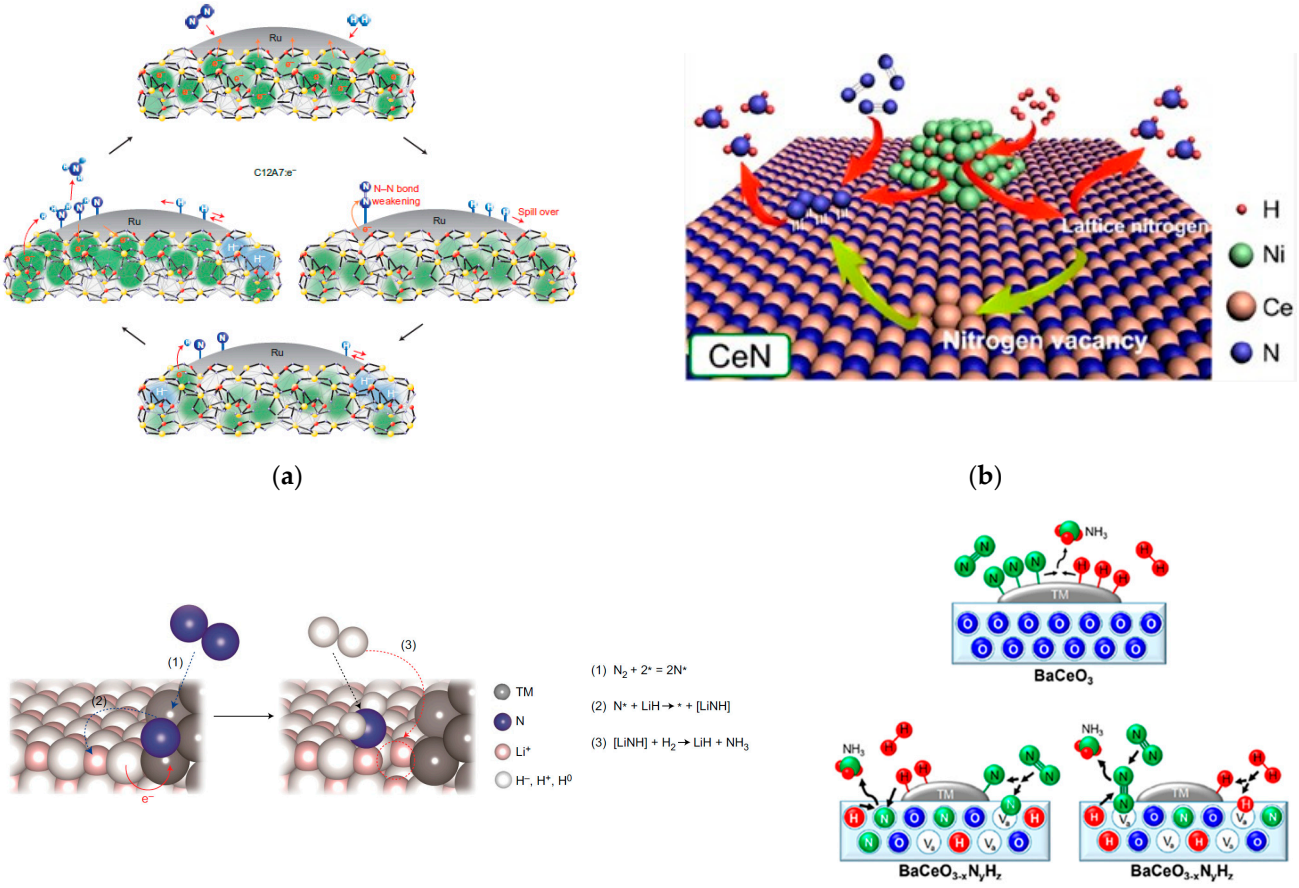

Figure 2. Ammonia synthesis mechanism scheme for (**a**) Ru/C12A7:e^- (electride). Reproduced with permission [26]. Copyright 2012, Springer Nature, (**b**) Ni/CeN (nitride). Reproduced with permission [56]. Copyright 2020, American Chemical Society, (**c**) TM-LiH (hydride). Reproduced with permission [59]. Copyright 2016, Springer Nature, and (**d**) $CaCeO_{3-x}N_yH_z$ (perovskite oxy-nitride hydride). Reproduced with permission [78]. Copyright 2019, American Chemical Society.

Significant differences can be found in the particular fundamentals for each support type, as shown in the Figure 2. However, any catalyst developed to date follows one of the catalytic mechanisms shown in the Table 2, even those which are not promoted by the action of second active centers, such as alkali/alkaline oxides or activated carbons. Oxygen vacancies, which arise as a consequence of the reversible reducibility of rare earth oxides and some particular surface electrides [63], lead to the promotion of electron transfer towards the TM, which drives nitrogen dissociation following the dissociative pathway, greatly outperforming traditional 2nd-generation catalysts kinetic mechanisms. Alkali, alkaline hydrides and their derivates perform on a similar way, since hydride ions can be exchanged by electrons which also boost the dissociative cleavage of dinitrogen. However, in this case, the transfer of electrons in the form of H^- anions makes hydrides attractive since they act as second active centers for hydrogen dissociation [20]. A combination of oxygen vacancies and reversible H^- donation makes oxyhydrides a promising branch of catalysts to consider for their high performance [71]. As aforementioned, nitrides typically follow the associative route: a reversible uptake of N* towards the nitride surface boost direct nitrogen reaction with dissociated hydrogen, which globally enables the catalyst to circumvent the nitrogen dissociation step, as demonstrated in several works [56,73]. In this case, the driving force for ammonia synthesis is directly related to the formation of NH_x species. According to these fundamentals, the nitride second active center for nitrogen dissociation enables the use of non-noble TMs with reasonable performances, which represents an advantage to most catalysts driven by the dissociative route, since electron transfer is not usually applicable to these materials.

It is noteworthy that novel technologies in addition to traditional thermochemical catalysis, such as photothermal or electrochemical catalysis, are ruled by either associative or dissociative mechanisms. As an example, in photothermal synthesis of ammonia using Ni/TiO_2 as catalyst, solar light activates and dissociate nitrogen by its interaction with photoelectrons trapped into the generated oxygen vacancies, while hydrogen is dissociated by the thermocatalytic action of Ni [12]. Therefore, although the driving force is photocatalytic action, the global mechanism follows the dissociative pathway. In contrast, chemical looping enables carrying out nitrogen and hydrogen cleavage steps independently. Ammonia synthesis materials used in chemical looping, such as lithium–palladium hydrides [7], act as intermediate cyclic carriers, i.e., the complex system Li-Pd-H leads to fix dinitrogen following a dissociative route, which is stored in the form of Li_2NH. This carrier is then hydrogenated to produce ammonia.

There is another key positive effect of the metal–support electronic promotion, which is the reduction in hydrogen poisoning, typical from 2nd-generation Ru-based catalysts. In that case, the dissociative adsorption of H_2 competes with the N_2 adsorption and cleavage and thus the reaction orders with respect to H_2 are usually negative, due to the accumulation of hydrogen adsorbed species inside the catalyst active sites. This phenomenon is more remarkable at higher pressures, which represents a challenge for the industrial operation of the Haber–Bosch system [5,59]. However, the electron donation from the support to the TM ensures a continuous supply of H^* by a reversible hydrogen migration [18,20,21,79], preventing hydrogen poisoning. Furthermore, the presence of H^- anions in the support from hydrides and their derivates is interesting since it gives a simultaneous backup of electrons and H^- (thus ensuring positive H_2 reaction orders) [59,80,81]. The impact on the electron transfer between support and TM in terms of hydrogen poisoning is shown in the Figure 3, were ammonia synthesis performance as a function of the operating pressure from 1 to 10 bar is plotted for Ru/C12A7:e^- (3rd generation) and Cs-Ru/MgO (2nd generation), at 360 °C [26]. In the case of Ru-Cs/MgO (black line), there is not a significant effect of increasing the operating pressure, as long as hydrogen poisoning suppresses its thermochemical and kinetic benefits. However, the ammonia synthesis rate increases with pressure for the Ru/C12A7:e^- (red line), since hydrogen poisoning is circumvented.

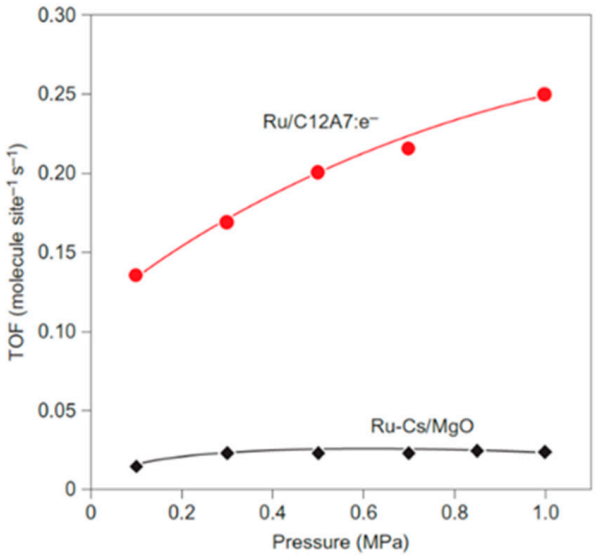

Figure 3. TOFs for Ru/C12A7:e$^-$ and Ru-Cs/MgO at 360 °C Reproduced with permission [26]. Copyright 2012, Springer Nature.

Another relevant aspect of the 3rd-generation catalysts resides in their application, since electron donation has been demonstrated to provide a high activity for ammonia decomposition to some catalysts, such as Ru/CeO_2 [82]. A reversible production of green ammonia has an outstanding potential, especially considering ammonia as a carbon neutral high-density fuel which can be directly used in fuel cells [83]. Furthermore, there are another environmental applications in which electron transfer plays a key role, such as CO_2 upgrading, in which oxygen vacancies from CeO_2 promote the thermochemical methanation process, catalyzed by Ru/CeO_2 [84].

As a global result of the phenomenology explained up to this point, the ammonia synthesis rate of the 3rd-generation ammonia synthesis catalysts is superior by at least one order of magnitude to 2nd-generation Ru-based catalyst [20,21,79] and their activation energies much lower (40–60 kJ mol^{-1} and 80–100 kJ mol^{-1}, respectively).

2.4. Metal—Support Interactions: Electron Transfer

The fundamentals behind the electron transfer between supports and TMs have been slightly explained and contrasted with the wide experimental background on the 3rd-generation ammonia synthesis catalysts. However, some works have recently been published in order to clear out the insights of metal–support interactions.

Particularly, a theoretical analysis of ammonia synthesis was performed, based on the application of DFT and microkinetic modelling for the Ru/Ca_2NH catalyst at atmospheric pressure and a temperature range of 300–400 °C [77]. The TOFs were simulated for every elementary step and contrasted with the experimental work performed for the same material [50], assuming the dissociative route as the correct pathway. The results shown in the Figure 4 demonstrated that the RDS is shifted from the N_2 dissociation towards NH_x species formation, which is in accordance with previous experimental works [20,85].

More precisely, the RDS was demonstrated to be given by the reaction of the dissociated N_2 and the hydrogen from the H lattice of the support in the TM–support interface through an associative mechanism, which is consistent with previous findings for other hydride catalysts [20,85].

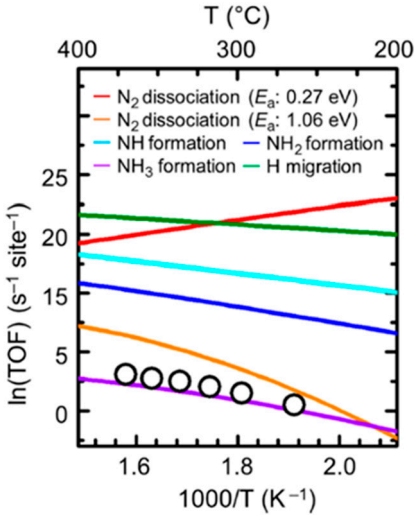

Figure 4. Comparison of ammonia synthesis rate for every elementary step (Table 2) and experimental results (white dots) for the Ru/Ca_2NH catalyst at 1 bar, as a function of temperature [77].

In addition, the key aspects of the electron transfer among TM and support for electride-like catalysts, as well as the support requirements for an efficient electronic promotion have been recently pointed out [86]: the difference between the work functions (the required energy to move an electron from the Fermi level to the void, i.e., the minimum energy to extract an electron from a solid) of the TM (4.2–5.1 eV) and support (2.1–3.0 eV) generates an electron transfer from the latter to the former and active sites on the structure are created. Therefore, it seems that the higher the difference in the work functions of TM and support, the better the electronic promotion.

The activation energy for the Ru/C12A7:e^- catalyst, as well as ammonia synthesis performance as a function of the electron concentration in the support are shown in the Figure 5 [86]: for the original material ($12CaO{\cdot}7Al_2O_3$), which corresponds to electron concentrations lower than 0.5×10^{21} cm^{-3}, the activation energy is similar to that found for 2nd-generation catalysts. However, as the electrons are doped on the material and their concentration is increased beyond 1×10^{21} cm^{-3}, the support acquires its electride behavior, thus leading a dramatic increase on its performance, due to the enhancement of the N_2 dissociation, which explains the previously discussed shift on the ammonia synthesis RDS [20,77,85].

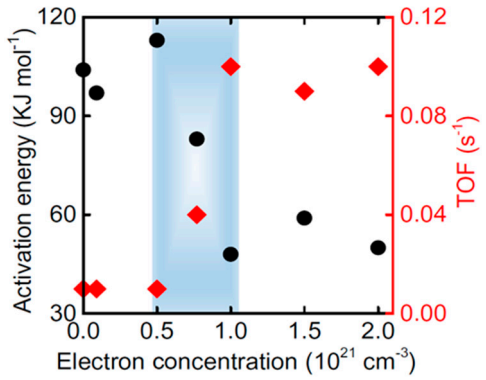

Figure 5. Ammonia synthesis activation energy and TOF as a function of the support electron concentration, for the Ru/C12A7:e^- catalyst. Reproduced with permission [86]. Copyright 2021, Springer Nature.

Furthermore, in the particular case of the supports based on hydrides, the deposition of the TM on the hydride support creates TM–hydride bonds, which gives an electride-like nature to some originally non-electride materials. This property, which is promoted by the formation of H^- at the TM–support interface, originates the so-called surface electrides [79]. Surface electrides such as Ru/Ca_2NH and Ru/Sr_2NH show very high ammonia yields at atmospheric pressure and temperatures below 300 °C, comparable with those of Ru/C12A7:e^- [87] and their activity is attributed to the above-mentioned surface electride nature.

In addition, a simple analysis of the electronic promotion of catalysts and their performance can be performed based on work function gaps between TM and support: for example, regarding the analysis developed about the performance of different 3d TMs (from the groups 6–9) supported on LiH [59], their ammonia synthesis rate is ordered as follows: Co~Fe > Cr > Mn, which matches with the order of the work functions of these TMs (Co: 5.0 eV, Fe: 4.8 eV, Cr: 4.5 eV, Mn: 4.1 eV).

In contrast, from an experimental study about the performance of $CaCN_2$ as a support for Ru [88], it was concluded that the ammonia synthesis rate of $CaCN_2$ is slightly higher than that of other high performance electrides such as Ca_2N and C12A7:e^-, even considering the higher work function of $CaCN_2$ (3.95 eV) compared with Ca_2N and C12A7:e^- (2.6 and 2.4 eV, respectively). In this case, the higher activity of the Ru/$CaCN_2$ is attributed to a better dispersion of Ru nanoparticles on the support.

Moreover, the activities of CeH_{2+x}, LaH_{2+x} and YH_{2+x} when supporting Ru are 1.63, 1.27 and 0.56 mmol g^{-1} h^{-1} at 300 °C and 1 bar, respectively [89], whose order does not correspond to the former metals work function sorting (2.9 eV for Ce, 3.5 eV for La and 3.1 eV for Y).

In addition, there are many other aspects influencing the performance of surface electride catalysts: for example, the ammonia synthesis rate varies approximately 1 order of magnitude for different Ru precursors when supporting it on Ru/Ba-Ca$(NH_2)_2$ by impregnation of Ba and Ca with liquid NH_3 at −40 °C [37], as shown in the Figure 6.

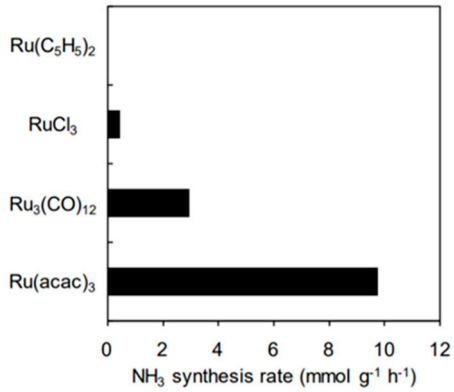

Figure 6. Ammonia synthesis rate for different Ru precursors supported on Ba-Ca$(NH_2)_2$, at 9 bar and 300 °C. Reproduced with permission [37]. Copyright 2018, Wiley Online Library.

Apart from this, the recently synthesized Ru/CaFH solid solution has 1 order of magnitude higher performance than any other catalyst tested at atmospheric pressure [37,43], but the estimated work function of CaFH is 2.2 eV, which is similar to that of C12A7:e^- (2.4 eV) and even higher than that of $Ca(NH_2)_2$ (2.1 eV). Therefore, the F^- repulsion effect and the superior electron donation from the CaFH cannot be solely explained by a work function analysis, but considering alternative phenomenology, as reported in Section 2.1.

Table 1. Classification and industrial progress of catalysts for ammonia synthesis.

Classification	Catalysts Nature	Catalysts Examples	Industrial Applications [1]	Ref
1st-generation catalysts	Iron-based (magnetite) Promoted iron-based	Fe/Al_2O_3 K-Fe/Al_2O_3-CaO	- Haber–Bosch process	[21] [20,21,28,29]
2nd-generation catalysts	Ruthenium on carbon Doubly promoted ruthenium on non-functional supports	Ru/C (Ba-Cs)-Ru/MgO (Ba-Cs)-Ru/C	- KAAP process	[22] [22]
3rd-generation catalysts	Electrides	Ru/C12A7:e^-, Ru/Ca2N:e^-	-	[26,85]
	Rare earth oxides	Ru/CeO_2, Ru/PrO, Ba-Co/La_2O_3		[44,74,90]
	Hydrides	Ru/LiH, Ru/Ca_2NH, Ru/CaFH		[59,60,87]
	Nitrides	Co_3Mo_3N, Ni/CeN		[56,91]
	Oxyhydrides (nitrides)	Ru/$CeH_{3-2x}O_x$, $BaCeO_{3-x}N_yH_z$		[37,71]
	Intermetallics	LaRuSi, CeRuSi, LaCoSi, $LaNi_5$		[66,67,73,92]

[1.] Relevant industrial scaling was only carried out in the Haber–Bosch (K-Fe/Al2O3-CaO) and KAAP ([Ba-Cs]-Ru/MgO, [Ba-Cs]-Ru/C) processes.

Table 2. Dissociative and associative mechanisms for ammonia synthesis [23].

	Dissociative Mechanism	Associative Mechanism
(1)	N_2 (g) + * → N_2*	N_2 (g) + * → N_2*
(2)	N_2* + * → 2N*	H_2 (g) + * → H_2*
(3)	N* + H* → NH* + *	H_2* → 2H*
(4)	NH* + H* → NH_2* + *	N_2* + 2H* → N_2H*
(5)	NH_2* + H* → NH_3* + *	N_2H* + H* → N_2H_2*
(6)	NH_3* → NH_3 (g) + *	N_2H_2* + H* → N_2H_3*
(7)	H_2 (g) + * → H_2*	N_2H_3* + H* → N_2H_4*
(8)	H_2* → 2H*	N_2H_4* → 2NH_2*
(9)		NH_2* + H* → NH_3*
(10)		NH_3* → NH_3 (g) + *

3. Discussion

Considering the background on the TM–support interactions and, particularly, the electron transfer issue, the search for suitable supports with enhanced electron donation capacity seems to be a reasonable strategy for the design of new 3rd-generation catalysts for ammonia synthesis. As explained in the previous sections, several works report a high interest to carefully consider the electronic promotion obtained when surface electrides are used as supports, given their capacity to break the scaling relation for the N_2 dissociation, which is as limit for the kinetic performance of 2nd-generation catalysts, opening a window for exploring different new formulas [20].

Some works presented in this review support their experimental investigations with simulations, mainly based on DFT, which reinforce the improvements of 3rd-generation catalysts in terms of enhanced kinetic mechanisms. For instance, the experimental data obtained for Ru/Ca_2NH catalysts was used to obtain microkinetic information regarding the reaction processes and mechanisms of ammonia synthesis, by means of DFT modelling [77]. The conclusions of this study led to understanding how nitrogen dissociation is promoted by the electron promotion of the TM from the support, as well as to determining the role of the hydrogen lattice (hydrogen vacancies) as a second active center for hydrogen dissociation. Interestingly, the RDS was identified as the NH_3 formation step, with a close match between the experimental results and the DFT simulation.

According to the background state of the art, a simple analysis of the work functions of supports could be a good criterion for the selection and design of new materials, as this property has been pointed out by Hosono and coworkers as a crucial parameter for electride materials [79].

However, as analyzed in Section 2.4., there are many other aspects with a strong influence on the performance of 3rd-generation catalysts for ammonia synthesis in addition to the electronic promotion in terms of the work function gap between TM and support, such as the surface properties of the catalyst and the TM dispersion on the support, the materials and methods for the synthesis of the catalyst, the operating reaction conditions or the addition of secondary species into the support, the tuning of internal structures or structural configurations in intermetallic materials, thus the work function gap between TM and support cannot solely explain differences between materials. Nevertheless, most supports that ensure the behavior of surface electride to catalysts have work functions in the range 2.1–2.4 eV [79]. Therefore, the use of low work function supports seems to be a reasonable first approach to screen new materials.

To summarize all the ideas presented in this work, a general scheme about the action of the 3rd-generation catalysts is shown in the Figure 7, which can be used as a conceptual approach for the requirements of new materials. An approach for general dissociative mechanism-like materials is presented in Figure 7a, while a scheme for catalysts that follow the associative route is shown in Figure 7b.

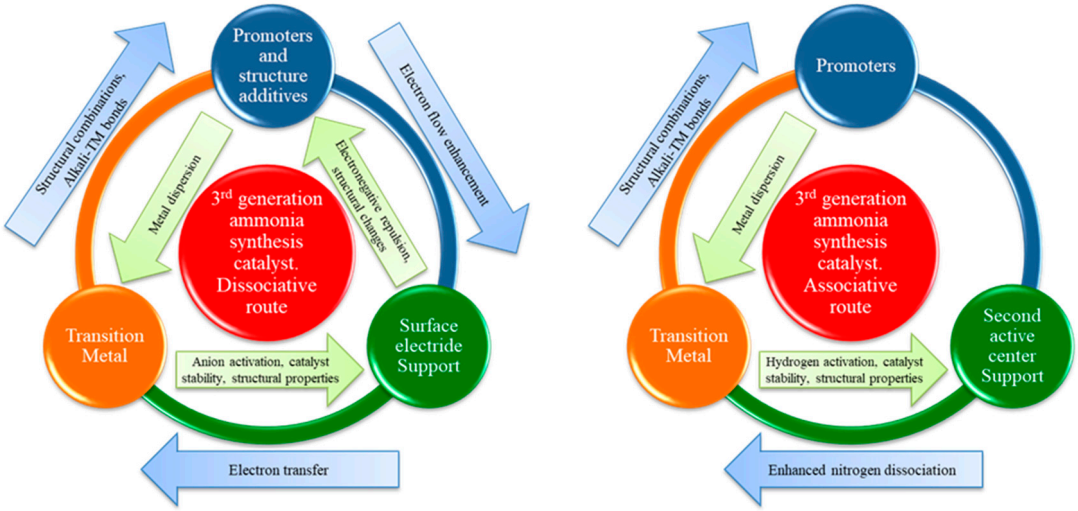

Figure 7. Conceptual approach for the requirements of new 3rd-generation catalysts for the (**a**) dissociative route and (**b**) associative route processes.

4. Conclusions

The present study highlights the fundamentals of thermocatalytic ammonia synthesis in terms of the reaction mechanisms, as well as the historical evolution of the 1st- and 2nd-generation ammonia synthesis catalysts, with a particular emphasis on the metal–support interactions for 3rd-generation catalysts.

For the electride-like supports, N_2 cleavage is no longer the RDS, but there is a switch towards NH_x species formation and continuous free electrons migration prevents hydrogen poisoning.

Surface electrides, particularly hydrides and amines, are promising supports under mild conditions to date, since the deposition of TMs on them ensures a continuous supply of both electrons and H^-, with activation energies in the range 20–66 kJ·mol^{-1}. Furthermore, the addition of secondary species such as electronegative and basic elements seems to provide surface electrides a superior performance. In addition, internal structure tuning of

novel materials and the coupling between structure versatility and stability of intermetallic compounds are promising approaches for high performance materials design.

However, many other factors influence ammonia synthesis, like TM precursor forms, the deposition process, TM loading, catalyst structural properties and operating conditions, thus a direct correlation between the electron donation of materials described by the simple form of the work functions and their performance is not truly representative, although it leads to an initial approach for the search for more efficient ammonia synthesis catalysts.

Finally, although there have been significant advances in recent decades in terms of ammonia synthesis performance and kinetic mechanisms for the new catalysts developed, there are several constraints to be solved in order to achieve technological implementation. For instance, the design of non-noble and stable materials, since some of them, such as hydrides and nitrides, are not stable under ambient conditions and handling under inert atmospheres is required. The search for a reasonable formula to couple ammonia synthesis with renewables, avoiding transient influences, should also be addressed. In addition, simple and scalable synthesis procedures are still necessary, since most novel catalysts are produced at a small scale following complex methodologies, which can hinder the industrial production of these materials.

Author Contributions: Conceptualization, J.C.S.-R. and M.A.D.-P. resources, J.C.S.-R.; writing—original draft preparation, J.A.-C.; writing—review and editing, M.A.L.-A. and M.A.D.-P.; funding acquisition, J.C.S.-R. All authors have read and agreed to the published version of the manuscript.

Funding: This research was funded by Universidad Loyola Andalucía through the project "Design and screening of catalysts for the synthesis of ammonia at mild temperature and pressure conditions". The independence of the institution enables us to be completely unbiased, so the work has been developed following exclusive scientific criteria. No private companies have participated in this work.

Data Availability Statement: No new data were created.

Conflicts of Interest: The authors declare no conflict of interest.

References

1. Alfa Laval HHTVSG. *Ammonfuel—An Industrial View of Ammonia as a Marine Fuel*; Alfa Laval HHTVSG: Nuremberg, Germany, 2020.
2. Ammonia Global Market Report 2023. Available online: https://www.reportlinker.com/p06323489/Ammonia-Global-Market-Report.html?utm_source=GNW (accessed on 20 June 2023).
3. Smith, C.; Hill, A.K.; Torrente-Murciano, L. Current and future role of Haber-Bosch ammonia in a carbon-free energy landscape. *Energy Environ. Sci.* **2020**, *13*, 331–344. [CrossRef]
4. Reese, M.; Marquart, C.; Malmali, M.; Wagner, K.; Buchanan, E.; McCormick, A.; Cussler, E.L. Performance of a Small-Scale Haber Process. *Ind. Eng. Chem. Res.* **2016**, *55*, 3742–3750. [CrossRef]
5. Wang, Q.; Guo, J.; Chen, P. Recent progress towards mild-condition ammonia synthesis. *J. Energy Chem.* **2019**, *36*, 25–36. [CrossRef]
6. Rouwenhorst, K.H.R.; Van der Ham, A.G.J.; Lefferts, L. Beyond Haber-Bosch: The renaissance of the Claude process. *Int. J. Hydrog. Energy* **2021**, *46*, 21566–21579. [CrossRef]
7. Yan, H.; Gao, W.; Wang, Q.; Guan, Y.; Feng, S.; Wu, H.; Guo, Q.; Cao, H.; Guo, J.; Chen, P. Lithium Palladium Hydride Promotes Chemical Looping Ammonia Synthesis Mediated by Lithium Imide and Hydride. *J. Phys. Chem. C* **2021**, *125*, 6716–6722. [CrossRef]
8. Moon, J.; Cheng, Y.; Daemen, L.; Novak, E.; Ramirez-Cuesta, A.J.; Wu, Z. On the Structural Transformation of Ni/BaH_2 During a N_2-H_2 Chemical Looping Process for Ammonia Synthesis: A Joint In Situ Inelastic Neutron Scattering and First-Principles Simulation Study. *Top. Catal.* **2021**, *64*, 685–692. [CrossRef]
9. Li, L.; Zhang, T.; Cai, J.; Cai, H.; Ni, J.; Lin, B.; Lin, J.; Wang, X.; Zheng, L.; Au, C.T.; et al. Operando spectroscopic and isotopic-label-directed observation of LaN-promoted Ru/ZrH_2 catalyst for ammonia synthesis via associative and chemical looping route. *J. Catal.* **2020**, *389*, 218–228. [CrossRef]
10. Zhao, Y.; Zhao, Y.; Shi, R.; Wang, B.; Waterhouse, G.I.; Wu, L.Z.; Tung, C.H.; Zhang, T. Tuning Oxygen Vacancies in Ultrathin TiO_2 Nanosheets to Boost Photocatalytic Nitrogen Fixation up to 700 nm. *Adv. Mater.* **2019**, *31*, 1806482. [CrossRef]
11. Medford, A.J.; Hatzell, M.C. Photon-Driven Nitrogen Fixation: Current Progress, Thermodynamic Considerations, and Future Outlook. *ACS Catal.* **2017**, *7*, 2624–2643. [CrossRef]

12. Wang, S.; Yu, W.; Xu, S.; Han, K.; Wang, F. Ammonia from Photothermal N_2Hydrogenation over Ni/TiO_2Catalysts under Mild Conditions. *ACS Sustain. Chem. Eng.* **2022**, *10*, 115–123. [CrossRef]
13. Hong, J.; Prawer, S.; Murphy, A.B. Plasma Catalysis as an Alternative Route for Ammonia Production: Status, Mechanisms, and Prospects for Progress. *ACS Sustain. Chem. Eng.* **2018**, *6*, 15–31. [CrossRef]
14. Carreon, M.L. Plasma catalytic ammonia synthesis: State of the art and future directions. *J. Phys. D Appl. Phys.* **2019**, *52*, 483001. [CrossRef]
15. Li, Y.; Wang, H.; Priest, C.; Li, S.; Xu, P.; Wu, G. Advanced Electrocatalysis for Energy and Environmental Sustainability via Water and Nitrogen Reactions. *Adv. Mater.* **2021**, *33*, 2000381. [CrossRef]
16. McEnaney, J.M.; Singh, A.R.; Schwalbe, J.A.; Kibsgaard, J.; Lin, J.C.; Cargnello, M.; Jaramillo, T.F.; Nørskov, J.K. Ammonia synthesis from N_2 and H_2O using a lithium cycling electrification strategy at atmospheric pressure. *Energy Environ. Sci.* **2017**, *10*, 1621–1630. [CrossRef]
17. Reichle, S.; Felderhoff, M.; Schüth, F. Mechanocatalytic Room-Temperature Synthesis of Ammonia from Its Elements Down to Atmospheric Pressure. *Angew. Chem.—Int. Ed.* **2021**, *60*, 26385–26389. [CrossRef]
18. Chang, F.; Gao, W.; Guo, J.; Chen, P. Emerging Materials and Methods toward Ammonia-Based Energy Storage and Conversion. *Adv. Mater.* **2021**, *33*, 2005721. [CrossRef]
19. Gao, W.; Guo, J.; Chen, P. Hydrides, Amides and Imides Mediated Ammonia Synthesis and Decomposition. *Chin. J. Chem.* **2019**, *37*, 442–451. [CrossRef]
20. Marakatti, V.S.; Gaigneaux, E.M. Recent Advances in Heterogeneous Catalysis for Ammonia Synthesis. *ChemCatChem* **2020**, *12*, 5838–5857. [CrossRef]
21. Humphreys, J.; Lan, R.; Tao, S. Development and Recent Progress on Ammonia Synthesis Catalysts for Haber–Bosch Process. *Adv. Energy Sustain. Res.* **2021**, *2*, 2000043. [CrossRef]
22. Saadatjou, N.; Jafari, A.; Sahebdelfar, S. Ruthenium Nanocatalysts for Ammonia Synthesis: A Review. *Chem. Eng. Commun.* **2015**, *202*, 420–448. [CrossRef]
23. Li, L.; Zhang, T.; Zhou, Y.; Wang, X.; Au, C.-T.; Jiang, L. Review on catalytic roles of rare earth elements in ammonia synthesis: Development and perspective. *J. Rare Earths* **2022**, *40*, 1–10. [CrossRef]
24. Nakaya, Y.; Furukawa, S. Catalysis of Alloys: Classification, Principles, and Design for a Variety of Materials and Reactions. *Chem. Rev.* **2022**, *123*, 5859–5947. [CrossRef] [PubMed]
25. Guo, J.; Chen, P. Interplay of Alkali, Transition Metals, Nitrogen, and Hydrogen in Ammonia Synthesis and Decomposition Reactions. *Acc. Chem. Res.* **2021**, *54*, 2434–2444. [CrossRef] [PubMed]
26. Kitano, M.; Inoue, Y.; Yamazaki, Y.; Hayashi, F.; Kanbara, S.; Matsuishi, S.; Yokoyama, T.; Kim, S.W.; Hara, M.; Hosono, H. Ammonia synthesis using a stable electride as an electron donor and reversible hydrogen store. *Nat. Chem.* **2012**, *4*, 934–940. [CrossRef]
27. Ojelade, O.A.; Zaman, S.F. Ammonia decomposition for hydrogen production: A thermodynamic study. *Chem. Pap.* **2021**, *75*, 57–65. [CrossRef]
28. Ertl, G. Surface Science and Catalysis—Studies on the Mechanism of Ammonia Synthesis: The P. *H. Emmett Award Address. Catal. Rev.* **1980**, *21*, 201–223. [CrossRef]
29. Almquist, J.A.; Crittenden, E.D. A Study of Pure-Iron and Promoted-iron Catalysts for Ammonia Synthesis. *Ind. Eng. Chem.* **1926**, *18*, 1307–1309. [CrossRef]
30. Aika, K.-I. Role of alkali promoter in ammonia synthesis over ruthenium catalysts—Effect on reaction mechanism. *Catal. Today* **2017**, *286*, 14–20. [CrossRef]
31. García-García, F.R.; Guerrero-Ruiz, A.; Rodríguez-Ramos, I. Role of B5-Type Sites in Ru Catalysts used for the NH_3 Decomposition Reaction. *Top. Catal.* **2009**, *52*, 758–764. [CrossRef]
32. van Hardeveld, R.; van Montfoort, A. The influence of crystallite size on the adsorption of molecular nitrogen on nickel, palladium and platinum: An infrared and electron-microscopic study. *Surf. Sci.* **1966**, *4*, 396–430. [CrossRef]
33. Raróg-Pilecka, W.; Szmigiel, D.; Kowalczyk, Z.; Jodzis, S.; Zielinski, J. Ammonia decomposition over the carbon-based ruthenium catalyst promoted with barium or cesium. *J. Catal.* **2003**, *218*, 465–469. [CrossRef]
34. Osozawa, M.; Hori, A.; Fukai, K.; Honma, T.; Oshima, K.; Satokawa, S. Improvement in ammonia synthesis activity on ruthenium catalyst using ceria support modified a large amount of cesium promoter. *Int. J. Hydrog. Energy* **2022**, *47*, 2433–2441. [CrossRef]
35. Zhang, Z.; Karakaya, C.; Kee, R.J.; Way, J.D.; Wolden, C.A. Barium-Promoted Ruthenium Catalysts on Yittria-Stabilized Zirconia Supports for Ammonia Synthesis. *ACS Sustain. Chem. Eng.* **2019**, *7*, 18038–18047. [CrossRef]
36. Nishi, M.; Chen, S.Y.; Takagi, H. Mild ammonia synthesis over Ba-promoted Ru/MPC catalysts: Effects of the Ba/Ru ratio and the mesoporous structure. *Catalysts* **2019**, *9*, 480. [CrossRef]
37. Kitano, M.; Inoue, Y.; Sasase, M.; Kishida, K.; Kobayashi, Y.; Nishiyama, K.; Tada, T.; Kawamura, S.; Yokoyama, T.; Hara, M.; et al. Self-organized Ruthenium-Barium Core-Shell Nanoparticles on a Mesoporous Calcium Amide Matrix for Efficient Low-Temperature Ammonia Synthesis. *Angew. Chem.* **2018**, *130*, 2678–2682. [CrossRef]
38. Guraya, M.; Sprenger, S.; Rarog-Pilecka, W.; Szmigiel, D.; Kowalczyk, Z.; Muhler, M. The effect of promoters on the electronic structure of ruthenium catalysts supported on carbon. *Appl. Surf. Sci.* **2004**, *238*, 77–81. [CrossRef]

39. Raróg-Pilecka, W.; Miśkiewicz, E.; Szmigiel, D.; Kowalczyk, Z. Structure sensitivity of ammonia synthesis over promoted ruthenium catalysts supported on graphitised carbon. *J. Catal.* **2005**, *231*, 11–19. [CrossRef]
40. Aika, K.-I.; Hori, H.; Ozaki, A. Activation of nitrogen by alkali metal promoted transition metal I. Ammonia synthesis over ruthenium promoted by alkali metal. *J. Catal.* **1972**, *27*, 424–431. [CrossRef]
41. Seetharamulu, P.; Hari Prasad Reddy, K.; Padmasri, A.H.; Rama Rao, K.S.; David Raju, B. Role of promoters on highly active nano-Ru catalyst supported on Mg–Al hydrotalcite precursor for the synthesis of ammonia. *Catal. Today* **2009**, *141*, 94–98. [CrossRef]
42. Wang, Y.; Wildfire, C.; Khan, T.S.; Shekhawat, D.; Hu, J.; Tavadze, P.; Quiñones-Fernández, R.; Moreno, S. Effects of support and promoter on Ru catalyst activity in microwave-assisted ammonia synthesis. *Chem. Eng. J.* **2021**, *425*, 130546. [CrossRef]
43. Miyahara, S.I.; Sato, K.; Kawano, Y.; Imamura, K.; Ogura, Y.; Tsujimaru, K.; Nagaoka, K. Ammonia synthesis over lanthanoid oxide–supported ruthenium catalysts. *Catal. Today* **2021**, *376*, 36–40. [CrossRef]
44. Lin, B.; Liu, Y.; Heng, L.; Wang, X.; Ni, J.; Lin, J.; Jiang, L. Morphology Effect of Ceria on the Catalytic Performances of Ru/CeO_2 Catalysts for Ammonia Synthesis. *Ind. Eng. Chem. Res.* **2018**, *57*, 9127–9135. [CrossRef]
45. Zhang, L.; Lin, J.; Ni, J.; Wang, R.; Wei, K. Highly efficient Ru/Sm_2O_3-CeO_2 catalyst for ammonia synthesis. *Catal. Commun.* **2011**, *15*, 23–26. [CrossRef]
46. Li, H.; Shang, J.; Ai, Z.; Zhang, L. Efficient visible light nitrogen fixation with BiOBr nanosheets of oxygen vacancies on the exposed {001} Facets. *J. Am. Chem. Soc.* **2015**, *137*, 6393–6399. [CrossRef]
47. Hirakawa, H.; Hashimoto, M.; Shiraishi, Y.; Hirai, T. Photocatalytic Conversion of Nitrogen to Ammonia with Water on Surface Oxygen Vacancies of Titanium Dioxide. *J. Am. Chem. Soc.* **2017**, *139*, 10929–10936. [CrossRef]
48. Li, C.; Wang, T.; Zhao, Z.J.; Yang, W.; Li, J.F.; Li, A.; Yang, Z.; Ozin, G.A.; Gong, J. Promoted Fixation of Molecular Nitrogen with Surface Oxygen Vacancies on Plasmon-Enhanced TiO_2 Photoelectrodes. *Angew. Chem. Int. Ed.* **2018**, *57*, 5278–5282. [CrossRef]
49. Dye, J.L. Electrons as anions. *Science* **2003**, *301*, 607–608. [CrossRef]
50. Kitano, M.; Inoue, Y.; Ishikawa, H.; Yamagata, K.; Nakao, T.; Tada, T.; Matsuishi, S.; Yokoyama, T.; Hara, M.; Hosono, H. Essential role of hydride ion in ruthenium-based ammonia synthesis catalysts. *Chem. Sci.* **2016**, *7*, 4036–4043. [CrossRef]
51. Lu, Y.; Li, J.; Ye, T.N.; Kobayashi, Y.; Sasase, M.; Kitano, M.; Hosono, H. Synthesis of rare-earth-based metallic electride nanoparticles and their catalytic applications to selective hydrogenation and ammonia synthesis. *ACS Catal.* **2018**, *8*, 11054–11058. [CrossRef]
52. Wu, J.; Gong, Y.; Inoshita, T.; Fredrickson, D.C.; Wang, J.; Lu, Y.; Kitano, M.; Hosono, H. Tiered Electron Anions in Multiple Voids of LaScSi and Their Applications to Ammonia Synthesis. *Adv. Mater.* **2017**, *29*, 1700924. [CrossRef]
53. Inoue, Y.; Kitano, M.; Kim, S.W.; Yokoyama, T.; Hara, M.; Hosono, H. Highly dispersed ru on electride $[Ca_{24}Al_{28}O_{64}]4+(e-)4$ as a catalyst for ammonia synthesis. *ACS Catal.* **2014**, *4*, 674–680. [CrossRef]
54. Kitano, M.; Kanbara, S.; Inoue, Y.; Kuganathan, N.; Sushko, P.V.; Yokoyama, T.; Hara, M.; Hosono, H. Electride support boosts nitrogen dissociation over ruthenium catalyst and shifts the bottleneck in ammonia synthesis. *Nat. Commun.* **2015**, *6*, 6371. [CrossRef] [PubMed]
55. Ye, T.N.; Park, S.W.; Lu, Y.; Li, J.; Sasase, M.; Kitano, M.; Tada, T.; Hosono, H. Vacancy-enabled N_2 activation for ammonia synthesis on an Ni-loaded catalyst. *Nature* **2020**, *583*, 391–395. [CrossRef] [PubMed]
56. Ye, T.N.; Park, S.W.; Lu, Y.; Li, J.; Sasase, M.; Kitano, M.; Hosono, H. Contribution of Nitrogen Vacancies to Ammonia Synthesis over Metal Nitride Catalysts. *J. Am. Chem. Soc.* **2020**, *142*, 14374–14383. [CrossRef]
57. Chang, F.; Guan, Y.; Chang, X.; Guo, J.; Wang, P.; Gao, W.; Wu, G.; Zheng, J.; Li, X.; Chen, P. Alkali and Alkaline Earth Hydrides-Driven N2 Activation and Transformation over Mn Nitride Catalyst. *J. Am. Chem. Soc.* **2018**, *140*, 14799–14806. [CrossRef]
58. Inoue, Y.; Kitano, M.; Kishida, K.; Abe, H.; Niwa, Y.; Sasase, M.; Fujita, Y.; Ishikawa, H.; Yokoyama, T.; Hara, M.; et al. Efficient and Stable Ammonia Synthesis by Self-Organized Flat Ru Nanoparticles on Calcium Amide. *ACS Catal.* **2016**, *6*, 7577–7584. [CrossRef]
59. Wang, P.; Chang, F.; Gao, W.; Guo, J.; Wu, G.; He, T.; Chen, P. Breaking scaling relations to achieve low-temperature ammonia synthesis through LiH-mediated nitrogen transfer and hydrogenation. *Nat. Chem.* **2017**, *9*, 64–70. [CrossRef]
60. Hattori, M.; Iijima, S.; Nakao, T.; Hosono, H.; Hara, M. Solid solution for catalytic ammonia synthesis from nitrogen and hydrogen gases at 50 °C. *Nat. Commun.* **2020**, *11*, 2001. [CrossRef]
61. Croisé, C.; Alabd, K.; Tencé, S.; Gaudin, E.; Villesuzanne, A.; Courtois, X.; Bion, N.; Can, F. Influence of the Rare Earth (R) Element in Ru-supported RScSi Electride-like Intermetallic Catalysts for Ammonia Synthesis at Low Pressure: Insight into NH_3 Formation Mechanism. *ChemCatChem* **2023**, *15*, e202201172. [CrossRef]
62. Croisé, C.; Alabd, K.; Villesuzanne, A.; Can, F.; Courtois, X.; Gaudin, E.; Tencé, S.; Bion, N. Role of hydride ion within Ru/LaScSi and Ru/CeTiGe catalysts for NH_3 synthesis: A combination of DFT and experimental nitrogen isotopic exchange studies. *Catal. Commun.* **2023**, *179*, 106689. [CrossRef]
63. Gong, Y.; Li, H.; Li, C.; Bao, X.; Hosono, H.; Wang, J. Insight into rare-earth-incorporated catalysts: The chance for a more efficient ammonia synthesis. *J. Adv. Ceram.* **2022**, *11*, 1499–1529. [CrossRef]

64. Gong, Y.; Li, H.; Wu, J.; Song, X.; Yang, X.; Bao, X.; Han, X.; Kitano, M.; Wang, J.; Hosono, H. Unique Catalytic Mechanism for Ru-Loaded Ternary Intermetallic Electrides for Ammonia Synthesis. *J. Am. Chem. Soc.* **2022**, *144*, 8683–8692. [CrossRef] [PubMed]
65. Wu, J.; Li, J.; Gong, Y.; Kitano, M.; Inoshita, T.; Hosono, H. Intermetallic Electride Catalyst as a Platform for Ammonia Synthesis. *Angew. Chem. Int. Ed.* **2019**, *58*, 825–829. [CrossRef] [PubMed]
66. Li, J.; Wu, J.; Wang, H.; Lu, Y.; Ye, T.; Sasase, M.; Wu, X.; Kitano, M.; Inoshita, T.; Hosono, H. Acid-durable electride with layered ruthenium for ammonia synthesis: Boosting the activity via selective etching. *Chem. Sci.* **2019**, *10*, 5712–5718. [CrossRef]
67. Jiang, Y.F.; Liu, J.C.; Xu, C.Q.; Li, J.; Xiao, H. Breaking the scaling relations for efficient N_2-to-NH_3 conversion by a bowl active site design: Insight from LaRuSi and isostructural electrides. *Chin. J. Catal.* **2022**, *43*, 2183–2192. [CrossRef]
68. Jacobsen, C.J.H.; Dahl, S.; Clausen, B.G.S.; Bahn, S.; Logadottir, A.; Nørskov, J.K. Catalyst design by interpolation in the periodic table: Bimetallic ammonia synthesis catalysts. *J. Am. Chem. Soc.* **2001**, *123*, 8404–8405. [CrossRef]
69. Sato, K.; Nagaoka, K. Boosting Ammonia Synthesis under Mild Reaction Conditions by Precise Control of the Basic Oxide–Ru Interface. *Chem. Lett.* **2021**, *50*, 687–696. [CrossRef]
70. Yan, H.; Gao, W.; Cui, J.; Zhang, W.; Pei, Q.; Wang, Q.; Guan, Y.; Feng, S.; Wu, H.; Cao, H.; et al. Dinitrogen fixation mediated by lanthanum hydride. *J. Energy Chem.* **2022**, *72*, 1–7. [CrossRef]
71. Ooya, K.; Li, J.; Fukui, K.; Iimura, S.; Nakao, T.; Ogasawara, K.; Sasase, M.; Abe, H.; Niwa, Y.; Kitano, M.; et al. Ruthenium Catalysts Promoted by Lanthanide Oxyhydrides with High Hydride-Ion Mobility for Low-Temperature Ammonia Synthesis. *Adv. Energy Mater.* **2021**, *11*, 2003723. [CrossRef]
72. Fukui, K.; Iimura, S.; Iskandarov, A.; Tada, T.; Hosono, H. Room-Temperature Fast H-Conduction in Oxygen-Substituted Lanthanum Hydride. *J. Am. Chem. Soc.* **2022**, *144*, 1523–1527. [CrossRef]
73. Ye, T.N.; Lu, Y.; Kobayashi, Y.; Li, J.; Park, S.W.; Sasase, M.; Kitano, M.; Hosono, H. Efficient Ammonia Synthesis over Phase-Separated Nickel-Based Intermetallic Catalysts. *J. Phys. Chem. C* **2020**, *124*, 28589–28595. [CrossRef]
74. Miyahara, S.I.; Sato, K.; Tsujimaru, K.; Wada, Y.; Ogura, Y.; Toriyama, T.; Yamamoto, T.; Matsumura, S.; Inazu, K.; Nagaoka, K. Co Nanoparticle Catalysts Encapsulated by BaO-La_2O_3Nanofractions for Efficient Ammonia Synthesis Under Mild Reaction Conditions. *ACS Omega* **2022**, *7*, 24452–24460. [CrossRef] [PubMed]
75. Che, M. Nobel Prize in chemistry 1912 to Sabatier: Organic chemistry or catalysis? *Catal. Today* **2013**, *218–219*, 162–171. [CrossRef]
76. Vojvodic, A.; Medford, A.J.; Studt, F.; Abild-Pedersen, F.; Khan, T.S.; Bligaard, T.; Nørskov, J.K. Exploring the limits: A low-pressure, low-temperature Haber-Bosch process. *Chem. Phys. Lett.* **2014**, *598*, 108–112. [CrossRef]
77. Nakao, T.; Tada, T.; Hosono, H. First-Principles and Microkinetic Study on the Mechanism for Ammonia Synthesis Using Ru-Loaded Hydride Catalyst. *J. Phys. Chem. C* **2020**, *124*, 2070–2078. [CrossRef]
78. Kitano, M.; Kujirai, J.; Ogasawara, K.; Matsuishi, S.; Tada, T.; Abe, H.; Niwa, Y.; Hosono, H. Low-Temperature Synthesis of Perovskite Oxynitride-Hydrides as Ammonia Synthesis Catalysts. *J. Am. Chem. Soc.* **2019**, *141*, 20344–20353. [CrossRef]
79. Hosono, H.; Kitano, M. Advances in Materials and Applications of Inorganic Electrides. *Chem. Rev.* **2021**, *121*, 3121–3185. [CrossRef]
80. Tang, Y.; Kobayashi, Y.; Masuda, N.; Uchida, Y.; Okamoto, H.; Kageyama, T.; Hosokawa, S.; Loyer, F.; Mitsuhara, K.; Yamanaka, K.; et al. Metal-Dependent Support Effects of Oxyhydride-Supported Ru, Fe, Co Catalysts for Ammonia Synthesis. *Adv. Energy Mater.* **2018**, *8*, 1801772. [CrossRef]
81. Gao, W.; Feng, S.; Yan, H.; Wang, Q.; Xie, H.; Jiang, L.; Zhang, W.; Guan, Y.; Wu, H.; Cao, H.; et al. In situ formed Co from a Co-Mg-O solid solution synergizing with LiH for efficient ammonia synthesis. *Chem. Commun.* **2021**, *57*, 8576–8579. [CrossRef]
82. Hu, Z.; Mahin, J.; Datta, S.; Bell, T.E.; Torrente-Murciano, L. Ru-Based Catalysts for H2 Production from Ammonia: Effect of 1D Support. *Top. Catal.* **2019**, *62*, 1169–1177. [CrossRef]
83. Zhu, L.; Cadigan, C.; Duan, C.; Huang, J.; Bian, L.; Le, L.; Hernandez, C.H.; Avance, V.; O'Hayre, R.; Sullivan, N.P. Ammonia-fed reversible protonic ceramic fuel cells with Ru-based catalyst. *Commun. Chem.* **2021**, *4*, 121. [CrossRef] [PubMed]
84. López-Rodríguez, S.; Davó-Quiñonero, A.; Bailón-García, E.; Lozano-Castelló, D.; Bueno-López, A. Effect of Ru loading on Ru/CeO_2 catalysts for CO_2 methanation. *Mol. Catal.* **2021**, *515*, 111911. [CrossRef]
85. Kobayashi, Y.; Kitano, M.; Kawamura, S.; Yokoyama, T.; Hosono, H. Kinetic evidence: The rate-determining step for ammonia synthesis over electride-supported Ru catalysts is no longer the nitrogen dissociation step. *Catal. Sci. Technol.* **2017**, *7*, 47–50. [CrossRef]
86. Hosono, H. Electron Transfer from Support/Promotor to Metal Catalyst: Requirements for Effective Support. *Catal. Lett.* **2022**, *152*, 307–314. [CrossRef]
87. Kitano, M.; Yamagata, K.; Hosono, H. Why Ca_2NH works as an efficient and stable support of Ru catalyst in ammonia synthesis. *Res. Chem. Intermed.* **2021**, *47*, 235–248. [CrossRef]
88. Kishida, K.; Kitano, M.; Sasase, M.; Sushko, P.V.; Abe, H.; Niwa, Y.; Ogasawara, K.; Yokoyama, T.; Hosono, H. Air-Stable Calcium Cyanamide-Supported Ruthenium Catalyst for Ammonia Synthesis and Decomposition. *ACS Appl. Energy Mater.* **2020**, *3*, 6573–6582. [CrossRef]
89. Mizoguchi, H.; Okunaka, M.; Kitano, M.; Matsuishi, S.; Yokoyama, T.; Hosono, H. Hydride-Based Electride Material, LnH_2 (Ln = La, Ce, or Y). *Inorg. Chem.* **2016**, *55*, 8833–8838. [CrossRef]
90. Sato, K.; Imamura, K.; Kawano, Y.; Miyahara, S.I.; Yamamoto, T.; Matsumura, S.; Nagaoka, K. A low-crystalline ruthenium nano-layer supported on praseodymium oxide as an active catalyst for ammonia synthesis. *Chem. Sci.* **2016**, *8*, 674–679. [CrossRef]

91. Hargreaves, J.S.J. Nitrides as ammonia synthesis catalysts and as potential nitrogen transfer reagents. *Appl. Petrochem. Res.* **2014**, *4*, 3–10. [CrossRef]
92. Gong, Y.; Wu, J.; Kitano, M.; Wang, J.; Ye, T.N.; Li, J.; Kobayashi, Y.; Kishida, K.; Abe, H.; Niwa, Y.; et al. Ternary intermetallic LaCoSi as a catalyst for N_2 activation. *Nat. Catal.* **2018**, *1*, 178–185. [CrossRef]

2. Chapter 2: $CeNi_x$ Alloys as Catalysts for Ammonia Synthesis: Insights on Ni-CeN Surface Layer Formation and Its Impact

Title: $CeNi_x$ Alloys as Catalysts for Ammonia Synthesis: Insights on Ni-CeN Surface Layer Formation and Its Impact.

Authors: Javier Arroyo−Caire, Yihao Jiang, Manuel Antonio Diaz−Perez, Mayra Anabel Lara−Angulo, Masayoshi Miyazaki, Juan Carlos Serrano−Ruiz, Masaaki Kitano and Hideo Hosono.

Reference: *ACS Catalysis* 2023, 13, 15715-15724. https://pubs.acs.org/doi/full/10.1021/acscatal.3c03654.

Published date: 21 November 2023.

Impact factor: JIF 11.7 (JCR, 2023).

Position: CHEMISTRY, PHYSICAL 21/178 (Q1).

ACS Catalysis

pubs.acs.org/acscatalysis Research Article

$CeNi_x$ Alloys as Catalysts for Ammonia Synthesis: Insights on Ni−CeN Surface Layer Formation and Its Impact

Javier Arroyo-Caire, Yihao Jiang, Manuel Antonio Diaz-Perez, Mayra Anabel Lara-Angulo, Masayoshi Miyazaki, Juan Carlos Serrano-Ruiz,* Masaaki Kitano,* and Hideo Hosono*

Cite This: *ACS Catal.* 2023, 13, 15715−15724 Read Online

ACCESS | Metrics & More | Article Recommendations | Supporting Information

ABSTRACT: Ammonia, which is widely used for the production of fertilizers, is becoming increasingly important as a hydrogen-containing energy vector. Typically, the ammonia synthesis activity of non-noble cheap metal-based catalysts (e.g., Ni) is well below that of ruthenium or cobalt. In this work, we unveil the performance of bulk $CeNi_x$ alloys as compact bimetallic catalysts for ammonia synthesis. The spontaneous formation of a crystalline CeN surface layer was responsible for the higher activity of $CeNi_2$ over $CeNi_5$ (1.012 and 0.067 mmol g^{-1} h^{-1}, respectively) at 400 °C and 0.9 MPa. The CeN layer was key since it served as a second active center for nitrogen dissociation, enhancing the ammonia synthesis rate to levels comparable to other rare earth-based alloys. Significant differences in the global kinetic mechanism were also found: $CeNi_2$ showed significantly lower apparent activation energies than $CeNi_5$ (55.3 vs 79.5 kJ mol^{-1}, respectively). Furthermore, $CeNi_2$ showed synthesis rates 1 order of magnitude higher than pure bulk CeN, thereby stressing the key role of Ni as an additional center for hydrogen and hydrogen-containing species (NH_x) activation. We also demonstrated that the chemical state of cerium (oxide vs nitride) is key for enhancing the ammonia synthesis reaction. We found that Ce is required to be in the form of nitride for enhancing the activity of $CeNi_2$, as revealed by the poor kinetic behavior (high activation energy, strong hydrogen poisoning, and poor affinity toward NH_x species) and low synthesis rates found for a nanopowder Ni/CeO_2 catalyst.

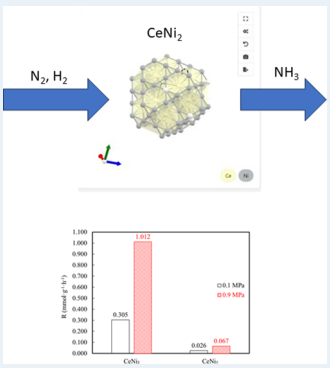

KEYWORDS: *nickel, $CeNi_x$ alloys, CeN surface layer, second active center, non-noble metal-based catalysts*

1. INTRODUCTION

Ammonia (NH_3) has recently gained attention as a chemical platform, not only for its increasing use in the fertilizer industry[1] but also due to its potential role as an energy carrier, owing to its large hydrogen content (18 wt %).[2−5] The Haber−Bosch (HB) process, traditionally used to produce ammonia, is highly energy-consuming since harsh operating conditions (i.e., 20−40 MPa and 400−600 °C) are required to achieve the dissociation of a very stable nitrogen molecule (N_2).[6]

In this context, strong efforts have been made to develop more efficient catalysts able to achieve reasonable ammonia synthesis performance at milder conditions.[3,7−11] This approach is particularly interesting for integrating NH_3 synthesis with renewable hydrogen production via water electrolysis, thereby paving the way for a new paradigmatic small-scale distributed green ammonia production.[12] 3d transition metals (TMs), such as ruthenium (Ru), have demonstrated high ammonia synthesis activities at milder conditions,[7,8] owing to its optimum nitrogen absorption energy.[13] However, despite its superior activity, the high cost of Ru hinders its widespread use at the industrial scale. Thus, the design of non-noble-metal-based catalysts for ammonia production is highly desirable. However, when selecting non-noble metals for this application, it is necessary to consider their affinity toward nitrogen (i.e., adsorption energy) since the adsorption and subsequent dissociation of N_2 is a key step in ammonia synthesis.[14] Some non-noble metals such as Ni present very low affinity toward N_2. This limitation has recently been overcome by using active supports with the ability to activate and dissociate N_2, such as hydrides (e.g., LiH[15]) or rare-earth (RE) nitrides (RE = Ce, La, Y).[16] While hydrides allow N_2 dissociation by promoting simultaneous electron and H^- transfer processes, nitrides promote N_2 adsorption and activation by providing nitrogen vacancy (N_V) surface sites.

RE elements have attracted significant attention in the field of ammonia synthesis at mild conditions.[17] Their versatile chemical nature allows them to generate different active centers, thereby facilitating the dispersion of TMs on their surface. In the case of RE oxides, the high reducibility of these materials results in the formation of surface oxygen vacancies upon reduction, promoting the so-called strong metal−support interaction (SMSI). The formation of these oxygen vacancies improves the dispersion of the TM while promoting electron transfer

Received: August 5, 2023
Revised: November 11, 2023
Accepted: November 13, 2023
Published: November 21, 2023

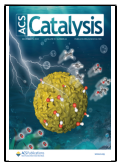

processes toward the metal, thereby facilitating the activation and dissociation of the N_2 molecule.[17,18] This strategy has demonstrated to be useful for metals with optimum nitrogen absorption energy, such as Ru[19,20] or Co.[21] RE hydrides and oxyhydrides have shown higher activities compared to RE oxides since the highly mobile H^- further enhances the electron donation process.[22,23] In general, the use of a suitable material as a secondary active center has been demonstrated to boost the activity of TMs with optimum nitrogen absorption energies.

In the case of metals with low affinity to nitrogen, such as Ni, RE oxides are less efficient and new strategies are required.[8] In this sense, Ni has recently demonstrated to have a superior performance when promoted with RE nitrides[16] since N_V sites can activate H_2 and, particularly, N_2. Among the RE nitrides, CeN has shown a superior performance for ammonia synthesis compared to LaN and YN because of its lower N_V formation energy (i.e., E_{N_V} = 1.3 eV). Bulk 5 wt % Ni/CeN has shown an outstanding ammonia synthesis activity of 3100 μmol g^{-1} h^{-1} at 400 °C and 1 bar.[16]

Intermetallic RETM compounds are currently gaining attention as ammonia synthesis catalysts[24−29] since the close interaction between RE and TM promotes N_2 dissociation efficiently. $RETM_x$ alloys (x = 2, 3, 5) have been found useful for several applications,[30,31] particularly as hydrogen storage materials,[32−35] in virtue of their ability to reversibly form hydrogenated complexes. This ability of $RETM_x$ intermetallics is particularly interesting for ammonia synthesis applications. Recently, $LaNi_5$ alloy nanoparticles (NPs) have shown outstanding ammonia synthesis activities (4500 μmol g^{-1} h^{-1} at 400 °C and 1 bar) with apparent activation energies as low as 53.8 kJ mol^{-1}. $LaNi_5$ has clearly outperformed other Ni-based materials, showing activities in the range (or even slightly higher) of those of Ru-based intermetallic compounds. The superior performance of $LaNi_5$ has been ascribed to the formation of a Ni−LaN surface layer upon reaction, resulting in a self-organized core (Ni)−shell (LaN) material.[36] The formation of secondary or intermediate phases has received growing interest in the field of ammonia synthesis and catalyst design. TM or primary phase encapsulation has demonstrated to lead to a dramatical increase in the ammonia synthesis performance of original materials, principally as a result of the formation of secondary active phases as in the case of $LaNi_5$[36] or for conventional TM/support materials, such as Co/BaO-La_2O_3[37] In this case, the formation of surface nanolayers encapsulating the TM is reported to enhance the electron transfer, further enhancing ammonia synthesis as compared to the original catalyst.

In this work, we provide new insights into the performance of bulk $CeNi_x$ (x = 2, 5) alloys. Remarkably, we found $CeNi_2$ alloys to outperform bulk $LaNi_5$ by 20% in terms of the ammonia production rate at similar conditions. We also demonstrated that the performance of $CeNi_x$ alloys relies on the formation of a CeN surface layer over the fresh catalyst and analyzed the relationship between the formation of this CeN phase and the ammonia synthesis rate. We found that the $CeNi_2$ performance and kinetic mechanism clearly exceed those of pure bulk CeN, with Ni playing a crucial role as a second active center for hydrogen dissociation and hydrogenation of the adsorbed nitrogen species. Furthermore, the importance of the chemical state of cerium in the nitride phase was highlighted. The $CeNi_2$ alloy catalyst showed significantly higher ammonia synthesis rates and lower apparent activation energies than did a regular Ni/CeO_2 catalyst. Ni/CeO_2 also showed negative and zero reaction orders toward hydrogen and ammonia, respectively, revealing a less efficient global kinetic mechanism as compared to the $CeNi_2$ alloy catalyst.

2. EXPERIMENTAL SECTION

2.1. Catalyst Preparation. $CeNi_x$ ingots were prepared by arc melting of specific mixtures (Ni/Ce molar ratio x = 2:5) of pure elemental Ce shots (99.9%, Rare Metallic Co.) and pellets of Ni powder (Kojundo Chemical Laboratory Co.), while bulk $CeNi_x$ powders were obtained by crushing the as-received ingots using an agate mortar, as reported previously.[36]

Bulk CeN samples were collected from previous batches and synthesized following a hydrogenation + nitridation process from pure Ce shots, as reported previously.[16]

Ni/CeO_2 NPs were prepared by loading Ni (20 wt %) over pure CeO_2 NPs through a solid-state reaction of nickelocene (>98.0%, Tokyo Chemical Industry Co.) and CeO_2 (Sigma-Aldrich), mixed in an agate mortar, followed by a reduction stage, as previously reported.[16]

Since Ce shots, nitrides, and alloys are air- and/or moisture-sensitive, material handling, crushing, and solid-state reaction procedures were all conducted inside an Ar-filled glovebox.

2.2. Ammonia Synthesis Tests. Catalytic reactions were carried out in a stainless-steel fixed-bed reactor under a stoichiometric N_2/H_2 (1:3) flow of 60 mL min^{-1}. A WHSV of 36000 mL g^{-1} h^{-1} was settled, so 0.1 g of the catalyst bed was used. The ammonia produced was monitored under steady-state conditions of temperature (340−400 °C) and pressure (0.1−0.9 MPa). A thermocouple was directly placed into the catalyst in order to minimize temperature errors. The ammonia produced was trapped in a 5 mM aqueous sulfuric acid solution, and the concentration of NH^{4+} ions was determined using an ion chromatograph (Prominence, Shimadzu) equipped with an electrical conductivity detector. Ar gas was used as an inert diluent gas for measuring the N_2 and H_2 reaction orders to ensure a total flow of 60 mL min^{-1} when changing the flow rate of N_2 and H_2.

2.3. Characterization. Crystal structures were analyzed using X-ray diffraction (XRD; D2 Phaser, Bruker) with Cu Kα radiation (λ = 0.15418 nm). All of the samples were placed in Ar-filled capsules to avoid air oxidation. Nitrogen adsorption measurements (BELSORP-mini II, BEL) were used to obtain the Brunauer−Emmet−Teller (BET) surface areas of the samples. X-ray photoelectron spectroscopy (XPS) (KRATOS ULTRA2, Shimadzu) analyses were carried out using Mg Kα radiation at <10^{-6} Pa, applying 8 kV voltage to the X-ray source. A sample holder was transported inside an ultrahigh vacuum (UHV) apparatus from an Ar-filled glovebox to avoid air contamination. Carbon 1s peak (binding energy = 284.6 eV) was used as a reference for sample measurements. Temperature-programmed desorption (TPD) analyses of hydrogen (m/z = 2), nitrogen (m/z = 28), and ammonia (m/z = 17) were performed to measure the amount of adsorbed gases in all samples using a BELCAT-A (BEL) instrument. Typically, 0.03−0.05 g of the sample was placed in a quartz glass cell inside an Ar-filled glovebox before the measurements. This cell was heated (10 °C min^{-1}) under an Ar stream (30 mL min^{-1}) and the concentrations of N_2, H_2, and NH_3 were monitored by a thermal conductivity detector (TCD) and a mass spectrometer (Bell Mass, BEL).

https://doi.org/10.1021/acscatal.3c03654
ACS Catal. 2023, 13, 15715−15724

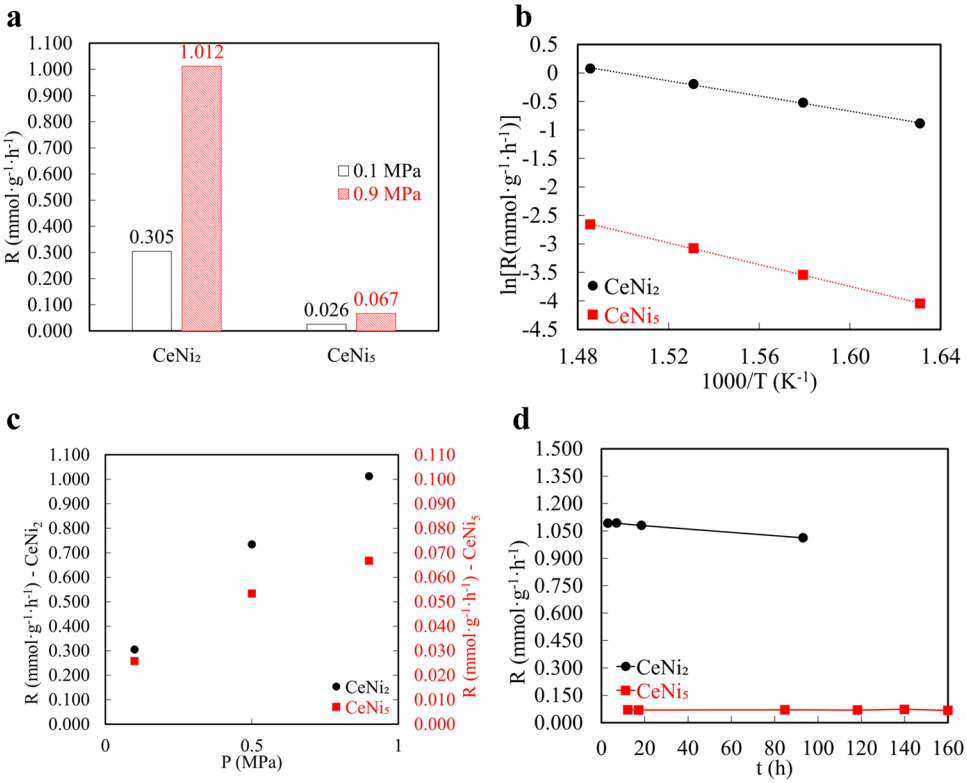

Figure 1. $CeNi_x$ alloy kinetic analysis results. (a) Ammonia synthesis rates at 0.1 and 0.9 MPa. Conditions: 400 °C, 36,000 mL g^{-1} h^{-1}, N_2/H_2 = 1:3, 0.1 g of the catalyst. (b) Arrhenius plots for ammonia synthesis at 0.9 MPa. (c) Ammonia synthesis rate as a function of pressure at 400 °C. (d) Time course of the ammonia synthesis at 0.9 MPa and 400 °C.

3. RESULTS AND DISCUSSION

3.1. Ammonia Synthesis Performance of $CeNi_x$. To study the catalytic behavior of Ce−Ni alloys, two catalysts with different Ni/Ce molar ratios were synthesized, as described in the Section 2. Kinetic experiments were conducted for both bulk $CeNi_2$ and bulk $CeNi_5$ to compare their performance. Prior to these kinetic tests, a preactivation stage was carried out for both catalysts during 2 h, at 500 °C, under a total gas flow (N_2/H_2 = 1:3) of 60 mL min^{-1}, at a pressure of 0.1 MPa, to make sure that the catalyst is homogeneously formed. A layer of CeN emerges during the activation stage for $CeNi_2$, and its formation process and impact on the ammonia synthesis are described in Section 3.2. Figure 1a shows the performances of $CeNi_2$ and $CeNi_5$ at 0.1 and 0.9 MPa, respectively. $CeNi_2$ showed ammonia production rates several orders of magnitude higher than $CeNi_5$ under similar conditions. Interestingly, $CeNi_2$ showed ammonia production rates 20% higher than previously reported bulk $LaNi_5$ (0.305 vs 0.250 mmol g^{-1} h^{-1}) at the same conditions (400 °C, 0.1 MPa, WHSV of 36,000 mL g^{-1} h^{-1}, N_2/H_2 = 1:3).[36]

With the aim to gain insight into the different kinetic behavior of $CeNi_2$ and $CeNi_5$, the Arrhenius plots for $CeNi_2$ and $CeNi_5$ were built (Figure 1b). Both alloys showed an appreciable difference, not only in terms of catalytic activity but also regarding the kinetic mechanism. Arrhenius plots revealed an apparent activation energy of 55.3 kJ mol^{-1} for $CeNi_2$, significantly lower than those of well-known Ru-based catalysts (80−150 kJ mol^{-1})[7] and lower than that of $CeNi_5$ (79.5 kJ mol^{-1}). Since traditional Ru-based catalysts are typically controlled by the nitrogen dissociation step, these results seem to indicate that the rate-determining step (RDS) for $CeNi_2$ is not N_2 dissociation, and it tends to shift toward the formation of NH_x species.[38] This is further confirmed by the reaction orders (Table 1), the experiments of which were driven at 0.9 MPa. The procedure for the reaction order calculation is detailed in the Supporting Information, Section S1. A nitrogen reaction order (α) closer to unity for $CeNi_5$ reveals a higher predominance of N_2 dissociation in the global kinetic scheme, as reported previously.[7,23,39,40] The positive hydrogen reaction orders (β) obtained for both $CeNi_2$ and $CeNi_5$ revealed the absence of hydrogen poisoning issues on these alloys.[7,39,41,42] $CeNi_2$ showed a significantly higher hydrogen reaction order than $CeNi_5$, thereby revealing hydrogen adsorption and dissociation processes to be much more relevant in the reaction mechanism on the former alloy.[7] The positive β values for both $CeNi_2$ and $CeNi_5$ were reflected in a positive and almost linear effect of the pressure on the reaction rate (Figure 1c), although the positive effect was more noticeable for the $CeNi_2$ alloy. The slopes of plots in Figure 1c, calculated as variations of the ammonia synthesis rate with pressure divided by the ammonia synthesis rate at 0.1 MPa, were found to be 2.9 and 2.0 MPa^{-1} for $CeNi_2$

Table 1. Kinetic Parameters of $CeNi_x$ Alloys in the Ammonia Synthesis Reaction[a]

catalyst	E_A (kJ mol^{-1})	α (N_2)	β (H_2)	γ (NH_3)
$CeNi_2$	55.3	0.663	1.089	−0.725
$CeNi_5$	79.5	0.884	0.633	−0.690

[a] E_A: apparent activation energy, α: nitrogen reaction order, β: hydrogen reaction order, γ: ammonia reaction order. Experimental conditions: 400 °C, 36,000 mL g^{-1} h^{-1}, N_2/H_2 = 1:3, 0.1 g of the catalyst.

https://doi.org/10.1021/acscatal.3c03654
ACS Catal. 2023, 13, 15715−15724

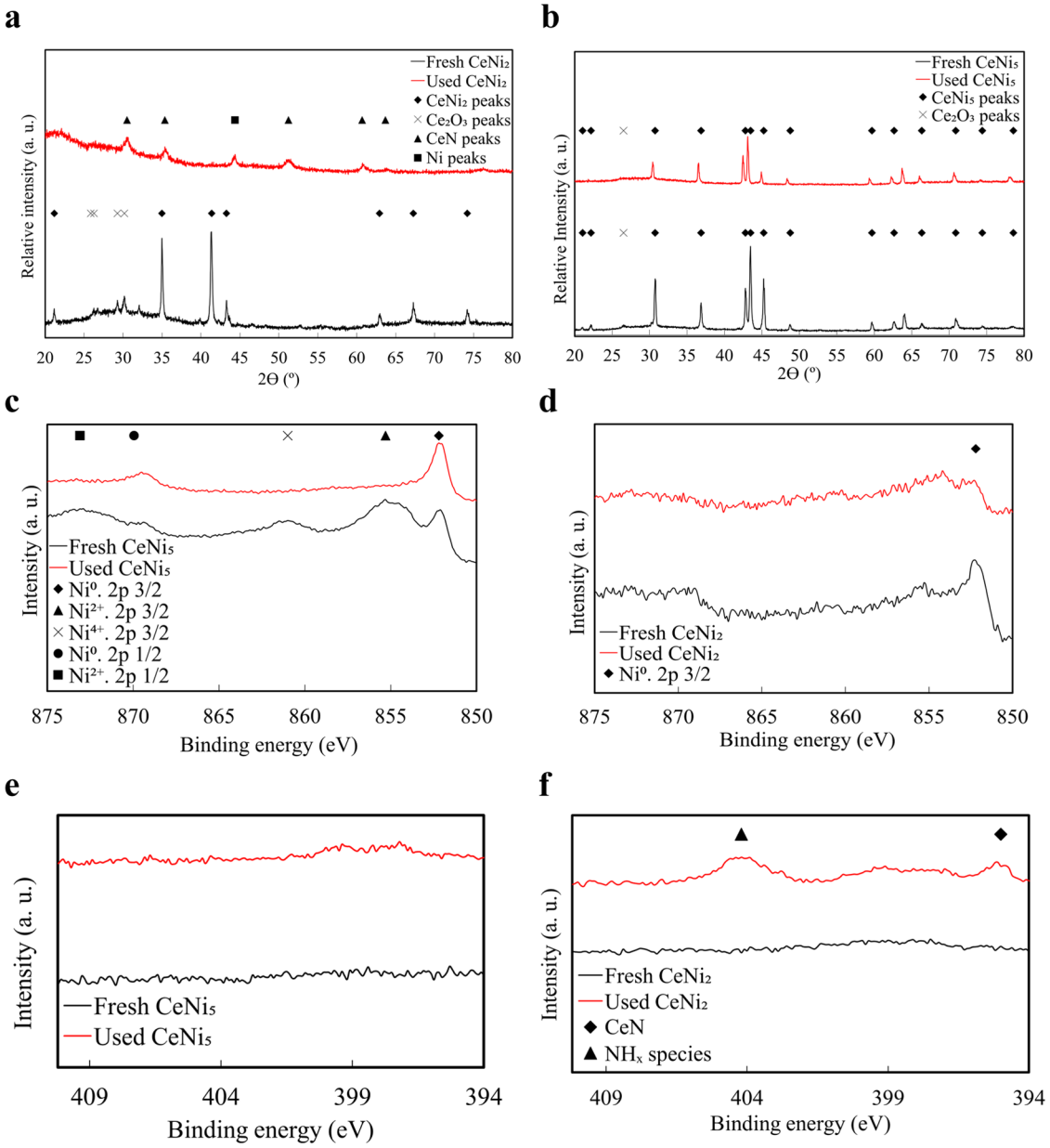

Figure 2. Characterization of $CeNi_x$ alloys. (a) XRD crystal structure of fresh and used $CeNi_2$. (b) XRD crystal structures of fresh and used $CeNi_5$. (c) Ni 2p XPS patterns of fresh and used $CeNi_5$. (d) Ni 2p XPS patterns of fresh and used $CeNi_2$. (e) N 1s XPS patterns of fresh and used $CeNi_5$. (f) N 1s XPS patterns of fresh and used $CeNi_2$.

and $CeNi_5$, respectively. The different β values for both catalysts can account for this different effect of pressure on the reaction rate.[7] For its part, ammonia reaction orders (γ) were very negative and nearly similar for both alloy catalysts.

Both $CeNi_2$ and $CeNi_5$ remained highly stable after 3 h on stream (Figure 1d). $CeNi_2$ (8% ammonia synthesis rate loss after 90 h on stream) and $CeNi_5$ (6% activity loss after 160 h on stream) were slightly deactivated with time. Therefore, total reaction times of 90 and 160 h were counted for $CeNi_2$ and $CeNi_5$, respectively.

To understand the differences between $CeNi_2$ and $CeNi_5$, BET surface analyses were carried out. Both catalysts showed similar surface areas (Table S1), thereby ruling out some effect of this parameter on the higher performance of $CeNi_2$ as compared to $CeNi_5$. Further characterization was required to understand the different behavior of both alloys. Crystal structures were determined by means of X-ray diffraction (XRD) analyses. XRD patterns of $CeNi_2$ and $CeNi_5$ are shown in Figure 2a,2b, respectively. From now on, note that all as-received catalysts, before the preactivation stage, will be defined as "fresh", while after-reaction materials will be named as "used".

As observed, crystal structures ascribed to $CeNi_2$ (Figure 2a) and $CeNi_5$ (Figure 2b) were confirmed for fresh samples (black lines), with minor peaks corresponding to Ce_2O_3 as a result of slight oxidation due to residual exposure to air inside the glovebox. After the reaction (red lines), $CeNi_5$ preserved its crystal structure, with slight angle shifting of the major $CeNi_5$ peaks. However, a change in crystal structure was observed for $CeNi_2$ after the reaction, showing a transformation from a nearly pure $CeNi_2$ phase to pure CeN, with one additional peak corresponding to Ni metal. Remarkably, no formation of the CeN phase was observed for $CeNi_5$ after the reaction. As it will

https://doi.org/10.1021/acscatal.3c03654
ACS Catal. 2023, 13, 15715−15724

be discussed later in Section 3.2, the formation of this crystalline phase of CeN can explain the outstanding performance of $CeNi_2$ as compared to $CeNi_5$.

The formation of nitrogen vacancies has been demonstrated to promote efficient N_2 dissociation over a Ni/CeN catalyst and in the absence of metal (pure CeN phase) in previous studies.[16] Bulk Ni/CeN (i.e., specific surface area of around 2 m^2 g^{-1}) showed a very low apparent activation energy (53.4 kJ mol^{-1}), which is very similar to that measured herein for $CeNi_2$ (55.3 kJ mol^{-1}, Table 1), which strongly supports the idea that the CeN phase plays a key role in the reaction by providing a second active center (i.e., nitrogen vacancies) for nitrogen dissociation. CeN generates nitrogen vacancies more easily (formation energy: 1.39 eV) than other nitrides such as LaN (1.72 eV),[16] which can explain the superior performance of bulk $CeNi_2$ versus bulk $LaNi_5$ since a self-organized nitride surface layer is generated spontaneously for both catalysts. In terms of ammonia synthesis activity and the complete kinetic mechanism, $CeNi_2$ and previously reported Ni/CeN cannot be easily contrasted since chemical composition and particle structure configuration are different for both materials. Nevertheless, the similarity in their apparent activation energy values leads to a switch of the RDS toward the formation of NH_x species for both materials, as aforementioned.

To further investigate CeN formation and the surface composition of both $CeNi_2$ and $CeNi_5$, X-ray photoelectron spectroscopy (XPS) experiments were conducted. As shown in Figure 2c, regarding Ni 2p XPS patterns, two positively charged Ni species (Ni^{2+} and Ni^{4+}) and metal Ni^0 were detected for the fresh $CeNi_5$ sample (black line). However, only Ni^0 species were detected for the used sample, revealing a reduction of metal on the $CeNi_5$ surface during the preactivation and initial reaction stages. In contrast, only Ni^0 species was detected for the fresh $CeNi_2$ sample (Figure 2d, black line). As in the case of $CeNi_5$, one could expect a clear presence of Ni^0 after the reaction for $CeNi_2$. However, metallic Ni was practically negligible for used $CeNi_2$ (Figure 2d, red line). This could indicate that a layer of CeN was formed in this catalyst during the reaction, encapsulating the Ni species. Similar conclusions can be obtained by analyzing the Ni 3p pattern (Figure S2c).

To confirm the formation of a surface nitride over the $CeNi_2$ catalyst, the N 1s XPS signals were analyzed (Figure 2e,f). No nitrogen species were detected over the used $CeNi_5$, which suggests that the formation of the CeN phase is negligible. However, two nitrogen peaks were clearly observed for $CeNi_2$ (Figure 2f). The peak at 394.8 eV was attributed to N^{3-} from CeN, in line with the only peak detected from the N 1s XPS pattern of bulk CeN (Figure S2e). Apart from this peak, $CeNi_2$ also showed an XPS peak at very high binding energies (404.0 eV), which can be ascribed to nitrogen species with high electron charge, most of them in the form of nitrates. Despite there are barely reported negatively charged N species around this binding energy, XPS N 1s patterns from previous investigations on Co−Cr−Mo alloys with implanted nitrogen ions[43] revealed the presence of nitrogen in the form of NH_3 or NH_4 over the alloy surface at higher binding energies (ca. 400 eV) than nitride N^{3-} species (ca. 397 eV). These findings suggest that the peak at 404.0 eV observed for the used $CeNi_2$ may correspond to species with a less negative charge than the N^{3-} species peak, i.e., N^{2-} or N^-, which could reveal the presence of NH_x species on the surface of used $CeNi_2$.

In summary, experimental characterization reveals that fresh $CeNi_2$ turns into a catalyst made of a crystalline phase of Ni and CeN (Figure 2a), in which a surface layer of CeN is spontaneously formed (Figure 2f), while the $CeNi_5$ structure remains unaltered.

3.2. Role of the CeN Surface Layer Formation: Temperature Effect. To further confirm the role of the CeN layer formation over the $CeNi_2$ alloy, a series of experimental runs were conducted. In these runs, 0.1 g of fresh $CeNi_2$ was loaded into the reactor and heated at a certain temperature (4 °C min^{-1}) under a total gas pressure (N_2/H_2 = 1:3) of 0.1 MPa and a WHSV of 36,000 mL g^{-1} h^{-1}. Once the set point temperature was reached for every run, the operating pressure was increased to 0.9 MPa and an activation stage of 5 h was performed for promoting CeN layer formation. Once this time lapse was over, the ammonia synthesis rate was measured. After each run, XRD analyses were conducted. The operating temperatures for every run are shown in Table 2 An additional preactivation stage, similar to that conducted in experiments from Section 3.1 (2 h at 500 °C), was carried out in run 8.

Table 2. Temperature Conditions of the Different Runs for CeN Surface Layer Formation Experiments

run	temperature (°C)	additional preactivation stage
1	100	no
2	200	
3	250	
4	300	
5	350	
6	380	
7	400	
8	400	500 °C for 2 h

The evolution of the crystal structure with the run number is shown in Figure 3a. Remarkably, modifications of the crystal structure of the original fresh $CeNi_2$ sample were found to take place at temperatures as low as 100 °C. Interestingly, during this transformation process, a completely amorphous phase was observed at temperatures below 380 °C (runs 1−5), while an incipient crystalline phase is only visible at 380 and 400 °C (runs 6−7). Thus, the crystal structure of the fresh catalyst was self-organized, turning eventually into a crystalline CeN surface layer after 500 °C pretreatment (run 8). Remarkably, this pretreatment is similar to that used for the experiments shown in Section 3.1, which highlights the relevance of this preactivation stage. Similar results were obtained previously for $LaNi_5$,[36] in which a self-organized LaN−Ni structure was spontaneously formed over the original alloy surface, increasing the ammonia synthesis performance by providing the LaN second phase with activity toward N_2 dissociation.

The ammonia synthesis rates for every run are listed in Figure 3b. The activities remained below the detection limit up to 350 °C. At 380 and 400 °C (runs 6 and 7), the CeN crystalline layer was not completely formed (Figure 3a) and ammonia synthesis rates were 1 order of magnitude lower than those reported in Section 3.1. The activation pretreatment at 500 °C (run 8) led to the complete formation of a crystalline surface CeN phase over the $CeNi_2$ catalysts, which was accompanied by a 4-fold increase of the reaction rate versus run 7 despite being carried out at the same temperature (Figure 3b). These results clearly demonstrate that the CeN phase generated upon pretreatment at 500 °C has a crucial role in the ammonia synthesis performance of $CeNi_2$.

https://doi.org/10.1021/acscatal.3c03654
ACS Catal. 2023, 13, 15715−15724

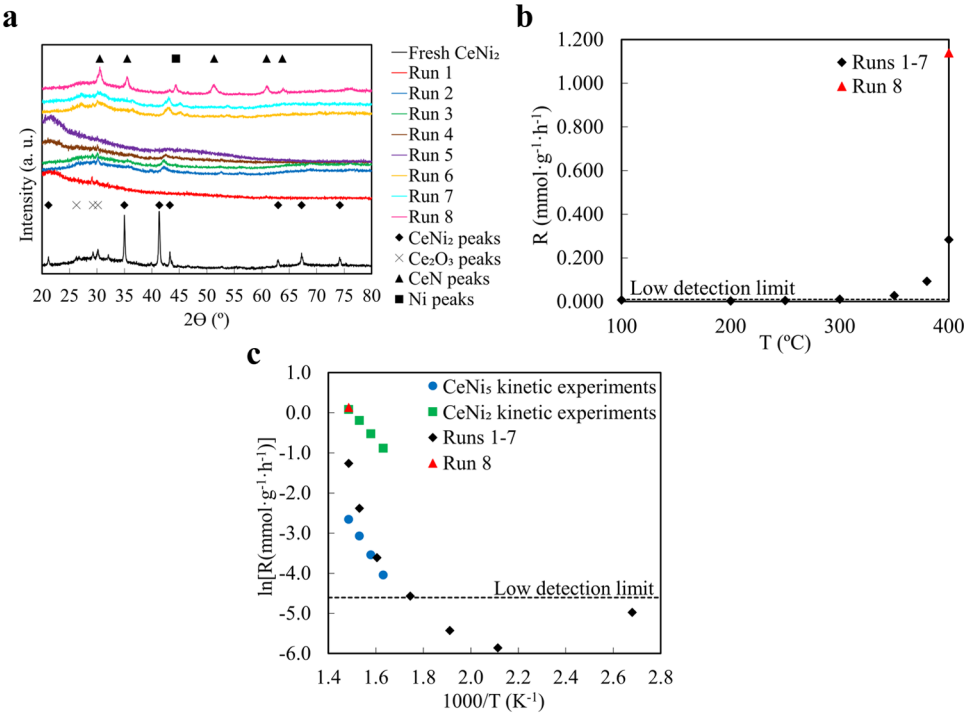

Figure 3. CeN formation layer analysis results. (a) XRD crystal structure of runs 1−8 for $CeNi_2$. (b) Ammonia synthesis rate of runs 1−8 of $CeNi_2$ at onset temperatures. (c) Arrhenius plots of runs 1−8 of $CeNi_2$, compared to $CeNi_x$ plots from kinetic experiments done in Section 3.1 (reaction conditions: 0.1 g of the catalyst, N_2/H_2 = 1:3, 36,000 mL g^{-1} h^{-1}, 0.9 MPa).

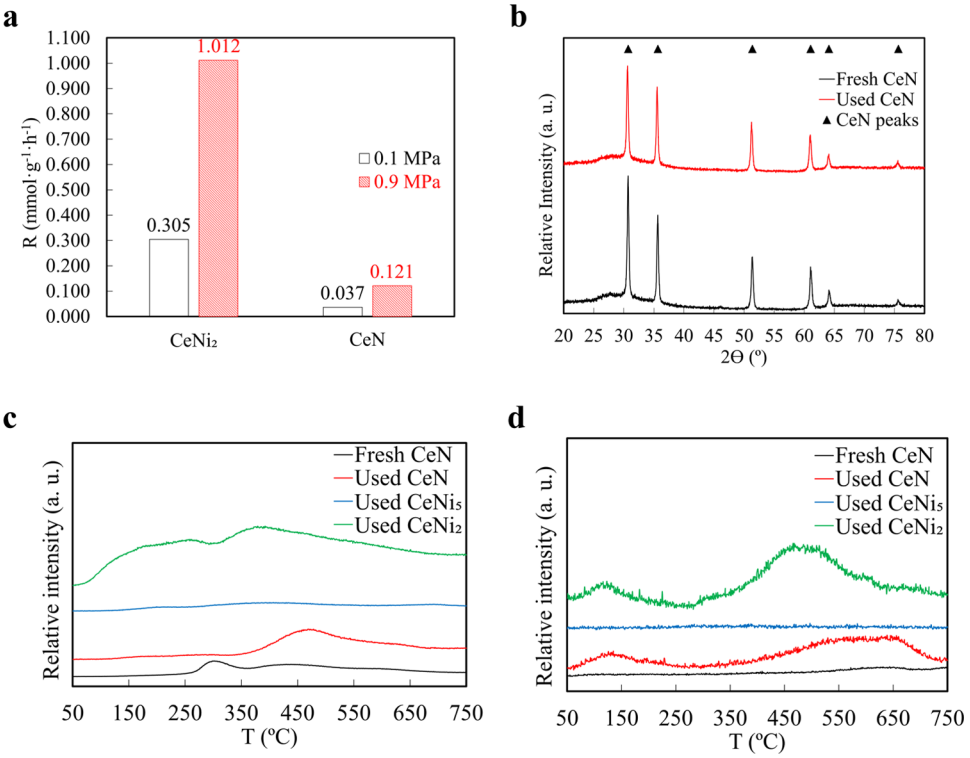

Figure 4. Bulk CeN results and characterization and TPD profiles. (a) Ammonia synthesis rates of $CeNi_2$ (red) and bulk CeN (black) at 0.1 and 0.9 MPa, 400 °C, 36000 mL g^{-1} h^{-1}, N_2/H_2 = 1:3, and 0.1 g of the catalyst. (b) XRD crystal structure of fresh and used CeN. (c) H_2 TPD profiles of fresh and used CeN and $CeNi_x$ alloys. (d) N_2 TPD profiles of fresh and used CeN and $CeNi_x$ alloys.

The ammonia synthesis rates from runs 1−7 were compared with those from previous kinetic experiments of $CeNi_2$ and $CeNi_5$ in the form of Arrhenius plots (Figure 3c). As expected, the rates from run 8 were similar to those obtained for $CeNi_2$ at 400 °C (Section 3.1) since both experiments were performed under similar operating conditions and with the same preactivation stage at 500 °C. At 350−380 °C (runs 6 and 7), the synthesis rates were close to those obtained for $CeNi_5$,

https://doi.org/10.1021/acscatal.3c03654
ACS Catal. 2023, 13, 15715−15724

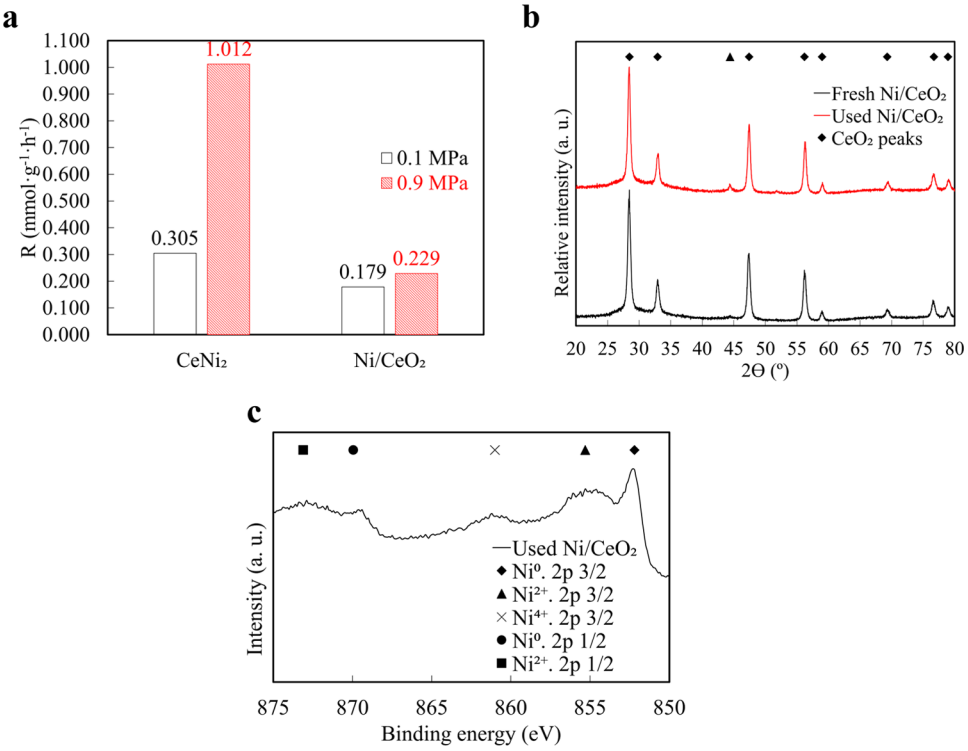

Figure 5. Ni/CeO_2 results and characterization. (a) Ammonia synthesis rates of $CeNi_2$ and Ni/CeO_2 at 0.1 and 0.9 MPa. Conditions: 400 °C, 36,000 mL g^{-1} h^{-1}, N_2/H_2 = 1:3, 0.1 g of the catalyst. (b) XRD crystal structure of fresh and used Ni/CeO_2. (c) Ni 2p XPS of the used Ni/CeO_2.

further suggesting that the strong difference in activity of both alloys originates from the formation of the CeN, which is absent in $CeNi_5$ (Figure 2b).

3.3. Role of Nickel in $CeNi_2$ and Bulk CeN Performance.

After the importance of the CeN surface layer formation was exposed, kinetic experiments were conducted for pure bulk CeN with no Ni loading. Despite having higher surface areas (2.78 vs 0.29 m^2 g^{-1}, Table S1), bulk CeN showed ammonia synthesis rates 1 order of magnitude lower than $CeNi_2$ at the same conditions (Figure 4a), thereby revealing the important role of Ni in the reaction. To further investigate these notable differences, additional experiments were carried out. The following kinetic parameters were obtained for bulk CeN—E_A: 72.1 kJ mol^{-1}, α: 0.806, β: 1.155, γ: −0.444. This material showed a higher apparent activation energy and nitrogen reaction order (α) than $CeNi_2$, while both catalysts showed very similar hydrogen reaction orders (β). This could indicate that bulk CeN is less efficient than $CeNi_2$ in dissociating N_2 (the importance of this step in the kinetic mechanism is higher) and, eventually, to generate ammonia,[7,44,45] which was further confirmed by the less negative (closer to 0) ammonia order (γ). CeN maintained its crystal structure after the reaction (Figure 4b), revealing that the material is stable under the operation conditions used herein.

Previous studies revealed that CeN nanoparticles have a similar reaction mechanism than Ni/CeN nanoparticles.[16] For both catalysts, N_V vacancies generated over the surface of the nitride layer can dissociate N_2 and activate H_2 to produce ammonia simultaneously, leading to a competition between activated N_2 and H_2 species to occupy those vacancies, which act as second active sites. However, since the adsorption energy of H_2 on Ni is lower than that on N_V vacancies,[16] Ni can act as an additional active center for H_2 activation, leading to a higher number of nitrogen vacancy sites available for N_2 dissociation over CeN after Ni loading, greatly enhancing ammonia synthesis of the pure nitride.

In order to clarify the role of Ni on the global ammonia synthesis performance of $CeNi_2$, temperature-programmed desorption (TPD) analyses were conducted for CeN (both fresh and used samples) and $CeNi_2$ and $CeNi_5$. The H_2 TPD patterns of fresh CeN (Figure 4c) showed a peak at 300 °C, which can be ascribed to hydrogen associated with residual amounts of CeH_3 from the material synthesis process.[22] Regarding the used samples, no H_2 peaks were observed for $CeNi_5$, thereby revealing that this material cannot activate hydrogen as efficiently as CeN, which showed a noticeable peak at ca. 450 °C attributed to hydrogen species activated on N_V vacancies. Interestingly, compared to CeN, the onset temperature of this high-temperature hydrogen peak decreased to 380 °C for $CeNi_2$, thereby revealing a higher mobility of H_2 species over the N_V vacancy sites in this material. $CeNi_2$ also showed a low-temperature hydrogen peak at ca. 200 °C, which has been previously associated with Ni.[36] Similar results were obtained for $LaNi_5$ alloys with two hydrogen peaks at ca. 150 and 365 °C ascribed to Ni and LaN, respectively. Thus, Ni improves the ammonia synthesis reaction by promoting H_2 dissociation and therefore increasing the number of available surface N_V sites for N_2 dissociation, enhancing both N_2 dissociation and NH_3 generation. This mechanism is in good agreement with the mechanism exhibited by Ni/CeN.[16] However, regarding the differences in performance and kinetic mechanism between $CeNi_2$ and $CeNi_5$ shown in Section 3.1 and considering that nitrogen dissociation takes place mainly over the N_V sites for $CeNi_2$ after the preactivation stage, maximizing CeN presence over the catalyst surface seems to be an advantage of $CeNi_2$ alloy over previously reported Ni/CeN. The role of Ni was further confirmed by N_2 TPD (Figure 4d). The CeN sample used showed a predominant peak at 550−650 °C ascribed to the

https://doi.org/10.1021/acscatal.3c03654
ACS Catal. 2023, 13, 15715−15724

release of N_2 from N_V sites. Remarkably, this peak shifted to significantly lower temperatures (480 °C) for the used $CeNi_2$, thereby suggesting a higher mobility of N_2 species over the N_V sites in the presence of Ni. The TPD peaks were integrated, and their normalized areas are shown in Table S2. The areas of both N_2 and H_2 peaks of the used $CeNi_2$ are 1 order of magnitude higher than those obtained for CeN and used $CeNi_5$. N 1s XPS patterns of both fresh and used pure CeN (Figure S2e) show that nitrogen is only in the form of CeN over the catalyst surface, unlike used $CeNi_2$, which is discussed in Section 3.1.

3.4. Role of Cerium Chemical State and Performance of Ni/CeO_2 Nanopowder. Once studied the roles of CeN (second active center for efficient N_2 dissociation) and Ni (promote the activation of hydrogen species),[16] we analyzed the role of Ce in the ammonia synthesis reaction. In order to study the chemical state of Ce and to verify Ce in a nitride form, the performance of $CeNi_2$ was compared to that of a simple catalyst of Ni supported on CeO_2. Thus, a Ni/CeO_2 (20 wt % of Ni) nanopowder catalyst was prepared and kinetic experiments were performed under the same conditions used for $CeNi_2$ (Section 3.1), with a previous preactivation stage at 500 °C for 2 h. The ammonia synthesis rates of Ni/CeO_2 and $CeNi_2$ are compared in Figure 5a. Despite the higher surface area of Ni/CeO_2 (30.35 vs 0.29 $m^2\ g^{-1}$ of $CeNi_2$, Table S1), this catalyst showed lower ammonia synthesis rates than $CeNi_2$. Furthermore, Ni/CeO_2 did not show a pressure effect as positive as expected (the rate only increased slightly at 0.9 MPa), considering the rest of the catalysts shown in this work.

The following kinetic parameters were obtained for Ni/CeO_2: E_A: 115.9 kJ mol^{-1}, α: 0.857, β: −0.649, γ: −0.062. An apparent activation energy as high as 115.9 kJ mol^{-1} and an ammonia order (γ) close to zero are clear indicatives of a less efficient mechanism as compared to other catalysts reported in Sections 3.1 and 3.2. Furthermore, a negative hydrogen order (β) reveals a noticeable hydrogen poisoning, which can explain the poor effect of pressure on the synthesis rate for this catalyst.[7]

The XRD pattern of Ni/CeO_2 (Figure 5b) revealed no significant changes in the crystal structure after the reaction. Ni was present on an amorphous phase over the fresh catalyst, and this could indicate that nickelocene is not properly reduced after the initial prereduction stage after the solid-state reaction. Furthermore, a very small peak corresponding to Ni can be observed after the reaction, which could suggest that a certain amount of amorphous Ni remains after the synthesis procedure. Moreover, the catalyst preserved the CeO_2 crystal structure, with no peaks ascribed to reduced Ce_2O_3.[20,46] XPS analysis of the used Ni/CeO_2 (Figure 5c) revealed an uncomplete reduction of Ni species to Ni^0 during the preactivation stage or the experimental reaction, in contrast with CeN or $CeNi_x$ alloys. This incomplete reduction of Ni can also account for the hydrogen poisoning effect observed for Ni/CeO_2 (β = −0.649).

Considering the above results, the positive role of Ce in this reaction seems to be associated with this element forming a nitride phase, which serves as a second active center for N_2 dissociation. When Ce is in the form of oxide, the promotional effect in the ammonia synthesis reaction is rather limited, showing high activation energies and significant hydrogen poisoning, which results in lower synthesis rates and poorer pressure effects as compared to $CeNi_2$.

4. CONCLUSIONS

The importance of intermetallic RETM materials as effective ammonia synthesis catalysts is highlighted herein. This work demonstrates that $CeNi_2$ can efficiently dissociate nitrogen and produce ammonia by the spontaneous formation of a second active phase (crystalline CeN surface layer) generated in situ during the preactivation stage. The formation of this CeN phase is key for promoting the ammonia synthesis reaction, as demonstrated by the poor performance of $CeNi_5$, which, unlike $CeNi_2$, operated with no formation of CeN. Pure bulk CeN was found to be less efficient in dissociating N_2 and in forming NH_x species as compared to $CeNi_2$, thereby stressing the crucial role of Ni in this reaction. Ni was found to be key in promoting H_2 dissociation while increasing the number of N_V nitrogen vacancy sites available to dissociate N_2 and generate NH_3. Eventually, the importance of the Ce chemical state (oxide versus nitride) was highlighted herein. Ni/CeO_2 nanopowder showed a less efficient kinetic mechanism (higher activation energies, strong hydrogen poisoning, and poor affinity toward NH_x species) and lower synthesis rates than $CeNi_2$. The optimization of the Ce/Ni ratio and the operating conditions leading to the formation of the CeN layer over the $CeNi_x$ alloy can pave the way for efficient non-noble metal ammonia synthesis catalysts, which could also have particular scalable interest if they demonstrate to be air-stable.

■ ASSOCIATED CONTENT

Supporting Information

The Supporting Information is available free of charge at https://pubs.acs.org/doi/10.1021/acscatal.3c03654.

Kinetic analysis results for $CeNi_2$ and $CeNi_5$ (Figure S1); XPS spectra for fresh and spent $CeNi_2$ and $CeNi_5$ (Figure S2); kinetic analysis results for bulk CeN (Figure S3); kinetic analysis results for Ni/CeO_2 (Figure S4); BET surface area data (Table S1); and normalized areas from TPD for $CeNi_x$ and CeN (Table S2) (PDF)

■ AUTHOR INFORMATION

Corresponding Authors

Juan Carlos Serrano-Ruiz − *Materials and Sustainability Group, Department of Engineering, Universidad Loyola Andalucía, 41704 Dos Hermanas, Seville, Spain;* orcid.org/0000-0002-9078-7390; Email: jcserrano@uloyola.es

Masaaki Kitano − *MDX Research Center for Element Strategy, International Research Frontiers Initiative, Tokyo Institute of Technology, Yokohama 226-8503, Japan;* orcid.org/0000-0003-4466-7387; Email: kitano.m.aa@m.titech.ac.jp

Hideo Hosono − *MDX Research Center for Element Strategy, International Research Frontiers Initiative, Tokyo Institute of Technology, Yokohama 226-8503, Japan;* orcid.org/0000-0001-9260-6728; Email: hosono@mces.titech.ac.jp

Authors

Javier Arroyo-Caire − *Materials and Sustainability Group, Department of Engineering, Universidad Loyola Andalucía, 41704 Dos Hermanas, Seville, Spain*

Yihao Jiang − *MDX Research Center for Element Strategy, International Research Frontiers Initiative, Tokyo Institute of Technology, Yokohama 226-8503, Japan;* orcid.org/0000-0001-5778-3446

Manuel Antonio Diaz-Perez − *Materials and Sustainability Group, Department of Engineering, Universidad Loyola Andalucía, 41704 Dos Hermanas, Seville, Spain*

Mayra Anabel Lara-Angulo − *Materials and Sustainability Group, Department of Engineering, Universidad Loyola Andalucía, 41704 Dos Hermanas, Seville, Spain*

Masayoshi Miyazaki − *MDX Research Center for Element Strategy, International Research Frontiers Initiative, Tokyo Institute of Technology, Yokohama 226-8503, Japan;* orcid.org/0000-0003-4343-1137

Complete contact information is available at: https://pubs.acs.org/10.1021/acscatal.3c03654

Author Contributions

This manuscript was written through contributions of all authors. All authors have given approval to the final version of the manuscript.

Funding

J.A.-C. would like to thank the University Loyola for the funds associated with the project "Design and screening of catalysts for the synthesis of ammonia at mild temperature and pressure conditions".

Notes

The authors declare no competing financial interest.

REFERENCES

(1) Food and Agriculture Organization of the United Nations. *World Fertilizer Trends and Outlook to 2022*; Rome, 2019.

(2) Smith, C.; Hill, A. K.; Torrente-Murciano, L. Current and Future Role of Haber-Bosch Ammonia in a Carbon-Free Energy Landscape. *Energy Environ. Sci.* **2020**, *13* (2), 331−344.

(3) Wang, Q.; Guo, J.; Chen, P. Recent Progress towards Mild-Condition Ammonia Synthesis. *J. Energy Chem.* **2019**, *36*, 25−36, DOI: 10.1016/j.jechem.2019.01.027.

(4) Rouwenhorst, K. H. R.; Van der Ham, A. G. J.; Lefferts, L. Beyond Haber-Bosch: The Renaissance of the Claude Process. *Int. J. Hydrogen Energy* **2021**, *46* (41), 21566−21579.

(5) 2020 Ammonfuel Report an Industrial View of Ammonia as a Marine Fuel, 2023. https://www.ocimf.org/?view=article&id=1289:2020-ammonfuel-report-an-industrial-view-of-ammonia-as-a-marine-fuel&catid=160. (accessed June 30, 2023).

(6) Ojelade, O. A.; Zaman, S. F. Ammonia Decomposition for Hydrogen Production: A Thermodynamic Study. *Chem. Pap.* **2021**, *75* (1), 57−65.

(7) Marakatti, V. S.; Gaigneaux, E. M. Recent Advances in Heterogeneous Catalysis for Ammonia Synthesis. *ChemCatChem* **2020**, *12*, 5838−5857, DOI: 10.1002/cctc.202001141.

(8) Humphreys, J.; Lan, R.; Tao, S. Development and Recent Progress on Ammonia Synthesis Catalysts for Haber−Bosch Process. *Adv. Energy Sustainability Res.* **2021**, *2* (1), No. 2000043.

(9) Li, L.; Zhang, T.; Zhou, Y.; Wang, X.; Au, C.-t.; Jiang, L. Review on Catalytic Roles of Rare Earth Elements in Ammonia Synthesis: Development and Perspective. *J. Rare Earths* **2022**, *11* (4), No. 2003723, DOI: 10.1016/j.jre.2021.06.014.

(10) Chang, F.; Gao, W.; Guo, J.; Chen, P. Emerging Materials and Methods toward Ammonia-Based Energy Storage and Conversion. *Adv. Mater.* **2021**, *33* (50), No. 2005721, DOI: 10.1002/adma.202005721.

(11) Hosono, H.; Kitano, M. Advances in Materials and Applications of Inorganic Electrides. *Chem. Rev.* **2021**, *121* (5), 3121−3185, DOI: 10.1021/acs.chemrev.0c01071.

(12) Reese, M.; Marquart, C.; Malmali, M.; Wagner, K.; Buchanan, E.; McCormick, A.; Cussler, E. L. Performance of a Small-Scale Haber Process. *Ind. Eng. Chem. Res.* **2016**, *55* (13), 3742−3750.

(13) Jacobsen, C. J. H.; Dahl, S.; Clausen, B. G. S.; Bahn, S.; Logadottir, A.; Nørskov, J. K. Catalyst Design by Interpolation in the Periodic Table: Bimetallic Ammonia Synthesis Catalysts. *J. Am. Chem. Soc.* **2001**, *123*, 8404−8405.

(14) Vojvodic, A.; Medford, A. J.; Studt, F.; Abild-Pedersen, F.; Khan, T. S.; Bligaard, T.; Nørskov, J. K. Exploring the Limits: A Low-Pressure, Low-Temperature Haber-Bosch Process. *Chem. Phys. Lett.* **2014**, *598*, 108−112.

(15) Wang, P.; Chang, F.; Gao, W.; Guo, J.; Wu, G.; He, T.; Chen, P. Breaking Scaling Relations to Achieve Low-Temperature Ammonia Synthesis through LiH-Mediated Nitrogen Transfer and Hydrogenation. *Nat. Chem.* **2017**, *9* (1), 64−70.

(16) Ye, T. N.; Park, S. W.; Lu, Y.; Li, J.; Sasase, M.; Kitano, M.; Hosono, H. Contribution of Nitrogen Vacancies to Ammonia Synthesis over Metal Nitride Catalysts. *J. Am. Chem. Soc.* **2020**, *142* (33), 14374−14383.

(17) Gong, Y.; Li, H.; Li, C.; Bao, X.; Hosono, H.; Wang, J. Insight into Rare-Earth-Incorporated Catalysts: The Chance for a More Efficient Ammonia Synthesis. *J. Adv. Ceram.* **2022**, *11* (10), 1499−1529.

(18) Lin, B.; Liu, Y.; Heng, L.; Wang, X.; Ni, J.; Lin, J.; Jiang, L. Morphology Effect of Ceria on the Catalytic Performances of Ru/CeO2 Catalysts for Ammonia Synthesis. *Ind. Eng. Chem. Res.* **2018**, *57* (28), 9127−9135.

(19) Sato, K.; Nagaoka, K. Boosting Ammonia Synthesis under Mild Reaction Conditions by Precise Control of the Basic Oxide−Ru Interface. *Chem. Lett.* **2021**, *50* (4), 687−696.

(20) Ma, Z.; Zhao, S.; Pei, X.; Xiong, X.; Hu, B. New Insights into the Support Morphology-Dependent Ammonia Synthesis Activity of Ru/CeO2 Catalysts. *Catal. Sci. Technol.* **2017**, *7* (1), 191−199.

(21) Wang, X.; Li, L.; Zhang, T.; Lin, B.; Ni, J.; Au, C. T.; Jiang, L. Strong Metal−Support Interactions of Co-Based Catalysts Facilitated by Dopamine for Highly Efficient Ammonia Synthesis: In Situ XPS and XAFS Spectroscopy Coupled with TPD Studies. *Chem. Commun.* **2019**, *55* (4), 474−477.

(22) Mizoguchi, H.; Okunaka, M.; Kitano, M.; Matsuishi, S.; Yokoyama, T.; Hosono, H. Hydride-Based Electride Material, LnH2 (Ln = La, Ce, or Y). *Inorg. Chem.* **2016**, *55* (17), 8833−8838, DOI: 10.1021/acs.inorgchem.6b01369.

(23) Ooya, K.; Li, J.; Fukui, K.; Iimura, S.; Nakao, T.; Ogasawara, K.; Sasase, M.; Abe, H.; Niwa, Y.; Kitano, M.; Hosono, H. Ruthenium Catalysts Promoted by Lanthanide Oxyhydrides with High Hydride-Ion Mobility for Low-Temperature Ammonia Synthesis. *Adv. Energy Mater.* **2021**, *11* (4), No. 2003723, DOI: 10.1002/aenm.202003723.

(24) Nakaya, Y.; Furukawa, S. Catalysis of Alloys: Classification, Principles, and Design for a Variety of Materials and Reactions. *Chem. Rev.* **2022**, *123* (9), 5859−5947, DOI: 10.1021/ACS.CHEMREV.2C00356/ASSET/IMAGES/MEDIUM/CR2C00356_0069.GIF.

(25) Croisé, C.; Alabd, K.; Tencé, S.; Gaudin, E.; Villesuzanne, A.; Courtois, X.; Bion, N.; Can, F. Influence of the Rare Earth (R) Element in Ru-Supported RScSi Electride-like Intermetallic Catalysts for Ammonia Synthesis at Low Pressure: Insight into NH3 Formation Mechanism. *ChemCatChem* **2023**, *15* (3), No. e202201172, DOI: 10.1002/cctc.202201172.

(26) Croisé, C.; Alabd, K.; Villesuzanne, A.; Can, F.; Courtois, X.; Gaudin, E.; Tencé, S.; Bion, N. Role of Hydride Ion within Ru/LaScSi and Ru/CeTiGe Catalysts for NH3 Synthesis: A Combination of DFT and Experimental Nitrogen Isotopic Exchange Studies. *Catal. Commun.* **2023**, *179*, No. 106689.

(27) Wu, J.; Li, J.; Gong, Y.; Kitano, M.; Inoshita, T.; Hosono, H. Intermetallic Electride Catalyst as a Platform for Ammonia Synthesis. *Angew. Chem., Int. Ed.* **2019**, *58* (3), 825−829.

(28) Li, J.; Wu, J.; Wang, H.; Lu, Y.; Ye, T.; Sasase, M.; Wu, X.; Kitano, M.; Inoshita, T.; Hosono, H. Acid-Durable Electride with Layered Ruthenium for Ammonia Synthesis: Boosting the Activity via Selective Etching. *Chem. Sci.* **2019**, *10* (22), 5712−5718.

(29) Gong, Y.; Wu, J.; Kitano, M.; Wang, J.; Ye, T. N.; Li, J.; Kobayashi, Y.; Kishida, K.; Abe, H.; Niwa, Y.; Yang, H.; Tada, T.; Hosono, H. Ternary Intermetallic LaCoSi as a Catalyst for N2 Activation. *Nat. Catal.* **2018**, *1* (3), 178−185.

(30) Latroche, M.; Percheron-Guégan, A. Structural and Thermodynamic Studies of Some Hydride Forming RM3-Type Compounds (R =

lanthanide, M = transition Metal). *J. Alloys Compd.* **2003**, *356*−*357*, 461−468.
(31) Joubert, J. M.; Paul-Boncour, V.; Cuevas, F.; Zhang, J.; Latroche, M. LaNi5 Related AB5 Compounds: Structure, Properties and Applications. *J. Alloys Compd.* **2021**, *862*, No. 158163.
(32) Santos, D. M. F.; Šljukić, B.; Amaral, L.; Macciò, D.; Saccone, A.; Sequeira, C. Nickel-Cerium Alloys for Borohydride Oxidation. *ECS Trans.* **2013**, *58* (1), 1893−1901.
(33) Tsukuda, R.; Ohhashi, S.; Xu, Y.; Nishimura, C.; Kameoka, S. Catalytic Hydrogenation of C2H2 over Amorphous CeNi2Hx and Crystalline CeNi2: Effects of Hydrogen-Induced Amorphization and Oxidation. *Mater. Trans.* **2022**, *63* (3), 343−350.
(34) Lushnikov, S. A. Desorption of Hydrogen from CeNi3 Intermetallic Hydrides. *Defect Diffus. Forum* **2010**, *297*−*301*, 35−39.
(35) Jiang, Y. F.; Liu, J. C.; Xu, C. Q.; Li, J.; Xiao, H. Breaking the Scaling Relations for Efficient N2-to-NH3 Conversion by a Bowl Active Site Design: Insight from LaRuSi and Isostructural Electrides. *Chin. J. Catal.* **2022**, *43* (8), 2183−2192.
(36) Ye, T. N.; Lu, Y.; Kobayashi, Y.; Li, J.; Park, S. W.; Sasase, M.; Kitano, M.; Hosono, H. Efficient Ammonia Synthesis over Phase-Separated Nickel-Based Intermetallic Catalysts. *J. Phys. Chem. C* **2020**, *124* (52), 28589−28595.
(37) Miyahara, S. I.; Sato, K.; Tsujimaru, K.; Wada, Y.; Ogura, Y.; Toriyama, T.; Yamamoto, T.; Matsumura, S.; Inazu, K.; Nagaoka, K. Co Nanoparticle Catalysts Encapsulated by BaO-La2O3Nanofractions for Efficient Ammonia Synthesis Under Mild Reaction Conditions. *ACS Omega* **2022**, *7* (28), 24452−24460.
(38) Kobayashi, Y.; Kitano, M.; Kawamura, S.; Yokoyama, T.; Hosono, H. Kinetic Evidence: The Rate-Determining Step for Ammonia Synthesis over Electride-Supported Ru Catalysts Is No Longer the Nitrogen Dissociation Step. *Catal. Sci. Technol.* **2017**, *7* (1), 47−50.
(39) Kitano, M.; Inoue, Y.; Yamazaki, Y.; Hayashi, F.; Kanbara, S.; Matsuishi, S.; Yokoyama, T.; Kim, S. W.; Hara, M.; Hosono, H. Ammonia Synthesis Using a Stable Electride as an Electron Donor and Reversible Hydrogen Store. *Nat. Chem.* **2012**, *4* (11), 934−940.
(40) Gong, Y.; Li, H.; Wu, J.; Song, X.; Yang, X.; Bao, X.; Han, X.; Kitano, M.; Wang, J.; Hosono, H. Unique Catalytic Mechanism for Ru-Loaded Ternary Intermetallic Electrides for Ammonia Synthesis. *J. Am. Chem. Soc.* **2022**, *144*, 8683−8692.
(41) Zheng, J.; Liao, F.; Wu, S.; Jones, G.; Chen, T.; Fellowes, J.; Sudmeier, T.; McPherson, I. J.; Wilkinson, I.; Tsang, S. C. E. Efficient Non-dissociative Activation of Dinitrogen to Ammonia over Lithium-Promoted Ruthenium Nanoparticles at Low Pressure. *Angew. Chem.* **2019**, *131* (48), 17496−17502.
(42) Miyahara, S.-i.; Sato, K.; Kawano, Y.; Imamura, K.; Ogura, Y.; Tsujimaru, K.; Nagaoka, K. Ammonia Synthesis over Lanthanoid Oxide−Supported Ruthenium Catalysts. *Catal. Today* **2021**, *376*, 36−40.
(43) Hiromoto, S.; Kano, K.; Suzuki, Y.; Asami, K.; Chiba, A.; Hanawa, T. Surface Characterization and Anodic Polarization of Nitrogen-Ion-Implanted Nickel-Free Co-Cr-Mo Alloy. *Mater. Trans.* **2005**, *46* (7), 1627−1632.
(44) Kitano, M.; Inoue, Y.; Ishikawa, H.; Yamagata, K.; Nakao, T.; Tada, T.; Matsuishi, S.; Yokoyama, T.; Hara, M.; Hosono, H. Essential Role of Hydride Ion in Ruthenium-Based Ammonia Synthesis Catalysts. *Chem. Sci.* **2016**, *7* (7), 4036−4043.
(45) Ye, T. N.; Park, S. W.; Lu, Y.; Li, J.; Sasase, M.; Kitano, M.; Tada, T.; Hosono, H. Vacancy-Enabled N2 Activation for Ammonia Synthesis on an Ni-Loaded Catalyst. *Nature* **2020**, *583* (7816), 391−395.
(46) Li, C.; Shi, Y.; Zhang, Z.; Ni, J.; Wang, X.; Lin, J.; Lin, B.; Jiang, L. Improving the Ammonia Synthesis Activity of Ru/CeO2 through Enhancement of the Metal−Support Interaction. *J. Energy Chem.* **2021**, *60*, 403−409.

https://doi.org/10.1021/acscatal.3c03654
ACS Catal. 2023, 13, 15715−15724

3. Chapter 3: Efficient CeO_2 and CeO_2-Al_2O_3 supports for Ru as 3rd generation ammonia synthesis catalysts: enhanced kinetic mechanism over commercial Ru/CeO_2

Title: Efficient CeO_2 and CeO_2-Al_2O_3 supports for Ru as 3rd generation ammonia synthesis catalysts: enhanced kinetic mechanism over commercial Ru/CeO_2.

Authors: Javier Arroyo−Caire, Mayra Anabel Lara−Angulo, Manuel Antonio Diaz−Perez and Juan Carlos Serrano−Ruiz.

Reference: *Catalysis Science & Technology* 2025, 13, 15715-15724. DOI: https://doi.org/10.1039/D5CY00122F.

Published date: 26 March 2025.

Impact factor: JIF 4.4 (JCR, 2023).

Position: CHEMISTRY, PHYSICAL 68/178 (Q2).

Catalysis Science & Technology

ROYAL SOCIETY OF CHEMISTRY

PAPER

View Article Online
View Journal

Cite this: DOI: 10.1039/d5cy00122f

Efficient CeO_2 and CeO_2–Al_2O_3 supports for Ru as 3rd generation ammonia synthesis catalysts: enhanced kinetic mechanism over commercial Ru/CeO_2†

Javier Arroyo-Caire, [a] Edgar S. Duran-Uribe, [b] Mayra Anabel Lara-Angulo,[a] Manuel Antonio Diaz-Perez,[a] Antonio Sepúlveda-Escribano [b] and Juan Carlos Serrano-Ruiz *[a]

Received 2nd February 2025,
Accepted 25th March 2025

DOI: 10.1039/d5cy00122f

rsc.li/catalysis

Ceria (CeO_2) has been previously reported as a functional support for ruthenium (Ru) as an ammonia synthesis catalyst. However, lab-synthesized ceria materials usually present low surface areas, thereby limiting the generation of oxygen vacancies and the ammonia synthesis activity as a result of weak metal–support interactions. With the aim of overcoming this issue, we prepared, by a simple impregnation method, high surface area ceria and ceria–alumina supported Ru catalysts with improved ammonia synthesis performance at moderate temperatures. In this sense, lab-synthesized Ru/CeO_2 (with higher specific surface area and lower crystallinity than commercial ceria) showed stronger metal–support interactions than the commercial sample, which resulted in a superior global ammonia synthesis kinetic mechanism with more positive hydrogen reaction orders (*i.e.*, more resistant to hydrogen inhibition) and significantly lower activation energies (46 *vs.* 61 kJ mol^{-1}). We found that the use of alumina as a structural support increased the surface area of ceria, thereby promoting the Ru–CeO_2 interaction and the catalytic performance. We analyzed the effect of the surface chemistry of two different commercial aluminas (acidic and basic) with similar surface areas. Basic alumina was found to increase the specific surface area of the catalyst to a larger extent as compared to acidic alumina. Thus, the Ru/CeO_2–Al_2O_3 catalyst with 50 wt% of basic alumina showed an ammonia synthesis activity of 1.9 mmol g^{-1} h^{-1} at 400 °C and ambient pressure and an activation energy as low as 44.8 kJ mol^{-1}.

Introduction

The change in the global energy paradigm during the last few decades shows a scenario in which green ammonia (NH_3) could be used as a chemical platform for decentralized green hydrogen (H_2) plants.[1–3] The current industrial process producing NH_3 from H_2 is incompatible with the use of renewables since harsh temperature (400–600 °C) and pressure (20–60 MPa) conditions are required to produce ammonia.[4] Such high temperatures are required to activate the N_2 molecule and break the stable N≡N triple bond. Thus, high pressures are on demand in order to circumvent both kinetic and thermodynamic limitations since the ammonia synthesis reaction is highly exothermic (*ca.* −92 kJ $mol_{NH_3}^{-1}$).[5]

Therefore, to successfully complete the transition into the new global green hydrogen scenario, the ammonia synthesis process needs to overcome several challenges, mainly related to the catalytic reaction system.[6,7] In this context, several alternatives to the conventional thermocatalytic ammonia synthesis process are being proposed by the research community, including plasma,[8,9] mechanocatalytic synthesis,[10] chemical looping,[11–13] photothermal catalysis[14] and electrocatalytic synthesis.[15,16]

However, given the early stage of research of these processes, the investigation efforts to design efficient catalysts for thermocatalytic ammonia synthesis under mild conditions have also grown exponentially within the last two decades.[17–19] The most recent studies are focused on the development of stable and efficient catalysts based on non-noble metals, although the complex synthesis methods and conditions required represent a difficulty for their application

[a] *Materials and Sustainability Group, Department of Engineering, Universidad Loyola Andalucía, Avda. de las Universidades s/n, Dos Hermanas, 41704 Seville, Spain. E-mail: jarroyo@uloyola.es, malangulo@uloyola.es, madiaz@uloyola.es, jcserrano@uloyola.es; Tel: +34 955 641 600 ext. 2579*

[b] *Instituto Universitario de Materiales de Alicante (IUMA), Departamento de Química Inorgánica, Universidad de Alicante – Instituto Universitario de Materiales de Alicante (IUMA), Apartado 99, Alicante 03080, Spain*

† Electronic supplementary information (ESI) available. See DOI: https://doi.org/10.1039/d5cy00122f

scalability.[20,21] In this sense, most novel catalysts mainly rely on the performance of complex and sometimes non-stable functional supports such as electrides, hydrides, nitrides or intermetallics,[17–19,22–25] which limits their practical applicability.

Rare earth metal oxides have been reported to present excellent electronic properties under strong metal–support interaction (SMSI) conditions, *i.e.*, they can serve as electron donors for the transition metal (TM), thereby promoting nitrogen dissociation, which is usually the rate determining step (RDS) of the process.[26] Cerium oxide, the most abundant rare earth oxide, forms oxygen vacancies upon reduction, thereby promoting the metal (*e.g.*, Ru, Co) by forming new interfacial metal–CeO_{2-x} sites[27] for the ammonia synthesis and promoting metal electronic donation. Thus, Ru/CeO_2-based catalysts have been reported to be more efficient than 1st generation Fe-based and 2nd generation Ru-based catalysts such as Ru/MgO or Ru/C.[19]

However, commercial ceria usually suffers from low surface area, which reduces the extent of the metal–support interaction and ultimately results in apparent activation energies significantly higher as compared to catalysts based on novel supports such as electrides and hydrides.[17,18] Therefore, the design of ceria-based catalysts with higher surface area and optimum metal–support interaction can increase both the number and activity of Ru sites in the ammonia synthesis reaction. One of the methods to increase the surface of ceria is the use of a high surface area material as a structural support. In this sense, alumina (Al_2O_3) is a widely used structural support in many applications in the field of thermocatalysis, since it has optimal structural properties. With regard to the ammonia synthesis, Al_2O_3 has been used as a structural promoter for Fe and some attempts were also made for Ru. However, it was concluded that acid sites from alumina can strongly interact with the NH_3 molecule, hindering its desorption.[22] Therefore, basic supports, such as rare earth-based materials, are usually preferred as structural promoters.[28] Also, considering that the SMSI between Ru and CeO_2 mainly takes place on the catalyst surface,[29] it could be interesting to substitute a fraction of the ceria-based support with cheaper alumina, as long as the support surface could be covered by ceria.

In this work, we analyse the differences in terms of performance between two different materials as supports for Ru: commercial ceria (to be named as $CeO_2|_C$) and cerium oxide made by a simple impregnation–calcination method from cerium nitrate (to be named as lab-synthesized cerium oxide: $CeO_2|_{AS}$). We demonstrate that the lab-synthesized ceria outperforms the commercial ceria as a result of its higher surface area and lower crystallinity, which led to the formation of a higher concentration of more reactive surface oxygen vacancies. The impregnation–calcination synthesis method used herein allowed preparation of a ceria support with improved kinetic properties in the ammonia synthesis reaction as compared to commercial ceria.

Furthermore, we study the impact of the structural promotion of ceria with two types of different Al_2O_3 materials using a similar impregnation–calcination procedure. We found that the acid sites of γ-Al_2O_3 played a detrimental role in the performance of the Ru/CeO_2–Al_2O_3 catalysts, whereas basic Al_2O_3 allowed the kinetic performance of Ru/CeO_2 to be improved.

Materials and methods

Catalyst preparation

The lab-synthesized ceria support was prepared using an aqueous solution of $Ce(NO_3)_3{\cdot}6H_2O$ (99 wt% trace metal basis, Sigma-Aldrich). After the complete dissolution of cerium nitrate, the solution was evaporated overnight and the resulting solid was calcined at 400 °C for 6 h (2 K min^{-1}). Cerium oxide was softened by hand-milling with an agate mortar.

Ceria–alumina supports were prepared by aqueous impregnation of $Ce(NO_3)_3{\cdot}6H_2O$ in an aqueous suspension of any of the two different aluminium oxide materials: basic alumina (activated basic, Brockmann I, Sigma-Aldrich) and acidic alumina (anhydrous γ-alumina, Merck). The impregnation was carried out by stirring the suspension at room temperature for 6 h. After the impregnation and subsequent overnight evaporation, the support materials were calcined at 400 °C for 6 h (2 K min^{-1}) and then softened by hand-milling with an agate mortar.

Ruthenium(III) acetylacetonate (Ruacac 97%, Sigma-Aldrich) was used as the Ru precursor. The catalysts with a 5 wt% loading of Ru were prepared by impregnation of Ruacac onto the supports previously synthesized in ethanol. After impregnation, the suspensions were evaporated, and the catalysts were homogenized using an agate mortar. A pre-reduction treatment was applied to all the catalysts, following previously reported methods.[30] During the pre-reduction stage, the catalyst was treated under a pure H_2 flow at 400 °C for 3 h, following a heating rate of 10 °C min^{-1}. Then, a treatment with a mixture of N_2 + H_2 = 1 : 3 was carried out for 15 h.

Kinetic experiments

The kinetic tests were carried out in a micro-reaction system with automated integral pressure, temperature, gas flow and composition control (Microactivity-Effi, PID, Micromeritics) in a 316SS fixed-bed reactor. A mixture of N_2/H_2 = 1 : 3 with a total gas flow of 60 N mL min^{-1} was set up, with a catalyst loading of 0.1 g and a space velocity of 36 000 mL g^{-1} h^{-1}. To ensure that the reaction conditions are far away from equilibrium limitations, the base case is set up at 400 °C and atmospheric pressure. For the calculation of N_2 and H_2 reaction orders, He was used as an inert diluent gas. With the aim of obtaining accurate temperature measurements, a thermocouple was placed into the catalyst bed. The produced ammonia was trapped in an aqueous solution of diluted sulfuric acid (5 mM) and the ammonium ion (NH_4^+)

concentration was measured by means of an ion chromatograph (Dionex Easion, Thermo Scientific).

The reproducibility of the kinetic experiments was checked as follows: a repetition of the whole kinetic mapping for each catalyst was carried out in different runs until the values of the ammonia reaction rate under the base case conditions and the activation energies showed a standard deviation below 10% over the average.

The procedure for the calculation of the reaction orders is shown in the ESI,† section S1.

Characterization

Nitrogen physisorption experiment measurements (ASAP 2020 Plus, Micromeritics) were used to obtain the Brunauer–Emmett–Teller (BET) specific surface areas of the catalysts. Crystalline patterns were analysed by means of X-ray diffraction (XRD, Bruker D8-Advance) with Cu Kα radiation. X-ray fluorescence spectroscopy (XRF, Zetium de PANalytical) was carried out to measure the bulk composition of all the catalysts. Surface analyses were done by means of X-ray photoelectron spectroscopy (XPS, NEXSA, Thermo-Scientific), using monochromatized Mg Kα radiation. Binding energies were calibrated with the carbon C–C 1s peak (284.6 eV). H_2 temperature programmed reduction (H_2-TPR) analyses were done to study the SMSI and the formation of oxygen vacancies. A gas flow of 100 mL min^{-1} with a composition of 5% H_2 into He was used, with a heating ramp of 10 °C min^{-1}. The outlet gas composition was measured using a mass spectrometer (Omnistar GSD 301 O_2, Pfeiffer Vacuum). High-angle annular dark-field scanning transmission electron microscopy (HAADF-STEM) experiments were conducted using a Talos F200X (Thermo Fisher Scientific) microscope, with high-resolution scanning (HRSTEM: 0.16 nm @200 kV). CO_2-TPD was carried out on a thermogravimetric analyzer (TGA SDT650, TA Instruments) coupled with a mass spectrometer (ThermoStar, Pfeiffer Vacuum). 35–60 mg of catalysts were loaded in a 90 μm alumina crucible. All the catalysts were pre-treated under pure Ar to 500 °C, after which the sample was cooled down to room temperature. Once at room temperature, CO_2 was fed to the reactor for 2 h to allow adsorption. Then, the temperature was raised to 40 °C under pure Ar to allow removal of the physisorbed CO_2. Finally, the TPD was conducted from 40 to 800 °C with a heating rate of 10 °C min^{-1}.

Inductively coupled plasma atomic emission spectroscopy (ICP-OES) experiments were conducted using the system Optima 7300 DV with dual vision (Perkin Elmer) in order to measure the Ru content of the catalysts and compare with the XRF results. Prior to the ICP experiments, the samples were dissolved in a mix of nitric acid and hydrochloric acid (1 : 3) under microwave conditions. Then, a scaling temperature program was followed up to 250 °C. After cooling down, the samples were filtered and diluted in ultrapure water.

Results and discussion

Lab-synthesized ceria *vs.* commercial ceria

The N_2 physisorption results for both commercial and lab-synthesized ceria-based catalysts are shown in Fig. 1a. The simple impregnation–calcination synthesis method used

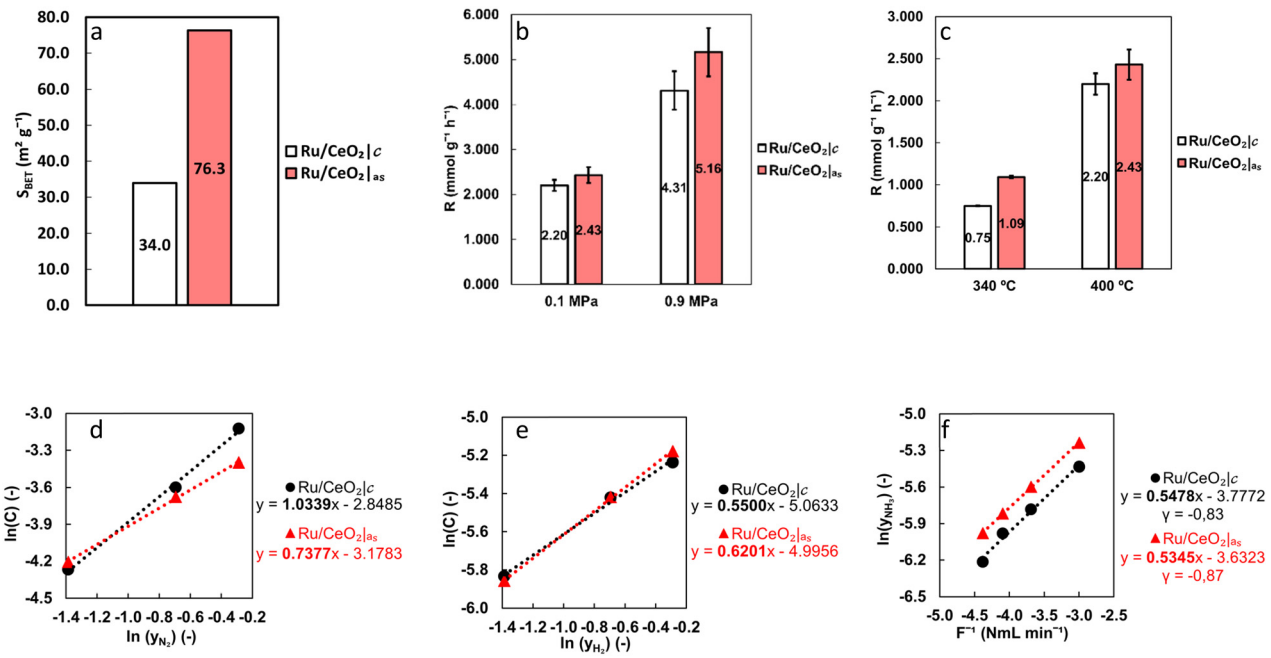

Fig. 1 (a) Specific surface area of $Ru/CeO_2|_C$ and $Ru/CeO_2|_{AS}$. (b) Ammonia synthesis rates at 0.1–0.9 MPa and 400 °C. (c) Ammonia synthesis rates at 340–400 °C and 0.1 MPa. (d) Nitrogen reaction order (α) plot, determined at 400 °C and 0.1 MPa. (e) Hydrogen reaction order (β) plot, determined at 400 °C and 0.1 MPa. (f) Ammonia reaction order (γ) plot, determined at 400 °C and 0.1 MPa.

herein resulted in a material with a significantly higher specific surface area as compared to the commercial sample (76.3 *vs.* 34.0 $m^2\ g^{-1}$). This difference in the specific surface area is important since the catalytic activity of Ru-based catalysts in this reaction has been found to be strongly influenced by the metal shape and particle size,[31,32] as well as by the support morphology.[29] Interestingly, the specific surface area obtained for $Ru/CeO_2|_{AS}$ was higher than other typical ceria-based catalysts (Table S1†), which highlights the success of our simple impregnation–calcination synthesis.

The ammonia synthesis rates for both catalysts at low and high pressure are shown in Fig. 1b. $Ru/CeO_2|_{AS}$ showed slightly higher activity than $Ru/CeO_2|_C$ at 0.1 MPa (2.43 *vs.* 2.20 mmol $g^{-1}\ h^{-1}$). Both values were higher than those reported for other Ru/CeO_2 catalysts under the same operating conditions.[27] The performance gap between both catalysts further increased to 20% at higher pressures (5.16 mmol $g^{-1}\ h^{-1}$ for $Ru/CeO_2|_{AS}$ and 4.31 mmol $g^{-1}\ h^{-1}$ for $Ru/CeO_2|_C$). This pressure effect is intimately related to the kinetic efficiency, in particular, to the resistance towards hydrogen poisoning.[33] Thus, these results revealed a more efficient global kinetic mechanism for $Ru/CeO_2|_{AS}$.[21,34]

The effect of the operating temperature on the ammonia synthesis performance was studied by performing runs at 400 (base case) and 340 °C (Fig. 1c). The relative difference in terms of performance between both catalysts was 4-fold higher at 340 °C, as compared to that observed at 400 °C. The Arrhenius analysis revealed an activation energy of 61.3 kJ mol^{-1} for $Ru/CeO_2|_C$ (Fig. S4b†), while a noticeably low value of 46.1 kJ mol^{-1} was obtained for $Ru/CeO_2|_{AS}$ (Fig. S4f†). This activation energy was significantly lower than those reported for other similar Ru/CeO_2 catalysts (Table S1†) and comparable to those of the best ammonia synthesis 3rd generation catalysts such as complex single atom catalysts (SACs), intermetallics and hydrides.[17–19,27] This outstanding performance highlights the success of the simple synthesis method used herein.

In the case of those catalysts following a dissociative mechanism, such as Ru/CeO_2, it is well known that the lower the activation energy, the more efficient the N_2 dissociation and activation step, which is usually the RDS of the reaction.[18,35–37] This was further confirmed by the N_2 reaction order analysis. Typical N_2 (α), H_2 (β) and NH_3 (γ) reaction order plots are shown in Fig. 1d–f, respectively. While β and γ were similar for both catalysts, α was 29% lower for $Ru/CeO_2|_{AS}$ (ref. 35) compared to $Ru/CeO_2|_C$, revealing a lower importance of the N_2 dissociation step for $Ru/CeO_2|_{AS}$. It is also remarkable that β was positive for both catalysts, which suggests that hydrogen poisoning is not relevant over these catalysts, in line with the positive pressure effect shown in Fig. 1b.[38] Interestingly, $Ru/CeO_2|_{AS}$ showed higher β values than the commercial sample (0.62 *vs.* 0.55, Fig. 1e), thereby revealing a higher resistance to hydrogen inhibition over these catalysts. Moreover, the highly negative values of γ (*ca.* −0.8) indicate that NH_3 is prone to be adsorbed over the catalysts, so the formation of NH_x species (rather than the N_2 dissociation step) plays a crucial role in the global kinetic scheme.[38]

With the aim of gaining insight into the reasons for the different performances of $Ru/CeO_2|_{AS}$ and $Ru/CeO_2|_C$, further characterization was carried out. Since the specific surface area of $Ru/CeO_2|_{AS}$ was significantly higher than that of the commercial sample, it is expected that ceria has a lower particle size in this sample, leading to an improved metal–support interaction upon reduction.[39]

An analysis of the Ru dispersion was carried out by means of HAADF-STEM with EDX mapping (Fig. 2a and b). Ru was found to be well dispersed over CeO_2 for both catalysts, although the lab-prepared sample showed optimum dispersion results (Fig. 2b). The HAADF-STEM pictures of all the catalysts characterized in this work are shown in Fig. S2,† whereas the EDX mapping with the contrast between Ru and Ce is shown in Fig. S3.† $Ru/CeO_2|_C$ (Fig. S2a†) was found to present an organized structure in the form of nanoplatelets, whereas $Ru/CeO_2|_{AS}$ (Fig. S2e†) seemed to be more amorphous. The $Ru/CeO_2|_{AS}$ sample showed minor Ru agglomeration, which can be ascribed to the simplicity of the synthesis method.

These results were further confirmed by XRD (Fig. 2c). The crystalline pattern showed peaks corresponding to the fluorite structure of CeO_2, which means that the support preserves the original Ce^{4+} crystalline lattice after the pre-reduction process. $Ru/CeO_2|_{AS}$ showed less intense and wider diffraction peaks than $Ru/CeO_2|_C$, revealing lower crystallinity. In order to quantify the difference in the crystallinity between both catalysts, the crystallite sizes of the first peak *i.e.*, $2\theta = 28.5°$, were obtained using the Scherrer equation shown in eqn (1).

$$D_C = \frac{K \cdot \lambda}{\beta \cdot \cos\theta} \quad (1)$$

where "D_C" is the crystallite size, "K" is the shape factor (a value of 0.9 was taken as an approximation in this case), "λ" is the X-ray wavelength, "β" is the full width at half maximum (FWHM) of the peak and "θ" is the peak angle (half of 2θ). Since the key point is a comparison between the crystallite sizes for both catalysts, an arbitrary value of 0 was taken for the instrumental line broadening, which leads to an approximation of the values of the crystallite sizes. As expected, $RuCeO_2|_C$ showed a significantly higher CeO_2 crystallite size than the $RuCeO_2|_{AS}$ sample (22.8 *vs.* 9.4 nm). As reported in previous studies, the lower the crystallinity, the higher the presence of structural defects. These results are in line with the improved kinetic mechanism for ammonia synthesis of the lab-synthesized sample as a result of an optimum Ru–CeO_2 contact.[40]

The surface oxygen vacancies generated upon hydrogen reduction at 400 °C promoted the formation of interfacial metal–CeO_{2-x} active sites[27] *via* metal–support interactions. In order to gain insight into the Ru–CeO_2 interaction, H_2-TPR experiments were conducted, from which the

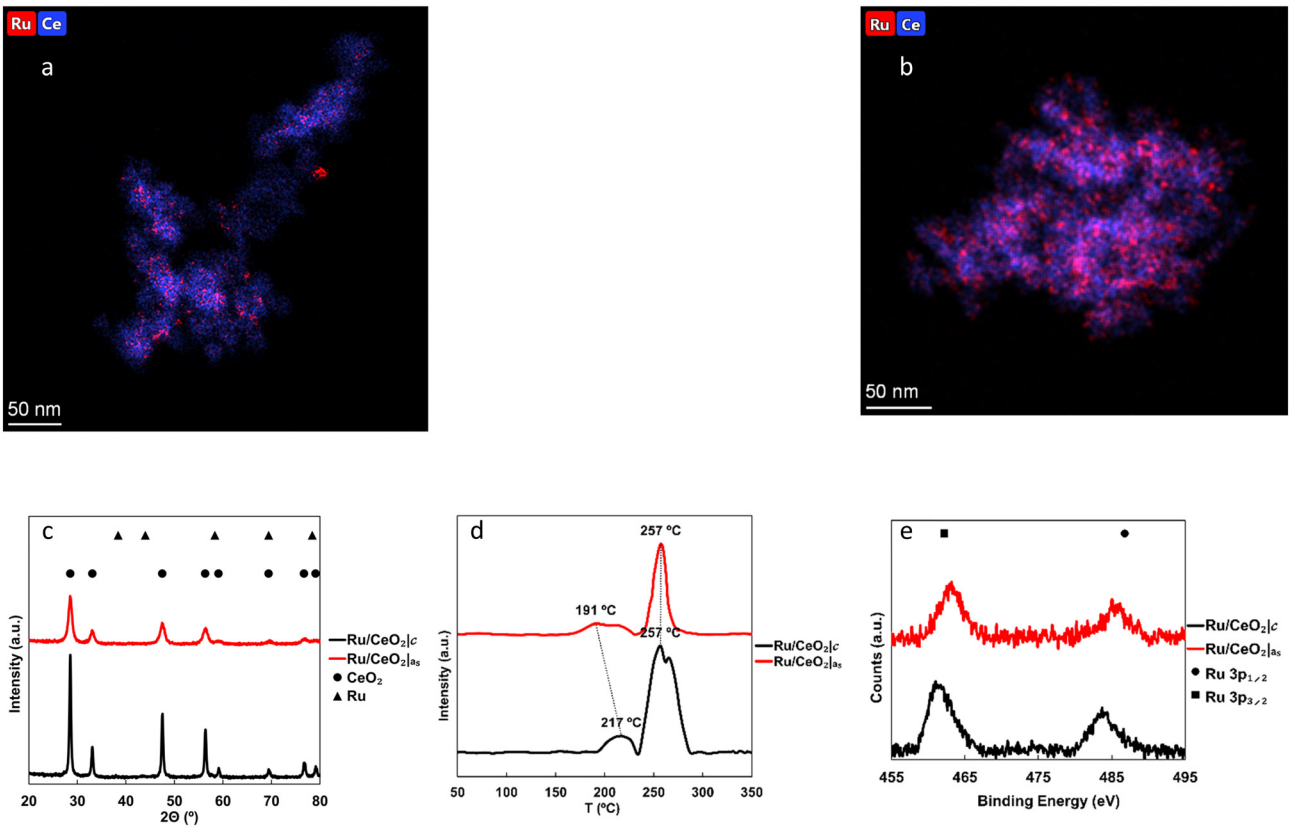

Fig. 2 Ru coupled to Ce elemental EDX mapping from HAADF-STEM results of the (a) commercial ceria catalyst and (b) lab-synthesized ceria catalyst. (c) XRD patterns. (d) H_2-TPR profiles. (e) Ru 3p XPS spectra.

generation of oxygen vacancies and the specific role of the interactions between Ru and CeO_2 can be inferred. The H_2 (m/z = 2) profiles for both catalysts are shown in Fig. 2d. No reduction peaks were found at temperatures typical of the reduction of Ru oxides[41] (below 180 °C), revealing that Ru is in the form of Ru^0. The fact that Ru is not present as oxidized species can explain the absence of large Ru particles and agglomerates revealed by TEM (Fig. 2a and b). Thus, the preparation method used herein led to well dispersed Ru particles avoiding the formation of Ru oxide patches which are typical of impregnation–calcination processes.[22] Two main reduction peaks were observed in the TPR profiles: one peak at low temperature (<250 °C) was attributed to the reduction of surface ceria in intimate contact with Ru, whereas the peak at higher temperature (>250 °C) corresponded to the reduction of surface ceria not in close contact with Ru. The reduction of surface ceria in close contact with Ru can be associated with SMSI between Ru and CeO_2.[29] By comparing the TPR profiles of the catalysts and the supports (Fig. S4a†), it can be inferred that Ru improved the reducibility of ceria, most likely by a hydrogen spillover process.[42] $Ru/CeO_2|_{AS}$ showed lower reduction temperatures for surface CeO_2 in contact with Ru as compared to $Ru/CeO_2|_C$ (191 *vs.* 217 °C, Fig. 2d). These results revealed a more intense metal–support interaction for $Ru/CeO_2|_{AS}$ and, potentially, an enhanced electron transfer between CeO_2 and Ru, which could account for its superior activity and the different kinetic mechanisms of both catalysts.[40] Reduction of the surface CeO_2 not in close in contact with Ru took place at a similar temperature for both catalysts (257 °C).

X-ray photoelectron spectroscopy (XPS) analyses were conducted to analyse surface Ru species (Fig. 2e). The Ru XPS spectra revealed the presence of two bands, namely, $3p_{1/2}$ attributed to Ru^{3+} species[43] and $3p_{2/3}$ assigned to Ru^0.[44] Thus, XPS results revealed the presence of oxidized Ru species which probably formed upon air exposure prior to XPS analyses. We note that, prior to the reaction kinetic measurements, the catalysts were pre-reduced *in situ* at 400 °C for 3 h to ensure that no oxidized Ru species were present on the catalyst surface before the reaction. This *in situ* pre-reduction step was also carried out before the TPR experiments such that no reduction peaks originating from Ru species are expected to appear in the TPR profiles.

In conclusion, the simple impregnation–calcination method used herein led to the formation of a low crystallinity cerium oxide with a higher surface area, as compared to the commercial ceria. $Ru/CeO_2|_{AS}$ showed a high degree of crystalline defects, which promote the formation of more active surface oxygen vacancies for those CeO_2 active sites in contact with Ru, showing an enhanced SMSI. This enhanced catalyst showed an outstanding performance for low-

Table 1 Nomenclature of $Ru/CeO_2–Al_2O_3$ catalysts

Sample	Alumina	Ceria	CeO_2 (wt%)
S1	—	Commercial	100
S2	Acidic		20
S3			50
S4			80
S5	—	Lab-synthesized	100
S6	Basic		20
S7			50
S8			80

temperature ammonia synthesis (*e.g.*, low activation energy) and a more efficient kinetic mechanism.

Structural promotion with basic and acidic alumina

As explained in the previous section, the formation of a high surface area low-crystallinity cerium oxide resulted in a Ru/CeO_2 catalyst with improved metal–support interaction and excellent low-temperature ammonia synthesis performance. With the aim of increasing the surface area of the cerium oxide and enhancing the $Ru–CeO_2$ interaction, we used alumina as a structural support. Two different aluminium oxide materials with similar specific surface areas (basic and acidic) were used as structural promoters.

The nomenclature of the samples is shown in Table 1, with samples S1 and S5 being respectively $Ru/CeO_2|_C$ and $Ru/CeO_2|_{AS}$ described in the previous section. The specific surface area of the samples is shown in Fig. 3a as a function of the ceria loading. As shown in Fig. 3a, the utilization of small amounts of alumina (*e.g.*, 20 wt%) resulted in a significant increase of the BET surface area, especially for basic alumina. In the case of acidic alumina, the specific surface area of the catalyst remained nearly unchanged as the alumina loading increased from 20 to 80 wt%. The N_2 isotherms for the specific surface area determination are shown in Fig. S1.†

The activity of the $Ru/CeO_2–Al_2O_3$ catalysts in the ammonia synthesis reaction was measured as a function of the ceria loading (Fig. 3b) under base case conditions (400 °C and 0.1 MPa). In the case of basic alumina, the ammonia synthesis rate increased continuously with the ceria loading, with a maximum value of 2.18 mmol g^{-1} h^{-1} for the sample with 80 wt% of ceria. In the case of the acidic alumina, the sample with 50 wt% of ceria showed an optimum activity (2.28 mmol g^{-1} h^{-1}) and only slightly lower activity than the pure ceria sample $Ru/CeO_2|_{AS}$ (S5) despite containing half of the ceria loading. These results also revealed that ceria plays a key role in promoting the ammonia synthesis reaction on Ru. In fact, once the ceria loading was reduced to 20 wt%, the ammonia synthesis rate decreased considerably, reaching values in the 0.5–0.7 mmol g^{-1} h^{-1} range for both basic and acidic alumina catalysts. This decrease can be explained by Ru–Ce sites being partially replaced with Ru–Al sites, which are not active considering that alumina is not a functional support for Ru.[45]

Significant differences were found in the kinetic behaviour of the catalysts for both aluminas. Thus, the catalysts supported on acidic alumina showed higher activation energies than those supported on basic alumina

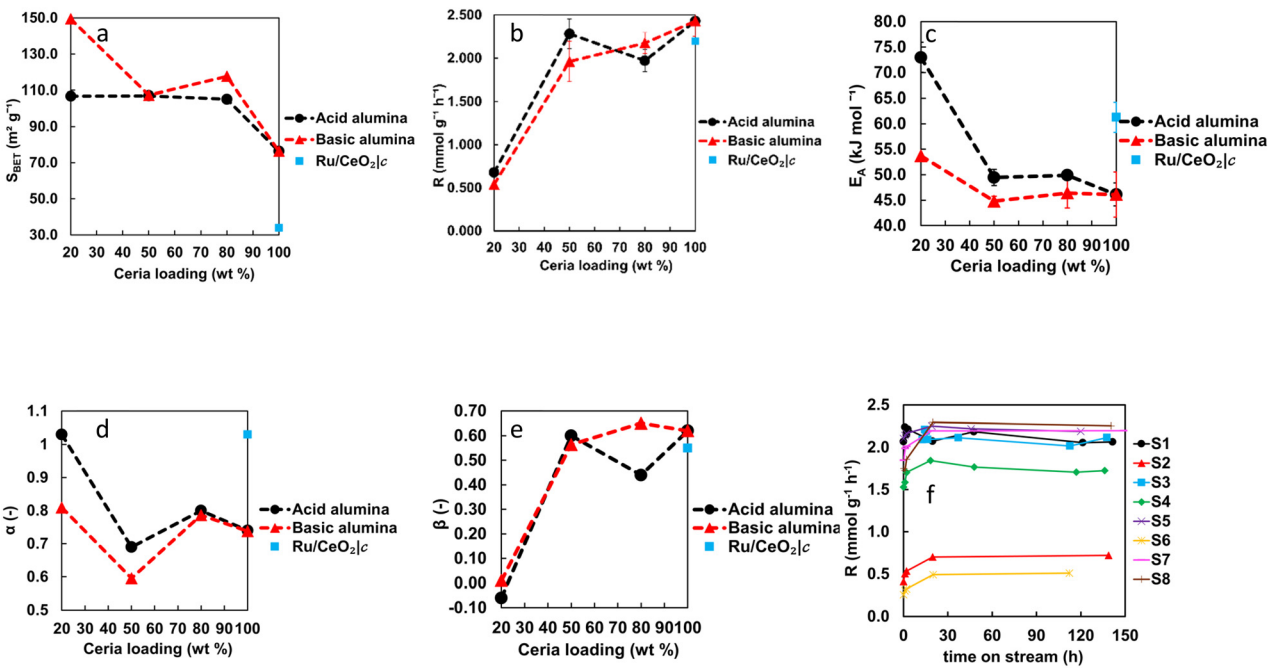

Fig. 3 (a) Specific surface area of $Ru/CeO_2–Al_2O_3$ catalysts as a function of the ceria loading. (b) Ammonia synthesis rates in the base case conditions as a function of the ceria loading. (c) Activation energies at 400 °C and 0.1 MPa as a function of the ceria loading. (d) Nitrogen reaction order at 400 °C and 0.1 MPa as a function of the ceria loading. (e) Hydrogen reaction order at 400 °C and 0.1 MPa as a function of the ceria loading. (f) Long-term performance at 400 °C and 0.1 MPa.

and $Ru/CeO_2|_{AS}$ (Fig. 3c). The Arrhenius plots for all the catalysts are shown in the ESI† (Fig. S3b–i). Interestingly, the activation energy of the 20 wt% ceria catalyst supported on acidic alumina was as high as 73.0 kJ mol^{-1} (*versus* 53.7 kJ mol^{-1} for the same catalyst supported on basic alumina). This result seems to indicate that the acid sites of γ-alumina have a detrimental effect on the $Ru–CeO_2$ interaction, thereby increasing the apparent activation energy for the reaction. Also, as previously reported, acid sites on the support strongly adsorb the ammonia produced (*i.e.*, ammonia poisoning), negatively affecting the global catalyst performance.[28,46] Basic alumina catalysts slightly outperformed $Ru/CeO_2|_{AS}$ in terms of an enhanced kinetic mechanism, with an optimum activation energy of 44.8 kJ mol^{-1} for a ceria loading of 50 wt%. This result is interesting in that 50% of ceria can be replaced with cheaper alumina with a minimum effect on the activity and an improved kinetic mechanism.

Nitrogen (α), hydrogen (β), and ammonia (γ) reaction orders are shown in Fig. S5a–c,† respectively. The dependence of α and β on the ceria loading is shown in Fig. 3d and e, respectively. For both acidic and basic alumina, the nitrogen reaction orders reached minimum values at a ceria loading of 50 wt% (0.69 and 0.60, respectively). Overall, catalysts supported on basic alumina showed lower nitrogen reaction orders than catalysts supported on acidic alumina. These results are in line with the Arrhenius results (Fig. 3c) revealing a facilitated nitrogen dissociation and activation pathway for catalysts supported on basic alumina. Noticeably, the 50 wt% ceria catalyst supported on basic alumina showed lower nitrogen reaction orders than $Ru/CeO_2|_{AS}$ (0.60 *vs.* 0.74). With regard to hydrogen reaction orders, positive values were obtained for ceria loadings higher than 50 wt%, thereby ruling out hydrogen inhibition (unlike catalysts with 20 wt% of ceria).

All the catalysts tested in this work showed excellent long-term stability (Fig. 3f). After an initial activation stage of *ca.* 24 h, variations in the ammonia synthesis rate below 10% under base case conditions (400 °C and 0.1 MPa) were found in all cases for more than 100 h on stream.

The HAADF-STEM pictures of the alumina-supported catalysts are shown in Fig. S2.† Unlike $Ru/CeO_2|_C$, none of the $Ru/CeO_2–Al_2O_3$ catalysts seem to present a clearly defined structure, probably because of the poor crystallinity of both

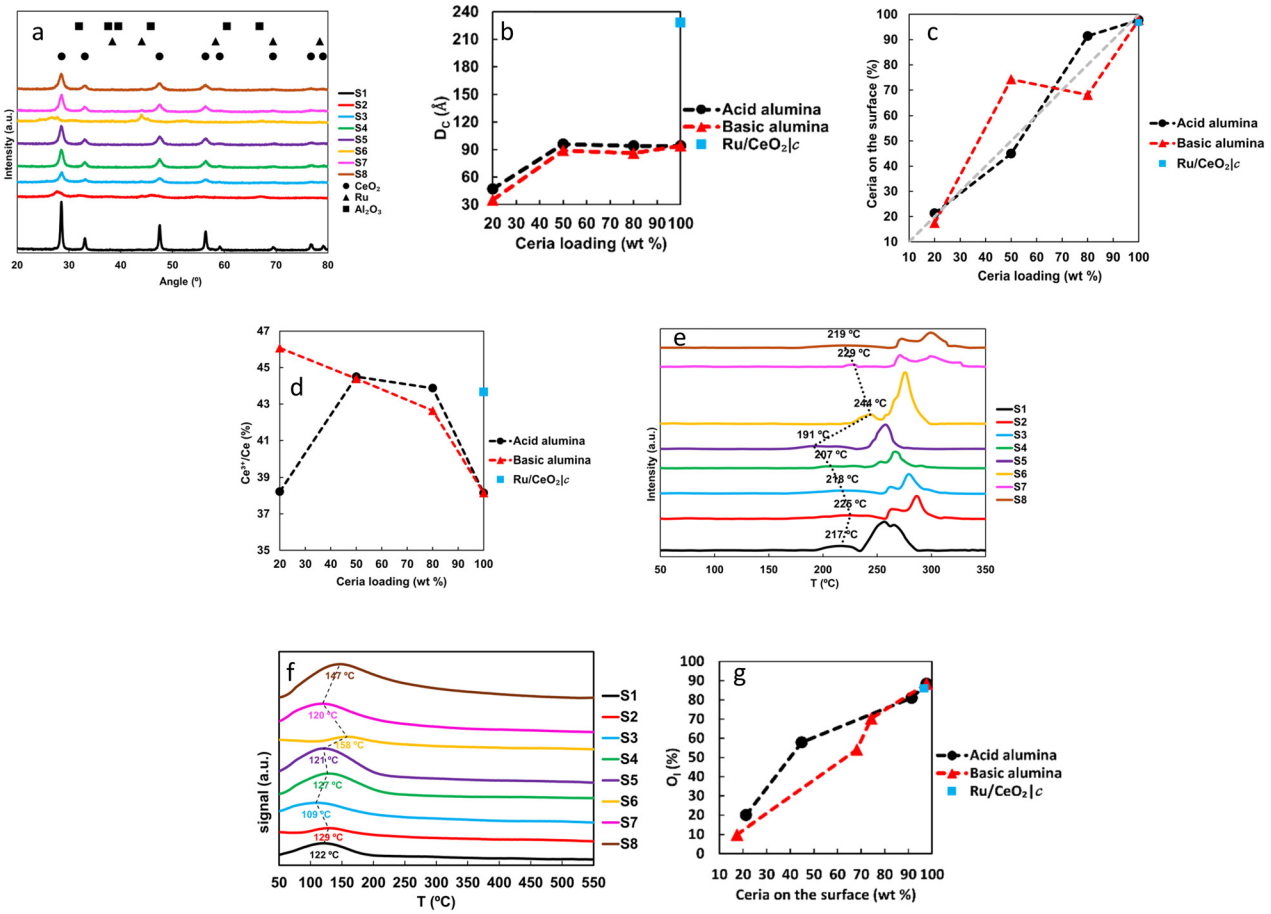

Fig. 4 Characterization of $Ru/CeO_2–Al_2O_3$ catalysts: (a) XRD patterns and (b) CeO_2 crystallite sizes. (c) Surface ceria content as a function of ceria loading determined by XPS. (d) Surface Ce^{3+} concentration as a function of ceria loading determined by XPS. (e) H_2-TPR profiles. (f) CO_2-TPD profiles. (g) Proportion of metal lattice oxygen species O_l from the O 1s XPS spectra as a function of the concentration of Ce on the catalyst surface.

aluminas after the calcination process (Fig. S5d†). Elemental EDX patterns of Ru, Ce and La (Fig. S3†) revealed poorer Ru dispersion for the alumina-based catalysts as compared to $Ru/CeO_2|_{AS}$ (Fig. S3e†).

The XRD patterns of the CeO_2–Al_2O_3 samples (Fig. 4a) showed no evidence of Al_2O_3 phases, in line with the poor crystallinity of these materials. CeO_2 crystallite sizes (calculated by the Scherrer equation, Fig. 4b) similar to those of $Ru/CeO_2|_{AS}$ were found for ceria loadings of 50 and 80 wt%, with samples supported on basic alumina showing slightly lower ceria crystallite sizes than their acidic alumina-supported counterparts. However, this difference seems to be marginal to explain the differences in terms of performance of both aluminas. Overall, the CeO_2 crystallite size for all the ceria–alumina based catalysts does not account for the different kinetic behaviour explained above. A simulation of the reference patterns from CeO_2, Al_2O_3 and Ru found in the database is shown in Fig. S5e† for clarity.

As aforementioned, the SMSI is related to the Ru–Ce interactions at the catalyst surface. In order to study the distribution of the different elements on the catalyst surface and their oxidation state, XPS analyses were conducted. The distribution of Al, Ce and Ru was calculated assuming that these elements were present on the surface in the form of Al_2O_3, CeO_2 and Ru^0, respectively, as an approximation, since those are the expected chemical species for Al, Ce and Ru, respectively. The amount of CeO_2 on the surface as a function of the ceria loading is shown in Fig. 4c. For acidic alumina catalysts, there is a direct relationship between the ceria loading and the amount of ceria present on the catalyst surface, with maximum deviations of 12 wt% between both parameters, thus revealing that cerium oxide is well dispersed over the alumina matrix. Conversely, the basic alumina catalysts with 50 wt% loading showed the highest deviation between the ceria contents on the catalyst surface and in the bulk, which could explain the good kinetic properties of this catalyst (*e.g.*, low activation energy, low nitrogen reaction order and positive hydrogen reaction order). In order to gain insight into the reducibility of the ceria on these catalysts, a previously reported method was used to calculate the distribution of Ce^{3+} and Ce^{4+} from the deconvoluted XPS patterns.[47] These results are shown in Fig. 4d, whereas the Ce 3d XPS patterns are shown in Fig. S6a.† For basic alumina catalysts, the lower the ceria loading, the higher the amount of surface Ce^{3+}. In the case of acidic alumina catalysts, the amount of surface Ce^{3+} reached a maximum for a ceria loading of 50 wt%, in line with the kinetic results revealing an optimum performance for this catalyst among the acidic alumina-based materials. The XPS patterns for Ru are shown in Fig. S6b.†

We have analysed the XPS results of our catalysts. In particular, the surface oxygen species on the catalysts were studied by analysing the O 1s spectra. Following the methodology of previous reports,[48,49] we have deconvoluted the O 1s band into three main peaks (Fig. S7†), which can be ascribed to different oxygen species. Thus, the peak at low binding energy (*ca.* 529.1–530.8 eV, O_l) is usually attributed to ceria lattice oxygen species in close contact with Ru (Ru–O–Ce), the second peak at *ca.* 530.9–532.0 eV is ascribed to ceria surface oxygen vacancies (O_v), while the third peak (*ca.* 531.5–533.5 eV) can be ascribed to adsorbed oxygenated species such as water and oxygen (O_s). The first two species (O_l and O_v) are associated with the presence of Ru–CeO_2 interactions leading to both electronic and structural interactions that result in catalytic promotion of Ru in this reaction. We quantified the amount of these species from the deconvoluted XPS spectra and the results are reported in a new table (Table 2). Interestingly, as shown in Fig. 4g, the number of O_l species was found to be directly related to the surface concentration of CeO_2 determined by XPS. On the other hand, the amount of ceria oxygen vacancies (O_v) increased with the alumina content since the structural promotion of Al_2O_3 leads to higher CeO_2 dispersions on the catalysts (Table 2). Thus, there seems to be a trade-off between the number of Ru–O–Ce sites (which increases with the ceria loading) and the number of oxygen vacancies (which increases with the alumina loading). This trade-off could explain the optimum activation energy found for the 50% CeO_2 supported on basic alumina (Fig. 3c).

XRF (Fig. S6c†) revealed similar tendencies to those observed in the XPS results for the surface ceria content. Furthermore, a Ru effective loading of 2–3% was achieved for all the catalysts reported in this work, with no significant relationship between Ru and CeO_2 loadings (Fig. S6d†) for both acidic and basic alumina-based catalysts.

The Ru loading was also determined by ICP-OES and the results are reported in Table 3. ICP results slightly differed

Table 2 Percentage amounts of O 1s species obtained by deconvolution of the XPS O 1s band

Sample	O_l (%)	O_v (%)	O_s (%)
S1	86.0	13.8	0.2
S2	19.9	65.6	14.5
S3	57.8	37.1	5.1
S4	81.0	14.2	4.8
S5	88.3	2.5	9.1
S6	9.9	71.2	18.9
S7	70.3	21.4	8.3
S8	54.0	29.8	16.2

Table 3 Ru loadings determined by XRF and ICP-OES experiments

Sample	Nominal Ru loading (wt%)	XRF Ru loading (wt%)	ICP-OES Ru loading (wt%)
S1	5.0	2.2	4.3
S2		2.4	1.1
S3		2.1	2.3
S4		2.5	1.4
S5		2.5	1.6
S6		3.1	2.1
S7		2.7	2.4
S8		2.6	2.7

from those obtained by XRF (Fig. S4d†). With the exception of S1, ICP revealed Ru loadings in the range of 1–3 wt% for all the catalysts synthesized herein. We note that these values are lower than the nominal content (5 wt%), and this could be explained by the well-known recalcitrance of Ru towards acids, which often results in incomplete dissolution.[50,51]

The H_2-TPR profiles of the ceria–alumina catalysts (Fig. 4e) showed two main peaks at low and high temperatures which can be ascribed to the reduction of surface ceria in close contact with Ru and surface ceria not in contact with Ru, respectively. The low temperature peaks appeared at lower temperatures as the ceria loading increased for both aluminas, with optimum values (207 and 219 °C) for 80 wt% ceria loading on acidic and basic alumina, respectively. Interestingly, alumina-supported catalysts showed reduction peaks at higher temperatures compared to $Ru/CeO_2|_{AS}$ (S5, Fig. 4e), which seems to indicate that the presence of alumina affects the net formation of surface oxygen vacancies as a consequence of a less intense interaction between Ru and CeO_2, particularly for basic alumina. Therefore, it seems clear that the strength of the metal–support interaction for the CeO_2–Al_2O_3 catalysts depends highly on the ceria loading rather than on the surface area. For instance, the S8 sample showed reduction peaks at higher temperatures than $Ru/CeO_2|_{AS}$ despite having significantly higher specific surface area.

We conducted CO_2-TPD experiments for all the catalysts tested in this work (Fig. 4f). The TPD profiles of the supports (basic alumina, acidic alumina, and lab-prepared CeO_2) are also reported in the ESI† (Fig. S6e). As shown in Fig. 4f, all the samples under study showed similar TPD profiles containing one single desorption peak at low temperatures (109–158 °C), thereby revealing weak surface basicity in all cases. This low-temperature desorption peak is normally ascribed to the decomposition of carbonates formed during CO_2 adsorption at room temperature, which takes place with the simultaneous release of CO_2 and H_2O (not shown). Both commercial (S1) and lab-synthesized (S5) Ru/CeO_2 samples showed surface sites with similar basicity strength (*i.e.*, desorption peaks at the same temperature), although the amount of surface basic sites was significantly higher for the lab-synthesized sample, in line with its higher surface area (Fig. 1). Thus, the number of ceria surface sites (and thus the improved Ru–CeO_2 interaction) rather than the basicity strength seems to explain the different kinetic behaviour of both samples (Fig. 1). The TPD profiles of the alumina-containing samples with low CeO_2 loading (20 wt%, S2 and S6) showed profiles very similar to those of their alumina parent supports (Fig. S6e†). As expected, the S6 sample supported on basic alumina showed a CO_2 desorption peak at higher temperatures than the S2 sample supported on acidic alumina (158 *vs.* 129 °C). Finally, the samples with higher CeO_2 content (50–80 wt%, S3, S4, S7, and S8) showed TPD profiles very similar to that of high surface area Ru/CeO_2 (S5). In this case, the samples supported on basic alumina (S7 and S8) showed desorption peaks with higher area than their counterparts supported on acidic alumina (S3 and S4), thereby revealing a higher CeO_2 dispersion on basic alumina (in line with the CeO_2 crystallite size data of Fig. 4b). These results could also explain the superior kinetic behaviour of basic alumina-supported samples S7 and S8 in terms of activation energy as compared to their acidic alumina-supported counterparts (Fig. 3c).

As a summary, the role of alumina as a structural promoter for ceria in Ru/CeO_2–Al_2O_3 catalysts has been unveiled. The use of alumina as a support allowed a high surface area, low crystalline and highly dispersed reducible cerium oxide to be generated, which helped improve the ammonia synthesis mechanism by decreasing the activation energy and the nitrogen reaction order, with an optimum loading of 50 wt% for both acidic and basic alumina supports. Acidic alumina had a negative effect on the catalytic performance, probably due to the strong adsorption of the ammonia produced in acid sites (ammonia inhibition). This poisoning effect was most relevant for low ceria loadings (*e.g.*, 20 wt%). The Ru/CeO_2–Al_2O_3 catalyst with 50 wt% ceria and basic alumina showed optimum kinetic performance with an activation energy as low as 44.8 kJ mol^{-1}.

Conclusions

A simple impregnation–calcination method was used herein for the synthesis of CeO_2 and CeO_2–Al_2O_3 supports for Ru. These catalysts showed an outstanding performance for the low-temperature ammonia synthesis reaction, with activation energies comparable to those of the best catalysts reported so far. In this sense, a lab-prepared high-surface-area sample $Ru/CeO_2|_{AS}$ showed an activation energy as low as 46.1 kJ mol^{-1}. This sample also showed excellent low-temperature kinetic behaviour with a very positive H_2 reaction order (thereby avoiding typical hydrogen inhibition issues associated with Ru) and a significantly lower N_2 reaction order as compared to the commercial counterpart (thereby allowing enhanced N_2 dissociation/activation).

Structural promotion of ceria with alumina led to the formation of catalysts with higher specific surface areas and lower ceria crystallinity. While acid sites from γ-alumina were found to negatively affect the ammonia synthesis performance, basic alumina allowed the ceria loading to be reduced while maintaining excellent activity and kinetic behaviour (activation energy as low as 44.8 kJ mol^{-1}) and reaction orders comparable to those of $Ru/CeO_2|_{AS}$.

The good performance of these easily prepared catalysts paves the way for a new family of 3rd generation catalysts which can be used as an alternative to complex electrides, hydrides and intermetallics, thereby providing new solutions for easier industrial catalyst scale up and effective integration of ammonia synthesis technology with renewables. We note that several improvements could be made to our catalysts. First, electropositive alkaline promoters could be added to

facilitate electronic transfer towards Ru, thereby facilitating N_2 dissociation by providing electrons to the antibonding molecular orbitals. Second, we could enhance the Ru–CeO_2 interaction by adding elements able to form a solid solution with CeO_2, such that the CeO_2 lattice is distorted and the formation of oxygen vacancies (*e.g.*, CeO_x) is facilitated.

Data availability

The data supporting this article have been included as part of the ESI.†

Author contributions

Javier Arroyo-Caire: conceptualization, methodology, validation, formal analysis, investigation, writing – original draft, visualization. Edgar. S. Duran-Uribe: methodology, formal analysis, resources. Mayra Anabel Lara-Angulo: resources, writing – review & editing. Manuel Antonio Diaz-Perez: conceptualization, writing – review & editing, supervision. Antonio Sepúlveda-Escribano: writing – review & editing, supervision. Juan Carlos Serrano-Ruiz: conceptualization, formal analysis, investigation, writing – review & editing, supervision, project administration, funding acquisition.

Conflicts of interest

There are no conflicts to declare.

Acknowledgements

This publication is part of the project BioEnH2, funded by MCIN/AEI/**https://doi.org/10.13039/501100011033** and by European Union NextGenerationEU/PRTR. The authors want to acknowledge the University of Cádiz (UCA) for their services in the microscopy field and their gentle analyses and reports.

References

1 M. Reese, C. Marquart, M. Malmali, K. Wagner, E. Buchanan, A. McCormick and E. L. Cussler, *Ind. Eng. Chem. Res.*, 2016, **55**, 3742–3750.
2 A. Laval, Hafnia, H. Tøpsoe, Vestas and S. Gamesa, *Ammonfuel. An industrial view of ammonia as a marine fuel*, 2020.
3 K. H. R. Rouwenhorst, A. G. J. Van der Ham and L. Lefferts, *Int. J. Hydrogen Energy*, 2021, **46**, 21566–21579.
4 C. Smith, A. K. Hill and L. Torrente-Murciano, *Energy Environ. Sci.*, 2020, **13**, 331–344.
5 O. A. Ojelade and S. F. Zaman, *Chem. Pap.*, 2021, **75**, 57–65.
6 Q. Wang, J. Guo and P. Chen, *J. Energy Chem.*, 2019, DOI: **10.1016/j.jechem.2019.01.027**.
7 F. Chang, W. Gao, J. Guo and P. Chen, *Adv. Mater.*, 2021, DOI: **10.1002/adma.202005721**.
8 M. L. Carreon, *J. Phys. D: Appl. Phys.*, 2019, **52**, 483001.
9 J. Hong, S. Prawer and A. B. Murphy, *ACS Sustainable Chem. Eng.*, 2018, **6**, 15–31.
10 S. Reichle, M. Felderhoff and F. Schüth, *Angew. Chem., Int. Ed.*, 2021, **60**, 26385–26389.
11 L. Li, T. Zhang, J. Cai, H. Cai, J. Ni, B. Lin, J. Lin, X. Wang, L. Zheng, C. T. Au and L. Jiang, *J. Catal.*, 2020, **389**, 218–228.
12 J. Moon, Y. Cheng, L. Daemen, E. Novak, A. J. Ramirez-Cuesta and Z. Wu, *Top. Catal.*, 2021, **64**, 685–692.
13 H. Yan, W. Gao, Q. Wang, Y. Guan, S. Feng, H. Wu, Q. Guo, H. Cao, J. Guo and P. Chen, *J. Phys. Chem. C*, 2021, **125**, 6716–6722.
14 S. Wang, W. Yu, S. Xu, K. Han and F. Wang, *ACS Sustainable Chem. Eng.*, 2022, **10**, 115–123.
15 Y. Li, H. Wang, C. Priest, S. Li, P. Xu and G. Wu, *Adv. Mater.*, 2021, **33**, 2000381.
16 J. M. McEnaney, A. R. Singh, J. A. Schwalbe, J. Kibsgaard, J. C. Lin, M. Cargnello, T. F. Jaramillo and J. K. Nørskov, *Energy Environ. Sci.*, 2017, **10**, 1621–1630.
17 J. Humphreys, R. Lan and S. Tao, *Adv. Energy Sustainability Res.*, 2021, **2**, 2000043.
18 V. S. Marakatti and E. M. Gaigneaux, *ChemCatChem*, 2020, DOI: **10.1002/cctc.202001141**.
19 J. Arroyo-Caire, M. A. Diaz-Perez, M. A. Lara-Angulo and J. C. Serrano-Ruiz, *Nanomaterials*, 2023, **13**, 2914.
20 C. Smith and L. Torrente-Murciano, *Chem Catal.*, 2021, DOI: **10.1016/j.checat.2021.09.015**.
21 H. Hosono and M. Kitano, *Chem. Rev.*, 2021, DOI: **10.1021/acs.chemrev.0c01071**.
22 N. Saadatjou, A. Jafari and S. Sahebdelfar, *Chem. Eng. Commun.*, 2015, DOI: **10.1080/00986445.2014.923995**.
23 L. Li, T. Zhang, Y. Zhou, X. Wang, C. tong Au and L. Jiang, *J. Rare Earths*, 2022, DOI: **10.1016/j.jre.2021.06.014**.
24 Y. Nakaya and S. Furukawa, *Chem. Rev.*, 2022, **123**, 5859–5947.
25 J. Guo and P. Chen, *Acc. Chem. Res.*, 2021, **54**, 2434–2444.
26 K. Sato and K. Nagaoka, *Chem. Lett.*, 2021, **50**, 687–696.
27 Y. Gong, H. Li, C. Li, X. Bao, H. Hosono and J. Wang, *J. Adv. Ceram.*, 2022, **11**(10), 1499–1529.
28 S. ichiro Miyahara, K. Sato, Y. Kawano, K. Imamura, Y. Ogura, K. Tsujimaru and K. Nagaoka, *Catal. Today*, 2021, **376**, 36–40.
29 Z. Ma, S. Zhao, X. Pei, X. Xiong and B. Hu, *Catal. Sci. Technol.*, 2017, **7**, 191–199.
30 M. Kitano, Y. Inoue, M. Sasase, K. Kishida, Y. Kobayashi, K. Nishiyama, T. Tada, S. Kawamura, T. Yokoyama, M. Hara and H. Hosono, *Angew. Chem.*, 2018, **130**, 2678–2682.
31 C. Fernández, C. Sassoye, D. P. Debecker, C. Sanchez and P. Ruiz, *Appl. Catal., A*, 2014, **474**, 194–202.
32 Z. Song, T. Cai, J. C. Hanson, J. A. Rodriguez and J. Hrbek, *J. Am. Chem. Soc.*, 2004, **126**, 8576–8584.
33 P. Wang, F. Chang, W. Gao, J. Guo, G. Wu, T. He and P. Chen, *Nat. Chem.*, 2017, **9**, 64–70.
34 H. Hosono, *Catal. Lett.*, 2022, **152**, 307–314.
35 K. Ooya, J. Li, K. Fukui, S. Iimura, T. Nakao, K. Ogasawara, M. Sasase, H. Abe, Y. Niwa, M. Kitano and H. Hosono, *Adv. Energy Mater.*, 2021, **11**, 2003723.
36 M. Kitano, Y. Inoue, Y. Yamazaki, F. Hayashi, S. Kanbara, S. Matsuishi, T. Yokoyama, S. W. Kim, M. Hara and H. Hosono, *Nat. Chem.*, 2012, **4**, 934–940.

37 Y. Gong, H. Li, J. Wu, X. Song, X. Yang, X. Bao, X. Han, M. Kitano, J. Wang and H. Hosono, *J. Am. Chem. Soc.*, 2022, **144**, 8683–8692.
38 Y. Kobayashi, M. Kitano, S. Kawamura, T. Yokoyama and H. Hosono, *Catal. Sci. Technol.*, 2017, **7**, 47–50.
39 W. Li, P. Liu, R. Niu, J. Li and S. Wang, *Solid State Sci.*, 2020, **99**, 105983.
40 K. Sato, K. Imamura, Y. Kawano, S. ichiro Miyahara, T. Yamamoto, S. Matsumura and K. Nagaoka, *Chem. Sci.*, 2016, **8**, 674–679.
41 X. Wang, X. Peng, Y. Zhang, J. Ni, C. T. Au and L. Jiang, *Inorg. Chem. Front.*, 2019, **6**, 396–406.
42 Z. Feng, F. Guo, Y. Zhang, T. Ichikawa and J. Zheng, *Appl. Catal., B*, 2025, 125059.
43 B. Folkesson, M. Bjorøy, J. Pappas, S. Skaarup, R. Aaltonen and C.-G. Swahn, *Acta Chem. Scand.*, 1973, **27**, 287–302.
44 M. M. T. Khan and S. Srivastava, *Polyhedron*, 1988, **7**, 1063–1065.
45 H. B. Kim and E. D. Park, *Catal. Today*, 2023, **411–412**, 113817.
46 M. Osozawa, A. Hori, K. Fukai, T. Honma, K. Oshima and S. Satokawa, *Int. J. Hydrogen Energy*, 2022, **47**, 2433–2441.
47 J. Silvestre-Albero, F. Rodríguez-Reinoso and A. Sepúlveda-Escribano, *J. Catal.*, 2002, **210**, 127–136.
48 Z. Peng, Y. Wang, C. Yin, S. Qiu, Y. Xia, Y. Zou, F. Xu, L. Sun and H. Chu, *Sustainable Energy Fuels*, 2023, **7**, 821–831.
49 Y. juan Hao, Y. guang Ma, X. Zhang, J. Li, S. Wang, X. Chen and F. tang Li, *Chem. Eng. J.*, 2022, **433**, 134619.
50 M. Balcerzak, *Crit. Rev. Anal. Chem.*, 2002, **32**, 181–226.
51 T. Suoranta, M. Niemelä and P. Perämäki, *Talanta*, 2014, **119**, 425–429.

4. Chapter 4: Ru/CeO_2-La_2O_3 catalysts for ammonia synthesis: on the search of an optimum Ce/La ratio

III. Section 3: Conclusions and future prospects

The objectives proposed in the Section I.2 of this Thesis have been successfully achieved. In general, a deep understanding of the thermocatalytic ammonia synthesis has been gained, particularly regarding the main kinetic aspects of this chemical reaction i.e., the kinetic mechanisms, N_2 dissociation, H_2 poisoning, the role of electron transfer, etc. The versatility of cerium has been demonstrated, since this metal exhibits an excellent performance, indistinctly as the bimetallic $CeNi_2$ alloy or as a support for Ru in the form of CeO_2.

The specific objective 1 was accomplished by the generation of the publication reported in the Chapter 1. The review in the state-of-the-art led to the comprehension of the ammonia thermocatalytic synthesis insights and reinforced the good performance of rare earths, particularly, cerium, in the design of 3rd generation ammonia synthesis catalysts.

The specific objective 2 was covered in the publication shown in the Chapter 2. The good performance of a non-noble metal-based catalyst was demonstrated by the synthesis of $CeNi_2$. The formation of a CeN surface layer under the reaction conditions was demonstrated to act as a second active center for the N_2 dissociation, while an efficient H_2 dissociation was given by the action of Ni via H_2 spillover. As a consequence, a performance of 1.0 mmol g^{-1} h^{-1} at 400 ºC and an apparent activation energy of 55.3 kJ mol^{-1} were achieved.

The specific objective 3 was completed with the publication from the Chapter 3. A Ru/CeO_2 catalyst with an excellent performance of 2.4 mmol g^{-1} h^{-1} and an apparent activation energy of 46.1 kJ mol^{-1} was produced by a simple impregnation-calcination method. Moreover, the structural promotion given by the impregnation of CeO_2 into Al_2O_3 led to a significant increase in the specific surface area. As a consequence, a superior formation of oxygen vacancies was reported. It was demonstrated that there is a trade-off between the metal-support interactions (Ru-O-Ce sites) and the structural promotion, which concludes with an optimum ceria loading over the Ce-Al support of 50 wt%, showing an apparent activation energy of 44.8 kJ mol^{-1}. This opens a potential window for an efficient transition between research a real application, considering that an easy-to-make, efficient, air stable and relatively low-cost material was obtained.

The specific objective 4 was accomplished by the results shown in the Chapter 4. The addition of La into the crystalline net of CeO_2 led to the formation of Ce-La solid

solution, with an optimum performance for the catalyst with a 50 mole% loading of Ce onto the support. Both superior structural and electronic properties were reported for the La-Ce mixed oxide supports i.e., a much higher Ru dispersion and concentration on the surface, a superior generation of surface crystalline defects, a higher formation of surface oxygen vacancies and enhanced metal-support interactions. As a result, the kinetic mechanism of Ru/CeO_2 showed in the Chapter 3 was outperformed by Ru/CeO_2-La_2O_3. A reaction rate of 2.7 mmol g^{-1} h^{-1} at 400 ºC and 0.1 MPa, as well as an apparent activation energy as low as 34.1 kJ mol^{-1} were obtained. This catalyst shows a good performance at low temperatures and an excellent pressure response, with an outstanding resistance to H_2 poisoning. In order to reinforce the results obtained, the realization of H_2-TPR experiments would be desirable in future works.

This Thesis demonstrates that the design of excellent ammonia synthesis materials made by simple materials and/or simple synthesis methods is not a utopia, but a real possibility. Further research efforts must be done in order to optimize and gain deeper understanding in the performance of Ru/CeO_2-based catalysts. There are several methodologies that could be applied, such as the enhancement of the electronic properties by the addition of alkaline elements or the structural promotion of the support, with the selection of the particle size and the increase in the catalyst homogeneity. Thus, this research line, focused on the rational design of materials for ammonia production with an eye on their scalability, holds great potential and could serve as a guidance for the development of new ammonia synthesis catalysts with the focus on the improvement of the industrial process.

In any case, this work states that a new generation of ammonia synthesis catalysts could rise from the change on the meaning of “novelty”, transitioning from the synthesis of complex and non-stable chemicals, towards the production of more available and useful materials. In this sense, we demonstrated that cerium could play a significant role in that transition. With the reader's indulgence, I will dare to name these materials as the 4th generation ammonia synthesis catalysts. This could look like a challenge, but as Dr. Albert Einstein said, “*if we knew what it is we were doing, it would not be called research. Would it?*”

IV. References

Manuscript. Introduction and Chapter 4

(1) Smil, V. Enriching the Earth: Fritz Haber, Carl Bosch, and the Transformation of World Food Production. *Enriching the Earth* **2000**. https://doi.org/10.7551/MITPRESS/2767.001.0001.

(2) Alfa Laval; Hafnia; Haldor Tøpsoe; Vestas; Siemens Gamesa. *Ammonfuel. An Industrial View of Ammonia as a Marine Fuel*; 2020.

(3) Smith, C.; Hill, A. K.; Torrente-Murciano, L. Current and Future Role of Haber-Bosch Ammonia in a Carbon-Free Energy Landscape. *Energy Environ Sci* **2020**, *13* (2), 331–344. https://doi.org/10.1039/c9ee02873k.

(4) Gambarotta, S.; Scott, J. Multimetallic Cooperative Activation of N2. *Angewandte Chemie International Edition* **2004**, *43* (40), 5298–5308. https://doi.org/10.1002/ANIE.200301669.

(5) Pool, J. A.; Lobkovsky, E.; Chirik, P. J. Hydrogenation and Cleavage of Dinitrogen to Ammonia with a Zirconium Complex. *Nature 2004 427:6974* **2004**, *427* (6974), 527–530. https://doi.org/10.1038/nature02274.

(6) Smil, V. Detonator of the Population Explosion. *Nature 1999 400:6743* **1999**, *400* (6743), 415–415. https://doi.org/10.1038/22672.

(7) Erisman, J. W.; Sutton, M. A.; Galloway, J.; Klimont, Z.; Winiwarter, W. How a Century of Ammonia Synthesis Changed the World. *Nature Geoscience 2008 1:10* **2008**, *1* (10), 636–639. https://doi.org/10.1038/ngeo325.

(8) Rouwenhorst, K. H. R.; Engelmann, Y.; Van 'T Veer, K.; Postma, R. S.; Bogaerts, A.; Lefferts, L. Plasma-Driven Catalysis: Green Ammonia Synthesis with Intermittent Electricity. *Green Chemistry* **2020**, *22* (19), 6258–6287. https://doi.org/10.1039/D0GC02058C.

(9) John Bøgild Hansen. Techno-Economic Challenges of Green Ammonia as an Energy Vector. *Techno-Economic Challenges of Green Ammonia as an Energy Vector* **2021**. https://doi.org/10.1016/C2019-0-01417-3.

(10) Techno-Economic Challenges of Green Ammonia as an Energy Vector. *Techno-Economic Challenges of Green Ammonia as an Energy Vector* **2021**. https://doi.org/10.1016/C2019-0-01417-3.

(11) Reese, M.; Marquart, C.; Malmali, M.; Wagner, K.; Buchanan, E.; McCormick, A.; Cussler, E. L. Performance of a Small-Scale Haber Process. *Ind Eng Chem Res* **2016**, *55* (13), 3742–3750. https://doi.org/10.1021/acs.iecr.5b04909.

(12) Smith, C.; Torrente-Murciano, L. Guidance for Targeted Development of Ammonia Synthesis Catalysts from a Holistic Process Approach. *Chem Catalysis*. Cell Press November 18, 2021, pp 1163–1172. https://doi.org/10.1016/j.checat.2021.09.015.

(13) Hansen, J. B.; Han, P. Roadmap to All Electric Ammonia Plants. In *NH3 Fuel Conference 2018*; Pittsburg, PA, 2018.

(14) Marakatti, V. S.; Gaigneaux, E. M. Recent Advances in Heterogeneous Catalysis for Ammonia Synthesis. *ChemCatChem*. Wiley Blackwell December 4, 2020, pp 5838–5857. https://doi.org/10.1002/cctc.202001141.

(15) Humphreys, J.; Lan, R.; Tao, S. Development and Recent Progress on Ammonia Synthesis Catalysts for Haber–Bosch Process. *Advanced Energy and Sustainability Research* **2021**, *2* (1), 2000043. https://doi.org/10.1002/aesr.202000043.

(16) Jacobsen, C. J. H.; Dahl, S.; Hansen, P. L.; Törnqvist, E.; Jensen, L.; Topsøe, H.; Prip, D. V.; Møenshaug, P. B.; Chorkendorff, I. Structure Sensitivity of Supported Ruthenium Catalysts for Ammonia Synthesis. *J Mol Catal A Chem* **2000**, *163* (1–2), 19–26. https://doi.org/10.1016/S1381-1169(00)00396-4.

(17) Hansen, T. W.; Hansen, P. L.; Dahl, S.; Jacobsen, C. J. H. Support Effect and Active Sites on Promoted Ruthenium Catalysts for Ammonia Synthesis. *Catal Letters* **2002**, *84* (1–2), 7–12. https://doi.org/10.1023/A:1021028718491/METRICS.

(18) Saadatjou, N.; Jafari, A.; Sahebdelfar, S. Ruthenium Nanocatalysts for Ammonia Synthesis: A Review. *Chem Eng Commun* **2015**, *202* (4), 420–448. https://doi.org/10.1080/00986445.2014.923995.

(19) Prieto, G.; Schüth, F. The Yin and Yang in the Development of Catalytic Processes: Catalysis Research and Reaction Engineering. *Angewandte Chemie International Edition* **2015**, *54* (11), 3222–3239. https://doi.org/10.1002/ANIE.201409885.

(20) Hinrichsen, O.; Rosowski, F.; Muhler, M.; Ertl, G. The Microkinetics of Ammonia Synthesis Catalyzed by Cesium-Promoted Supported Ruthenium. *Chem Eng Sci* **1996**, *51* (10), 1683–1690. https://doi.org/10.1016/0009-2509(96)00027-9.

(21) Jacobsen, C. J. H.; Dahl, S.; Boisen, A.; Clausen, B. S.; Topsøe, H.; Logadottir, A.; Nørskov, J. K. Optimal Catalyst Curves: Connecting Density Functional Theory Calculations with Industrial Reactor Design and Catalyst Selection. *J Catal* **2002**, *205* (2), 382–387. https://doi.org/10.1006/JCAT.2001.3442.

(22) Kowalczyk, Z.; Krukowski, M.; Raróg-Pilecka, W.; Szmigiel, D.; Zielinski, J. Carbon-Based Ruthenium Catalyst for Ammonia Synthesis: Role of the Barium and Caesium Promoters and Carbon Support. *Appl Catal A Gen* **2003**, *248* (1–2), 67–73. https://doi.org/10.1016/S0926-860X(03)00150-9.

(23) Kitano, M.; Kanbara, S.; Inoue, Y.; Kuganathan, N.; Sushko, P. V.; Yokoyama, T.; Hara, M.; Hosono, H. Electride Support Boosts Nitrogen Dissociation over Ruthenium Catalyst and Shifts the Bottleneck in Ammonia Synthesis. *Nature Communications 2015 6:1* **2015**, *6* (1), 1–9. https://doi.org/10.1038/ncomms7731.

(24) Liu, H. Ammonia Synthesis Catalysts: Innovation and Practice. *Ammonia Synthesis Catalysts: Innovation and Practice* **2013**, 1–872. https://doi.org/10.1142/8199.

(25) Liu, H. Ammonia Synthesis Catalyst 100 Years: Practice, Enlightenment and Challenge. *Chinese Journal of Catalysis* **2014**, *35* (10), 1619–1640. https://doi.org/10.1016/S1872-2067(14)60118-2.

(26) Laursen, A. B.; Sehested, J.; Chorkendorff, I.; Vesborg, P. C. K. Availability of Elements for Heterogeneous Catalysis: Predicting the Industrial Viability of Novel Catalysts. *Chinese Journal of Catalysis* **2018**, *39* (1), 16–26. https://doi.org/10.1016/S1872-2067(17)62979-6.

(27) Nielsen, Anders. Ammonia : Catalysis and Manufacture. **1995**, 346.

(28) Li, L.; Zhang, T.; Zhou, Y.; Wang, X.; Au, C. tong; Jiang, L. Review on Catalytic Roles of Rare Earth Elements in Ammonia Synthesis: Development and Perspective. *Journal of Rare Earths*. Editorial Office of Chinese Rare Earths January 1, 2022, pp 1–10. https://doi.org/10.1016/j.jre.2021.06.014.

(29) Zhang, Y.; Li, J.; Zhou, Y.; Au, C.; Wang, X.; Jiang, L. Recent Progress of Thermocatalytic Ammonia Synthesis via an Associative Mechanism. *Fundamental Research* **2024**. https://doi.org/10.1016/J.FMRE.2023.11.016.

(30) Pool, J. A.; Lobkovsky, E.; Chirik, P. J. Hydrogenation and Cleavage of Dinitrogen to Ammonia with a Zirconium Complex. *Nature 2004 427:6974* **2004**, *427* (6974), 527–530. https://doi.org/10.1038/nature02274.

(31) Gambarotta, S.; Scott, J. Multimetallic Cooperative Activation of N2. *Angewandte Chemie International Edition* **2004**, *43* (40), 5298–5308. https://doi.org/10.1002/ANIE.200301669.

(32) Jacobsen, C. J. H.; Dahl, S.; Clausen, B. G. S.; Bahn, S.; Logadottir, A.; Nørskov, J. K. Catalyst Design by Interpolation in the Periodic Table: Bimetallic Ammonia Synthesis Catalysts [2]. *Journal of the American Chemical Society*. 2001, pp 8404–8405. https://doi.org/10.1021/ja010963d.

(33) Logadottir, A.; Rod, T. H.; Nørskov, J. K.; Hammer, B.; Dahl, S.; Jacobsen, C. J. H. The Brønsted–Evans–Polanyi Relation and the Volcano Plot for Ammonia Synthesis over Transition Metal Catalysts. *J Catal* **2001**, *197* (2), 229–231. https://doi.org/10.1006/JCAT.2000.3087.

(34) Chang, F.; Gao, W.; Guo, J.; Chen, P. Emerging Materials and Methods toward Ammonia-Based Energy Storage and Conversion. *Advanced Materials*. John Wiley and Sons Inc December 1, 2021. https://doi.org/10.1002/adma.202005721.

(35) Wang, Q.; Guo, J.; Chen, P. Recent Progress towards Mild-Condition Ammonia Synthesis. *Journal of Energy Chemistry*. Elsevier B.V. September 1, 2019, pp 25–36. https://doi.org/10.1016/j.jechem.2019.01.027.

(36) McEnaney, J. M.; Singh, A. R.; Schwalbe, J. A.; Kibsgaard, J.; Lin, J. C.; Cargnello, M.; Jaramillo, T. F.; Nørskov, J. K. Ammonia Synthesis from N2 and H2O Using a Lithium Cycling Electrification Strategy at Atmospheric Pressure. *Energy Environ Sci* **2017**, *10* (7), 1621–1630. https://doi.org/10.1039/c7ee01126a.

(37) Cui, X.; Tang, C.; Zhang, Q. A Review of Electrocatalytic Reduction of Dinitrogen to Ammonia under Ambient Conditions. *Adv Energy Mater* **2018**, *8* (22). https://doi.org/10.1002/AENM.201800369.

(38) Kibsgaard, J.; Nørskov, J. K.; Chorkendorff, I. The Difficulty of Proving Electrochemical Ammonia Synthesis. *ACS Energy Lett* **2019**, *4* (12), 2986–2988. https://doi.org/10.1021/ACSENERGYLETT.9B02286/ASSET/IMAGES/LARGE/NZ9B02286_0002.JPEG.

(39) Chen, X.; Li, N.; Kong, Z.; Ong, W. J.; Zhao, X. Photocatalytic Fixation of Nitrogen to Ammonia: State-of-the-Art Advancements and Future Prospects. *Mater Horiz* **2018**, *5* (1), 9–27. https://doi.org/10.1039/C7MH00557A.

(40) Xue, X.; Chen, R.; Yan, C.; Zhao, P.; Hu, Y.; Zhang, W.; Yang, S.; Jin, Z. Review on Photocatalytic and Electrocatalytic Artificial Nitrogen Fixation for Ammonia Synthesis at Mild Conditions: Advances, Challenges and Perspectives. *Nano Res* **2019**, *12* (6), 1229–1249. https://doi.org/10.1007/S12274-018-2268-5.

(41) Ithisuphalap, K.; Zhang, H.; Guo, L.; Yang, Q.; Yang, H.; Wu, G. Photocatalysis and Photoelectrocatalysis Methods of Nitrogen Reduction for Sustainable Ammonia Synthesis. *Small Methods* **2019**, *3* (6). https://doi.org/10.1002/SMTD.201800352.

(42) Medford, A. J.; Hatzell, M. C. Photon-Driven Nitrogen Fixation: Current Progress, Thermodynamic Considerations, and Future Outlook. *ACS Catal* **2017**, *7* (4), 2624–2643. https://doi.org/10.1021/ACSCATAL.7B00439.

(43) Huang, P.; Liu, W.; He, Z.; Xiao, C.; Yao, T.; Zou, Y.; Wang, C.; Qi, Z.; Tong, W.; Pan, B.; Wei, S.; Xie, Y. Single Atom Accelerates Ammonia Photosynthesis. *Sci China Chem* **2018**, *61* (9), 1187–1196. https://doi.org/10.1007/S11426-018-9273-1.

(44) Swearer, D. F.; Knowles, N. R.; Everitt, H. O.; Halas, N. J. Light-Driven Chemical Looping for Ammonia Synthesis. *ACS Energy Lett* **2019**, *4* (7), 1505–1512. https://doi.org/10.1021/ACSENERGYLETT.9B00860/SUPPL_FILE/NZ9B00860_SI_001.PDF.

(45) Yan, H.; Gao, W.; Wang, Q.; Guan, Y.; Feng, S.; Wu, H.; Guo, Q.; Cao, H.; Guo, J.; Chen, P. Lithium Palladium Hydride Promotes Chemical Looping Ammonia Synthesis Mediated by Lithium Imide and Hydride. *Journal of Physical Chemistry C* **2021**, *125* (12), 6716–6722. https://doi.org/10.1021/acs.jpcc.1c01230.

(46) Moon, J.; Cheng, Y.; Daemen, L.; Novak, E.; Ramirez-Cuesta, A. J.; Wu, Z. On the Structural Transformation of Ni/BaH2 During a N2-H2 Chemical Looping Process for Ammonia Synthesis: A Joint In Situ Inelastic Neutron Scattering and First-Principles Simulation Study. *Top Catal* **2021**, *64* (9–12), 685–692. https://doi.org/10.1007/s11244-021-01445-w.

(47) Wang, P.; Chang, F.; Gao, W.; Guo, J.; Wu, G.; He, T.; Chen, P. Breaking Scaling Relations to Achieve Low-Temperature Ammonia Synthesis through LiH-Mediated Nitrogen Transfer and Hydrogenation. *Nat Chem* **2017**, *9* (1), 64–70. https://doi.org/10.1038/nchem.2595.

(48) Lazouski, N.; Manthiram, K. Ambient Lithium-Mediated Ammonia Synthesis. *Trends Chem* **2019**, *1* (1), 141–142. https://doi.org/10.1016/J.TRECHM.2019.02.008.

(49) Lazouski, N.; Schiffer, Z. J.; Williams, K.; Manthiram, K. Understanding Continuous Lithium-Mediated Electrochemical Nitrogen Reduction. *Joule* **2019**, *3* (4), 1127–1139. https://doi.org/10.1016/J.JOULE.2019.02.003.

(50) Reichle, S.; Felderhoff, M.; Schüth, F. Mechanocatalytic Room-Temperature Synthesis of Ammonia from Its Elements Down to Atmospheric Pressure. *Angewandte Chemie - International Edition* **2021**, *60* (50), 26385–26389. https://doi.org/10.1002/anie.202112095.

(51) Reichle, S.; Kang, L.; Demirbas, D.; Weidenthaler, C.; Felderhoff, M.; DeBeer, S.; Schüth, F. Mechanocatalytic Synthesis of Ammonia: State of the Catalyst During Reaction and Deactivation Pathway. *Angewandte Chemie - International Edition* **2024**, *63* (14). https://doi.org/10.1002/ANIE.202317038.

(52) Hosono, H.; Kitano, M. Advances in Materials and Applications of Inorganic Electrides. *Chemical Reviews*. American Chemical Society March 10, 2021, pp 3121–3185. https://doi.org/10.1021/acs.chemrev.0c01071.

(53) Inoue, Y.; Kitano, M.; Kim, S. W.; Yokoyama, T.; Hara, M.; Hosono, H. Highly Dispersed Ru on Electride [Ca24Al28O 64]4+(e-)4 as a Catalyst for Ammonia Synthesis. *ACS Catal* **2014**, *4* (2), 674–680. https://doi.org/10.1021/CS401044A/SUPPL_FILE/CS401044A_SI_001.PDF.

(54) Kitano, M.; Inoue, Y.; Yamazaki, Y.; Hayashi, F.; Kanbara, S.; Matsuishi, S.; Yokoyama, T.; Kim, S. W.; Hara, M.; Hosono, H. Ammonia Synthesis Using a Stable Electride as an Electron Donor and Reversible Hydrogen Store. *Nat Chem* **2012**, *4* (11), 934–940. https://doi.org/10.1038/nchem.1476.

(55) Arroyo-Caire, J.; Diaz-Perez, M. A.; Lara-Angulo, M. A.; Serrano-Ruiz, J. C. A Conceptual Approach for the Design of New Catalysts for Ammonia Synthesis: A Metal—Support Interactions Review. *Nanomaterials 2023, Vol. 13, Page 2914* **2023**, *13* (22), 2914. https://doi.org/10.3390/NANO13222914.

(56) Hosono, H. Electron Transfer from Support/Promotor to Metal Catalyst: Requirements for Effective Support. *Catal Letters* **2022**, *152* (2), 307–314. https://doi.org/10.1007/s10562-021-03648-y.

(57) Nakao, T.; Tada, T.; Hosono, H. First-Principles and Microkinetic Study on the Mechanism for Ammonia Synthesis Using Ru-Loaded Hydride Catalyst. *Journal of Physical Chemistry C* **2020**, *124* (3), 2070–2078. https://doi.org/10.1021/acs.jpcc.9b10850.

(58) Kobayashi, Y.; Kitano, M.; Kawamura, S.; Yokoyama, T.; Hosono, H. Kinetic Evidence: The Rate-Determining Step for Ammonia Synthesis over Electride-Supported Ru Catalysts Is No Longer the Nitrogen Dissociation Step. *Catal Sci Technol* **2017**, *7* (1), 47–50. https://doi.org/10.1039/c6cy01962e.

(59) Ye, T. N.; Park, S. W.; Lu, Y.; Li, J.; Wu, J.; Sasase, M.; Kitano, M.; Hosono, H. Dissociative and Associative Concerted Mechanism for Ammonia Synthesis over Co-Based Catalyst. *J Am Chem Soc* **2021**, *143* (32), 12857–12866. https://doi.org/10.1021/jacs.1c06657.

(60) Li, L.; Zhang, T.; Cai, J.; Cai, H.; Ni, J.; Lin, B.; Lin, J.; Wang, X.; Zheng, L.; Au, C. T.; Jiang, L. Operando Spectroscopic and Isotopic-Label-Directed Observation of LaN-Promoted Ru/ZrH2 Catalyst for Ammonia Synthesis via Associative and Chemical Looping Route. *J Catal* **2020**, *389*, 218–228. https://doi.org/10.1016/j.jcat.2020.05.039.

(61) Ye, T. N.; Park, S. W.; Lu, Y.; Li, J.; Sasase, M.; Kitano, M.; Hosono, H. Contribution of Nitrogen Vacancies to Ammonia Synthesis over Metal Nitride Catalysts. *J Am Chem Soc* **2020**, *142* (33), 14374–14383. https://doi.org/10.1021/jacs.0c06624.

(62) Hattori, M.; Iijima, S.; Nakao, T.; Hosono, H.; Hara, M. Solid Solution for Catalytic Ammonia Synthesis from Nitrogen and Hydrogen Gases at 50 °C. *Nat Commun* **2020**, *11* (1). https://doi.org/10.1038/s41467-020-15868-8.

(63) Ye, T. N.; Lu, Y.; Kobayashi, Y.; Li, J.; Park, S. W.; Sasase, M.; Kitano, M.; Hosono, H. Efficient Ammonia Synthesis over Phase-Separated Nickel-Based Intermetallic Catalysts. *Journal of Physical Chemistry C* **2020**, *124* (52), 28589–28595. https://doi.org/10.1021/ACS.JPCC.0C09590/SUPPL_FILE/JP0C09590_SI_001.PDF.

(64) Li, J.; Wu, J.; Wang, H.; Lu, Y.; Ye, T.; Sasase, M.; Wu, X.; Kitano, M.; Inoshita, T.; Hosono, H. Acid-Durable Electride with Layered Ruthenium for Ammonia Synthesis: Boosting the Activity via Selective Etching. *Chem Sci* **2019**, *10* (22), 5712–5718. https://doi.org/10.1039/C9SC01539F.

(65) Nakaya, Y.; Furukawa, S. Catalysis of Alloys: Classification, Principles, and Design for a Variety of Materials and Reactions. *Chem Rev* **2022**. https://doi.org/10.1021/ACS.CHEMREV.2C00356/ASSET/IMAGES/MEDIUM/CR2C00356_0069.GIF.

(66) Croisé, C.; Alabd, K.; Tencé, S.; Gaudin, E.; Villesuzanne, A.; Courtois, X.; Bion, N.; Can, F. Influence of the Rare Earth (R) Element in Ru-Supported RScSi Electride-like Intermetallic Catalysts for Ammonia Synthesis at Low Pressure: Insight into NH3 Formation Mechanism. *ChemCatChem* **2023**, *15* (3). https://doi.org/10.1002/CCTC.202201172.

(67) Croisé, C.; Alabd, K.; Villesuzanne, A.; Can, F.; Courtois, X.; Gaudin, E.; Tencé, S.; Bion, N. Role of Hydride Ion within Ru/LaScSi and Ru/CeTiGe Catalysts for NH3 Synthesis: A Combination of DFT and Experimental Nitrogen Isotopic Exchange Studies. *Catal Commun* **2023**, *179*, 106689. https://doi.org/10.1016/J.CATCOM.2023.106689.

(68) Gong, Y.; Li, H.; Li, C.; Bao, X.; Hosono, H.; Wang, J. Insight into Rare-Earth-Incorporated Catalysts: The Chance for a More Efficient Ammonia Synthesis. *Journal of Advanced Ceramics 2022 11:10* **2022**, *11* (10), 1499–1529. https://doi.org/10.1007/S40145-022-0633-Z.

(69) Jiang, Y. F.; Liu, J. C.; Xu, C. Q.; Li, J.; Xiao, H. Breaking the Scaling Relations for Efficient N2-to-NH3 Conversion by a Bowl Active Site Design: Insight from LaRuSi

and Isostructural Electrides. *Chinese Journal of Catalysis* **2022**, *43* (8), 2183–2192. https://doi.org/10.1016/S1872-2067(22)64129-9.

(70) Fang, H.; Liu, D.; Luo, Y.; Zhou, Y.; Liang, S.; Wang, X.; Lin, B.; Jiang, L. Challenges and Opportunities of Ru-Based Catalysts toward the Synthesis and Utilization of Ammonia. *ACS Catal* **2022**, *12* (7), 3938–3954. https://doi.org/10.1021/ACSCATAL.2C00090.

(71) Carballo, J. M. G.; Yang, J.; Holmen, A.; García-Rodríguez, S.; Rojas, S.; Ojeda, M.; Fierro, J. L. G. Catalytic Effects of Ruthenium Particle Size on the Fischer–Tropsch Synthesis. *J Catal* **2011**, *284* (1), 102–108. https://doi.org/10.1016/J.JCAT.2011.09.008.

(72) Li, L.; Jiang, Y. F.; Zhang, T.; Cai, H.; Zhou, Y.; Lin, B.; Lin, X.; Zheng, Y.; Zheng, L.; Wang, X.; Xu, C. Q.; Au, C. tong; Jiang, L.; Li, J. Size Sensitivity of Supported Ru Catalysts for Ammonia Synthesis: From Nanoparticles to Subnanometric Clusters and Atomic Clusters. *Chem* **2022**, *8* (3), 749–768. https://doi.org/10.1016/J.CHEMPR.2021.11.008.

(73) Xuanbei Peng; Mingyuan Zhang; Tianhua Zhang; Yanliang Zhou; Jun Ni; Xiuyun Wang; Lilong Jiang. Single-Atom and Cluster Catalysts for Thermocatalytic Ammonia Synthesis at Mild Conditions. *Chem Sci* **2024**. https://doi.org/10.1039/D3SC06998B.

(74) Azofra, L. M.; Morlanés, N.; Poater, A.; Samantaray, M. K.; Vidjayacoumar, B.; Albahily, K.; Cavallo, L.; Basset, J. M. Single-Site Molybdenum on Solid Support Materials for Catalytic Hydrogenation of N2-into-NH3. *Angewandte Chemie International Edition* **2018**, *57* (48), 15812–15816. https://doi.org/10.1002/ANIE.201810409.

(75) Wang, X.; Peng, X.; Chen, W.; Liu, G.; Zheng, A.; Zheng, L.; Ni, J.; Au, C. tong; Jiang, L. Insight into Dynamic and Steady-State Active Sites for Nitrogen Activation to Ammonia by Cobalt-Based Catalyst. *Nature Communications 2020 11:1* **2020**, *11* (1), 1–10. https://doi.org/10.1038/s41467-020-14287-z.

(76) Qiu, J. Z.; Hu, J.; Lan, J.; Wang, L. F.; Fu, G.; Xiao, R.; Ge, B.; Jiang, J. Pure Siliceous Zeolite-Supported Ru Single-Atom Active Sites for Ammonia Synthesis. *Chemistry of Materials* **2019**, *31* (22), 9413–9421. https://doi.org/10.1021/ACS.CHEMMATER.9B03099/SUPPL_FILE/CM9B03099_SI_001.PDF.

(77) Wang, X.; Li, L.; Fang, Z.; Zhang, Y.; Ni, J.; Lin, B.; Zheng, L.; Au, C. T.; Jiang, L. Atomically Dispersed Ru Catalyst for Low-Temperature Nitrogen Activation to

Ammonia via an Associative Mechanism. *ACS Catal* **2020**, *10* (16), 9504–9514. https://doi.org/10.1021/ACSCATAL.0C00549/SUPPL_FILE/CS0C00549_SI_001.PDF.

(78) Hu, X. C.; Fu, X. P.; Wang, W. W.; Wang, X.; Wu, K.; Si, R.; Ma, C.; Jia, C. J.; Yan, C. H. Ceria-Supported Ruthenium Clusters Transforming from Isolated Single Atoms for Hydrogen Production via Decomposition of Ammonia. *Appl Catal B* **2020**, *268*, 118424. https://doi.org/10.1016/J.APCATB.2019.118424.

(79) Wang, A.; Li, J.; Zhang, T. Heterogeneous Single-Atom Catalysis. *Nat Rev Chem* **2018**, *2* (6), 65–81. https://doi.org/10.1038/S41570-018-0010-1.

(80) Manaka, Y.; Nagata, Y.; Kobayashi, K.; Kobayashi, D.; Nanba, T. The Effect of a Ruthenium Precursor on the Low-Temperature Ammonia Synthesis Activity over Ru/CeO2. *Dalton Transactions* **2020**, *49* (47), 17143–17146. https://doi.org/10.1039/D0DT01974G.

(81) Miyahara, S. ichiro; Sato, K.; Kawano, Y.; Imamura, K.; Ogura, Y.; Tsujimaru, K.; Nagaoka, K. Ammonia Synthesis over Lanthanoid Oxide–Supported Ruthenium Catalysts. *Catal Today* **2021**, *376*, 36–40. https://doi.org/10.1016/J.CATTOD.2020.08.031.

(82) Niwa, Y.; Aika, K. I. The Effect of Lanthanide Oxides as a Support for Ruthenium Catalysts in Ammonia Synthesis. *J Catal* **1996**, *162* (1), 138–142. https://doi.org/10.1006/JCAT.1996.0268.

(83) Ma, Z.; Zhao, S.; Pei, X.; Xiong, X.; Hu, B. New Insights into the Support Morphology-Dependent Ammonia Synthesis Activity of Ru/CeO2 Catalysts. *Catal Sci Technol* **2017**, *7* (1), 191–199. https://doi.org/10.1039/C6CY02089E.

(84) Lin, B.; Liu, Y.; Heng, L.; Wang, X.; Ni, J.; Lin, J.; Jiang, L. Morphology Effect of Ceria on the Catalytic Performances of Ru/CeO2 Catalysts for Ammonia Synthesis. *Ind Eng Chem Res* **2018**, *57* (28), 9127–9135. https://doi.org/10.1021/acs.iecr.8b02126.

(85) Wang, X.; Peng, X.; Zhang, Y.; Ni, J.; Au, C. T.; Jiang, L. Efficient Ammonia Synthesis over a Core–Shell Ru/CeO2 Catalyst with a Tunable CeO2 Size: DFT Calculations and XAS Spectroscopy Studies. *Inorg Chem Front* **2019**, *6* (2), 396–406. https://doi.org/10.1039/C8QI01244J.

(86) Li, L.; Chen, F.; Lu, J. Q.; Luo, M. F. Study of Defect Sites in Ce1-Xmxo2-δ (x = 0.2) Solid Solutions Using Raman Spectroscopy. *Journal of Physical Chemistry A* **2011**, *115* (27), 7972–7977. https://doi.org/10.1021/JP203921M/SUPPL_FILE/JP203921M_SI_001.PDF.

(87) Ma, Z.; Xiong, X.; Song, C.; Hu, B.; Zhang, W. Electronic Metal–Support Interactions Enhance the Ammonia Synthesis Activity over Ruthenium Supported on Zr-Modified CeO2 Catalysts. *RSC Adv* **2016**, *6* (56), 51106–51110. https://doi.org/10.1039/C6RA10540H.

(88) Luo, X.; Wang, R.; Ni, J.; Lin, J.; Lin, B.; Xu, X.; Wei, K. Effect of La2O3 on Ru/CeO2-La 2O3 Catalyst for Ammonia Synthesis. *Catal Letters* **2009**, *133* (3–4), 382–387. https://doi.org/10.1007/S10562-009-0177-7.

(89) Iglesias González, A. Ceria Modificada Con Estaño Como Soporte Catalítico Del Cobre. Aplicación a Las Reacciones de Eliminación de CO. **2016**.

(90) Mizoguchi, H.; Okunaka, M.; Kitano, M.; Matsuishi, S.; Yokoyama, T.; Hosono, H. Hydride-Based Electride Material, LnH2 (Ln = La, Ce, or Y). *Inorganic Chemistry*. American Chemical Society September 6, 2016, pp 8833–8838. https://doi.org/10.1021/acs.inorgchem.6b01369.

(91) Ooya, K.; Li, J.; Fukui, K.; Iimura, S.; Nakao, T.; Ogasawara, K.; Sasase, M.; Abe, H.; Niwa, Y.; Kitano, M.; Hosono, H. Ruthenium Catalysts Promoted by Lanthanide Oxyhydrides with High Hydride-Ion Mobility for Low-Temperature Ammonia Synthesis. *Adv Energy Mater* **2021**, *11* (4). https://doi.org/10.1002/aenm.202003723.

(92) Fukui, K.; Iimura, S.; Iskandarov, A.; Tada, T.; Hosono, H. Room-Temperature Fast H-Conduction in Oxygen-Substituted Lanthanum Hydride. *J Am Chem Soc* **2022**, *144* (4), 1523–1527. https://doi.org/10.1021/jacs.1c11353.

(93) Garagounis, I.; Vourros, A.; Stoukides, D.; Dasopoulos, D.; Stoukides, M. Electrochemical Synthesis of Ammonia: Recent Efforts and Future Outlook. *Membranes 2019, Vol. 9, Page 112* **2019**, *9* (9), 112. https://doi.org/10.3390/MEMBRANES9090112.

(94) Meloni, E.; Cafiero, L.; Martino, M.; Palma, V. Structured Catalysts for Non-Thermal Plasma-Assisted Ammonia Synthesis. *Energies 2023, Vol. 16, Page 3218* **2023**, *16* (7), 3218. https://doi.org/10.3390/EN16073218.

(95) Zhang, S.; Zhao, Y.; Shi, R.; Waterhouse, G. I. N.; Zhang, T. Photocatalytic Ammonia Synthesis: Recent Progress and Future. *EnergyChem* **2019**, *1* (2), 100013. https://doi.org/10.1016/J.ENCHEM.2019.100013.

Compendium of publications

Chapter 1

(1) Alfa Laval, H. H. T. V. S. G. *Ammonfuel. An Industrial View of Ammonia as a Marine Fuel*; 2020.

(2) *Ammonia Global Market Report 2023*. https://www.reportlinker.com/p06323489/Ammonia-Global-Market-Report.html?utm_source=GNW (accessed 2023-06-20).

(3) Smith, C.; Hill, A. K.; Torrente-Murciano, L. Current and Future Role of Haber-Bosch Ammonia in a Carbon-Free Energy Landscape. *Energy Environ Sci* **2020**, *13* (2), 331–344. https://doi.org/10.1039/c9ee02873k.

(4) Reese, M.; Marquart, C.; Malmali, M.; Wagner, K.; Buchanan, E.; McCormick, A.; Cussler, E. L. Performance of a Small-Scale Haber Process. *Ind Eng Chem Res* **2016**, *55* (13), 3742–3750. https://doi.org/10.1021/acs.iecr.5b04909.

(5) Wang, Q.; Guo, J.; Chen, P. Recent Progress towards Mild-Condition Ammonia Synthesis. *Journal of Energy Chemistry*. Elsevier B.V. September 1, 2019, pp 25–36. https://doi.org/10.1016/j.jechem.2019.01.027.

(6) Rouwenhorst, K. H. R.; van der Ham, A. G. J.; Lefferts, L. Beyond Haber-Bosch: The Renaissance of the Claude Process. *Int J Hydrogen Energy* **2021**, *46* (41), 21566–21579. https://doi.org/10.1016/j.ijhydene.2021.04.014.

(7) Yan, H.; Gao, W.; Wang, Q.; Guan, Y.; Feng, S.; Wu, H.; Guo, Q.; Cao, H.; Guo, J.; Chen, P. Lithium Palladium Hydride Promotes Chemical Looping Ammonia Synthesis Mediated by Lithium Imide and Hydride. *Journal of Physical Chemistry C* **2021**, *125* (12), 6716–6722. https://doi.org/10.1021/acs.jpcc.1c01230.

(8) Moon, J.; Cheng, Y.; Daemen, L.; Novak, E.; Ramirez-Cuesta, A. J.; Wu, Z. On the Structural Transformation of Ni/BaH2 During a N2-H2 Chemical Looping Process for Ammonia Synthesis: A Joint In Situ Inelastic Neutron Scattering and First-Principles Simulation Study. *Top Catal* **2021**, *64* (9–12), 685–692. https://doi.org/10.1007/s11244-021-01445-w.

(9) Li, L.; Zhang, T.; Cai, J.; Cai, H.; Ni, J.; Lin, B.; Lin, J.; Wang, X.; Zheng, L.; Au, C. T.; Jiang, L. Operando Spectroscopic and Isotopic-Label-Directed Observation of LaN-Promoted Ru/ZrH2 Catalyst for Ammonia Synthesis via Associative and Chemical Looping Route. *J Catal* **2020**, *389*, 218–228. https://doi.org/10.1016/j.jcat.2020.05.039.

(10) Zhao, Y.; Zhao, Y.; Shi, R.; Wang, B.; Waterhouse, G. I. N.; Wu, L. Z.; Tung, C. H.; Zhang, T. Tuning Oxygen Vacancies in Ultrathin TiO2 Nanosheets to Boost Photocatalytic Nitrogen Fixation up to 700 Nm. *Advanced Materials* **2019**, *31* (16), 1806482. https://doi.org/10.1002/ADMA.201806482.

(11) Medford, A. J.; Hatzell, M. C. Photon-Driven Nitrogen Fixation: Current Progress, Thermodynamic Considerations, and Future Outlook. *ACS Catal* **2017**, *7* (4), 2624–2643. https://doi.org/10.1021/ACSCATAL.7B00439/ASSET/IMAGES/MEDIUM/CS-2017-00439R_0012.GIF.

(12) Wang, S.; Yu, W.; Xu, S.; Han, K.; Wang, F. Ammonia from Photothermal N2Hydrogenation over Ni/TiO2Catalysts under Mild Conditions. *ACS Sustain Chem Eng* **2022**, *10* (1), 115–123. https://doi.org/10.1021/ACSSUSCHEMENG.1C04931/SUPPL_FILE/SC1C04931_SI_001.PDF.

(13) Hong, J.; Prawer, S.; Murphy, A. B. Plasma Catalysis as an Alternative Route for Ammonia Production: Status, Mechanisms, and Prospects for Progress. *ACS Sustain Chem Eng* **2018**, *6* (1), 15–31. https://doi.org/10.1021/ACSSUSCHEMENG.7B02381/ASSET/IMAGES/MEDIUM/SC-2017-02381B_0021.GIF.

(14) Carreon, M. L. Plasma Catalytic Ammonia Synthesis: State of the Art and Future Directions. *J Phys D Appl Phys* **2019**, *52* (48), 483001. https://doi.org/10.1088/1361-6463/AB3B2C.

(15) Li, Y.; Wang, H.; Priest, C.; Li, S.; Xu, P.; Wu, G. Advanced Electrocatalysis for Energy and Environmental Sustainability via Water and Nitrogen Reactions. *Advanced Materials* **2021**, *33* (6). https://doi.org/10.1002/ADMA.202000381.

(16) McEnaney, J. M.; Singh, A. R.; Schwalbe, J. A.; Kibsgaard, J.; Lin, J. C.; Cargnello, M.; Jaramillo, T. F.; Nørskov, J. K. Ammonia Synthesis from N2 and H2O Using a Lithium Cycling Electrification Strategy at Atmospheric Pressure. *Energy Environ Sci* **2017**, *10* (7), 1621–1630. https://doi.org/10.1039/c7ee01126a.

(17) Reichle, S.; Felderhoff, M.; Schüth, F. Mechanocatalytic Room-Temperature Synthesis of Ammonia from Its Elements Down to Atmospheric Pressure. *Angewandte Chemie - International Edition* **2021**, *60* (50), 26385–26389. https://doi.org/10.1002/anie.202112095.

(18) Chang, F.; Gao, W.; Guo, J.; Chen, P. Emerging Materials and Methods toward Ammonia-Based Energy Storage and Conversion. *Advanced Materials*. John Wiley and Sons Inc December 1, 2021. https://doi.org/10.1002/adma.202005721.

(19) Gao, W.; Guo, J.; Chen, P. Hydrides, Amides and Imides Mediated Ammonia Synthesis and Decomposition. *Chin J Chem* **2019**, *37* (5), 442–451. https://doi.org/10.1002/cjoc.201800586.

(20) Marakatti, V. S.; Gaigneaux, E. M. Recent Advances in Heterogeneous Catalysis for Ammonia Synthesis. *ChemCatChem*. Wiley Blackwell December 4, 2020, pp 5838–5857. https://doi.org/10.1002/cctc.202001141.

(21) Humphreys, J.; Lan, R.; Tao, S. Development and Recent Progress on Ammonia Synthesis Catalysts for Haber–Bosch Process. *Advanced Energy and Sustainability Research* **2021**, *2* (1), 2000043. https://doi.org/10.1002/aesr.202000043.

(22) Saadatjou, N.; Jafari, A.; Sahebdelfar, S. Ruthenium Nanocatalysts for Ammonia Synthesis: A Review. *Chemical Engineering Communications*. Taylor and Francis Ltd. May 1, 2015, pp 420–448. https://doi.org/10.1080/00986445.2014.923995.

(23) Li, L.; Zhang, T.; Zhou, Y.; Wang, X.; Au, C. tong; Jiang, L. Review on Catalytic Roles of Rare Earth Elements in Ammonia Synthesis: Development and Perspective. *Journal of Rare Earths*. Editorial Office of Chinese Rare Earths January 1, 2022, pp 1–10. https://doi.org/10.1016/j.jre.2021.06.014.

(24) Nakaya, Y.; Furukawa, S. Catalysis of Alloys: Classification, Principles, and Design for a Variety of Materials and Reactions. *Chem Rev* **2022**. https://doi.org/10.1021/ACS.CHEMREV.2C00356/ASSET/IMAGES/MEDIUM/CR2C00356_0069.GIF.

(25) Guo, J.; Chen, P. Interplay of Alkali, Transition Metals, Nitrogen, and Hydrogen in Ammonia Synthesis and Decomposition Reactions. *Acc Chem Res* **2021**, *54* (10), 2434–2444. https://doi.org/10.1021/acs.accounts.1c00076.

(26) Kitano, M.; Inoue, Y.; Yamazaki, Y.; Hayashi, F.; Kanbara, S.; Matsuishi, S.; Yokoyama, T.; Kim, S. W.; Hara, M.; Hosono, H. Ammonia Synthesis Using a Stable Electride as an Electron Donor and Reversible Hydrogen Store. *Nat Chem* **2012**, *4* (11), 934–940. https://doi.org/10.1038/nchem.1476.

(27) Ojelade, O. A.; Zaman, S. F. Ammonia Decomposition for Hydrogen Production: A Thermodynamic Study. *Chemical Papers* **2021**, *75* (1), 57–65. https://doi.org/10.1007/s11696-020-01278-z.

(28) Ertl, G. Surface Science and Catalysis—Studies on the Mechanism of Ammonia Synthesis: The P. H. Emmett Award Address. *Catalysis Reviews* **1980**, *21* (2), 201–223. https://doi.org/10.1080/03602458008067533.

(29) Almquist, J. A.; Crittenden, E. D. A Study of Pure-Iron and Promoted-Iron Catalysts for Ammonia Synthesis. *Ind Eng Chem* **1926**, *18* (12), 1307–1309. https://doi.org/10.1021/IE50204A036/ASSET/IE50204A036.FP.PNG_V03.

(30) Aika, K. ichi. Role of Alkali Promoter in Ammonia Synthesis over Ruthenium Catalysts—Effect on Reaction Mechanism. *Catal Today* **2017**, *286*, 14–20. https://doi.org/10.1016/J.CATTOD.2016.08.012.

(31) García-García, F. R.; Guerrero-Ruiz, A.; Rodríguez-Ramos, I. Role of B5-Type Sites in Ru Catalysts Used for the NH3 Decomposition Reaction. *Topics in Catalysis 2009 52:6* **2009**, *52* (6), 758–764. https://doi.org/10.1007/S11244-009-9203-7.

(32) van Hardeveld, R.; van Montfoort, A. The Influence of Crystallite Size on the Adsorption of Molecular Nitrogen on Nickel, Palladium and Platinum: An Infrared and Electron-Microscopic Study. *Surf Sci* **1966**, *4* (4), 396–430. https://doi.org/10.1016/0039-6028(66)90016-1.

(33) Raróg-Pilecka, W.; Szmigiel, D.; Kowalczyk, Z.; Jodzis, S.; Zielinski, J. Ammonia Decomposition over the Carbon-Based Ruthenium Catalyst Promoted with Barium or Cesium. *J Catal* **2003**, *218* (2), 465–469. https://doi.org/10.1016/S0021-9517(03)00058-7.

(34) Osozawa, M.; Hori, A.; Fukai, K.; Honma, T.; Oshima, K.; Satokawa, S. Improvement in Ammonia Synthesis Activity on Ruthenium Catalyst Using Ceria Support Modified a Large Amount of Cesium Promoter. *Int J Hydrogen Energy* **2022**, *47* (4), 2433–2441. https://doi.org/10.1016/J.IJHYDENE.2021.10.204.

(35) Zhang, Z.; Karakaya, C.; Kee, R. J.; Way, J. D.; Wolden, C. A. Barium-Promoted Ruthenium Catalysts on Yittria-Stabilized Zirconia Supports for Ammonia Synthesis. *ACS Sustain Chem Eng* **2019**, *7* (21), 18038–18047. https://doi.org/10.1021/ACSSUSCHEMENG.9B04929/SUPPL_FILE/SC9B04929_SI_001.PDF.

(36) Nishi, M.; Chen, S. Y.; Takagi, H. Mild Ammonia Synthesis over Ba-Promoted Ru/MPC Catalysts: Effects of the Ba/Ru Ratio and the Mesoporous Structure. *Catalysts* **2019**, *9* (5). https://doi.org/10.3390/CATAL9050480.

(37) Kitano, M.; Inoue, Y.; Sasase, M.; Kishida, K.; Kobayashi, Y.; Nishiyama, K.; Tada, T.; Kawamura, S.; Yokoyama, T.; Hara, M.; Hosono, H. Self-Organized Ruthenium-Barium Core-Shell Nanoparticles on a Mesoporous Calcium Amide Matrix for Efficient Low-Temperature Ammonia Synthesis. *Angewandte Chemie* **2018**, *130* (10), 2678–2682. https://doi.org/10.1002/ange.201712398.

(38) Guraya, M.; Sprenger, S.; Rarog-Pilecka, W.; Szmigiel, D.; Kowalczyk, Z.; Muhler, M. The Effect of Promoters on the Electronic Structure of Ruthenium Catalysts Supported on Carbon. *Appl Surf Sci* **2004**, *238* (1–4), 77–81. https://doi.org/10.1016/J.APSUSC.2004.05.214.

(39) Raróg-Pilecka, W.; Miśkiewicz, E.; Szmigiel, D.; Kowalczyk, Z. Structure Sensitivity of Ammonia Synthesis over Promoted Ruthenium Catalysts Supported on Graphitised Carbon. *J Catal* **2005**, *231* (1), 11–19. https://doi.org/10.1016/J.JCAT.2004.12.005.

(40) Aika, K. ichi; Hori, H.; Ozaki, A. Activation of Nitrogen by Alkali Metal Promoted Transition Metal I. Ammonia Synthesis over Ruthenium Promoted by Alkali Metal. *J Catal* **1972**, *27* (3), 424–431. https://doi.org/10.1016/0021-9517(72)90179-0.

(41) Seetharamulu, P.; Hari Prasad Reddy, K.; Padmasri, A. H.; Rama Rao, K. S.; David Raju, B. Role of Promoters on Highly Active Nano-Ru Catalyst Supported on Mg–Al Hydrotalcite Precursor for the Synthesis of Ammonia. *Catal Today* **2009**, *141* (1–2), 94–98. https://doi.org/10.1016/J.CATTOD.2008.05.010.

(42) Wang, Y.; Wildfire, C.; Khan, T. S.; Shekhawat, D.; Hu, J.; Tavadze, P.; Quiñones-Fernández, R.; Moreno, S. Effects of Support and Promoter on Ru Catalyst Activity in Microwave-Assisted Ammonia Synthesis. *Chemical Engineering Journal* **2021**, *425*. https://doi.org/10.1016/J.CEJ.2021.130546.

(43) Miyahara, S. ichiro; Sato, K.; Kawano, Y.; Imamura, K.; Ogura, Y.; Tsujimaru, K.; Nagaoka, K. Ammonia Synthesis over Lanthanoid Oxide–Supported Ruthenium Catalysts. *Catal Today* **2021**, *376*, 36–40. https://doi.org/10.1016/J.CATTOD.2020.08.031.

(44) Lin, B.; Liu, Y.; Heng, L.; Wang, X.; Ni, J.; Lin, J.; Jiang, L. Morphology Effect of Ceria on the Catalytic Performances of Ru/CeO2 Catalysts for Ammonia Synthesis. *Ind Eng Chem Res* **2018**, *57* (28), 9127–9135. https://doi.org/10.1021/acs.iecr.8b02126.

(45) Zhang, L.; Lin, J.; Ni, J.; Wang, R.; Wei, K. Highly Efficient Ru/Sm2O3-CeO2 Catalyst for Ammonia Synthesis. *Catal Commun* **2011**, *15* (1), 23–26. https://doi.org/10.1016/J.CATCOM.2011.08.003.

(46) Li, H.; Shang, J.; Ai, Z.; Zhang, L. Efficient Visible Light Nitrogen Fixation with BiOBr Nanosheets of Oxygen Vacancies on the Exposed {001} Facets. *J Am Chem Soc* **2015**, *137* (19), 6393–6399. https://doi.org/10.1021/JACS.5B03105/SUPPL_FILE/JA5B03105_SI_001.PDF.

(47) Hirakawa, H.; Hashimoto, M.; Shiraishi, Y.; Hirai, T. Photocatalytic Conversion of Nitrogen to Ammonia with Water on Surface Oxygen Vacancies of Titanium Dioxide. *J Am Chem Soc* **2017**, *139* (31), 10929–10936. https://doi.org/10.1021/JACS.7B06634/SUPPL_FILE/JA7B06634_SI_001.PDF.

(48) Li, C.; Wang, T.; Zhao, Z. J.; Yang, W.; Li, J. F.; Li, A.; Yang, Z.; Ozin, G. A.; Gong, J. Promoted Fixation of Molecular Nitrogen with Surface Oxygen Vacancies on Plasmon-Enhanced TiO2 Photoelectrodes. *Angewandte Chemie International Edition* **2018**, *57* (19), 5278–5282. https://doi.org/10.1002/ANIE.201713229.

(49) Dye, J. L. Electrons as Anions. *Science (1979)* **2003**, *301* (5633), 607–608. https://doi.org/10.1126/SCIENCE.1088103/ASSET/2642FB52-1D3E-4E1C-9718-AA37302B4114/ASSETS/SCIENCE.1088103.FP.PNG.

(50) Kitano, M.; Inoue, Y.; Ishikawa, H.; Yamagata, K.; Nakao, T.; Tada, T.; Matsuishi, S.; Yokoyama, T.; Hara, M.; Hosono, H. Essential Role of Hydride Ion in Ruthenium-Based Ammonia Synthesis Catalysts. *Chem Sci* **2016**, *7* (7), 4036–4043. https://doi.org/10.1039/c6sc00767h.

(51) Lu, Y.; Li, J.; Ye, T. N.; Kobayashi, Y.; Sasase, M.; Kitano, M.; Hosono, H. Synthesis of Rare-Earth-Based Metallic Electride Nanoparticles and Their Catalytic Applications to Selective Hydrogenation and Ammonia Synthesis. *ACS Catal* **2018**, *8* (12), 11054–11058. https://doi.org/10.1021/ACSCATAL.8B03743/SUPPL_FILE/CS8B03743_SI_001.PDF.

(52) Wu, J.; Gong, Y.; Inoshita, T.; Fredrickson, D. C.; Wang, J.; Lu, Y.; Kitano, M.; Hosono, H. Tiered Electron Anions in Multiple Voids of LaScSi and Their Applications to Ammonia Synthesis. *Advanced Materials* **2017**, *29* (36), 1700924. https://doi.org/10.1002/ADMA.201700924.

(53) Inoue, Y.; Kitano, M.; Kim, S. W.; Yokoyama, T.; Hara, M.; Hosono, H. Highly Dispersed Ru on Electride [Ca24Al28O 64]4+(e-)4 as a Catalyst for Ammonia Synthesis. *ACS Catal* **2014**, *4* (2), 674–680. https://doi.org/10.1021/CS401044A/SUPPL_FILE/CS401044A_SI_001.PDF.

(54) Kitano, M.; Kanbara, S.; Inoue, Y.; Kuganathan, N.; Sushko, P. v.; Yokoyama, T.; Hara, M.; Hosono, H. Electride Support Boosts Nitrogen Dissociation over Ruthenium Catalyst and Shifts the Bottleneck in Ammonia Synthesis. *Nat Commun* **2015**, *6*. https://doi.org/10.1038/NCOMMS7731.

(55) Ye, T. N.; Park, S. W.; Lu, Y.; Li, J.; Sasase, M.; Kitano, M.; Tada, T.; Hosono, H. Vacancy-Enabled N2 Activation for Ammonia Synthesis on an Ni-Loaded Catalyst. *Nature* **2020**, *583* (7816), 391–395. https://doi.org/10.1038/s41586-020-2464-9.

(56) Ye, T. N.; Park, S. W.; Lu, Y.; Li, J.; Sasase, M.; Kitano, M.; Hosono, H. Contribution of Nitrogen Vacancies to Ammonia Synthesis over Metal Nitride Catalysts. *J Am Chem Soc* **2020**, *142* (33), 14374–14383. https://doi.org/10.1021/jacs.0c06624.

(57) Chang, F.; Guan, Y.; Chang, X.; Guo, J.; Wang, P.; Gao, W.; Wu, G.; Zheng, J.; Li, X.; Chen, P. Alkali and Alkaline Earth Hydrides-Driven N2 Activation and Transformation over Mn Nitride Catalyst. *J Am Chem Soc* **2018**, *140* (44), 14799–14806. https://doi.org/10.1021/jacs.8b08334.

(58) Inoue, Y.; Kitano, M.; Kishida, K.; Abe, H.; Niwa, Y.; Sasase, M.; Fujita, Y.; Ishikawa, H.; Yokoyama, T.; Hara, M.; Hosono, H. Efficient and Stable Ammonia Synthesis by Self-Organized Flat Ru Nanoparticles on Calcium Amide. *ACS Catal* **2016**, *6* (11), 7577–7584. https://doi.org/10.1021/ACSCATAL.6B01940/SUPPL_FILE/CS6B01940_SI_001.PDF.

(59) Wang, P.; Chang, F.; Gao, W.; Guo, J.; Wu, G.; He, T.; Chen, P. Breaking Scaling Relations to Achieve Low-Temperature Ammonia Synthesis through LiH-Mediated Nitrogen Transfer and Hydrogenation. *Nat Chem* **2017**, *9* (1), 64–70. https://doi.org/10.1038/nchem.2595.

(60) Hattori, M.; Iijima, S.; Nakao, T.; Hosono, H.; Hara, M. Solid Solution for Catalytic Ammonia Synthesis from Nitrogen and Hydrogen Gases at 50 °C. *Nat Commun* **2020**, *11* (1). https://doi.org/10.1038/s41467-020-15868-8.

(61) Croisé, C.; Alabd, K.; Tencé, S.; Gaudin, E.; Villesuzanne, A.; Courtois, X.; Bion, N.; Can, F. Influence of the Rare Earth (R) Element in Ru-Supported RScSi Electride-like Intermetallic Catalysts for Ammonia Synthesis at Low Pressure: Insight into NH3 Formation Mechanism. *ChemCatChem* **2023**, *15* (3). https://doi.org/10.1002/CCTC.202201172.

(62) Croisé, C.; Alabd, K.; Villesuzanne, A.; Can, F.; Courtois, X.; Gaudin, E.; Tencé, S.; Bion, N. Role of Hydride Ion within Ru/LaScSi and Ru/CeTiGe Catalysts for NH3 Synthesis: A Combination of DFT and Experimental Nitrogen Isotopic Exchange Studies. *Catal Commun* **2023**, *179*, 106689. https://doi.org/10.1016/J.CATCOM.2023.106689.

(63) Gong, Y.; Li, H.; Li, C.; Bao, X.; Hosono, H.; Wang, J. Insight into Rare-Earth-Incorporated Catalysts: The Chance for a More Efficient Ammonia Synthesis.

Journal of Advanced Ceramics 2022 11:10 **2022**, *11* (10), 1499–1529. https://doi.org/10.1007/S40145-022-0633-Z.

(64) Gong, Y.; Li, H.; Wu, J.; Song, X.; Yang, X.; Bao, X.; Han, X.; Kitano, M.; Wang, J.; Hosono, H. Unique Catalytic Mechanism for Ru-Loaded Ternary Intermetallic Electrides for Ammonia Synthesis. *J Am Chem Soc* **2022**. https://doi.org/10.1021/jacs.2c01899.

(65) Wu, J.; Li, J.; Gong, Y.; Kitano, M.; Inoshita, T.; Hosono, H. Intermetallic Electride Catalyst as a Platform for Ammonia Synthesis. *Angewandte Chemie International Edition* **2019**, *58* (3), 825–829. https://doi.org/10.1002/ANIE.201812131.

(66) Li, J.; Wu, J.; Wang, H.; Lu, Y.; Ye, T.; Sasase, M.; Wu, X.; Kitano, M.; Inoshita, T.; Hosono, H. Acid-Durable Electride with Layered Ruthenium for Ammonia Synthesis: Boosting the Activity via Selective Etching. *Chem Sci* **2019**, *10* (22), 5712–5718. https://doi.org/10.1039/C9SC01539F.

(67) Jiang, Y. F.; Liu, J. C.; Xu, C. Q.; Li, J.; Xiao, H. Breaking the Scaling Relations for Efficient N2-to-NH3 Conversion by a Bowl Active Site Design: Insight from LaRuSi and Isostructural Electrides. *Chinese Journal of Catalysis* **2022**, *43* (8), 2183–2192. https://doi.org/10.1016/S1872-2067(22)64129-9.

(68) Jacobsen, C. J. H.; Dahl, S.; Clausen, B. G. S.; Bahn, S.; Logadottir, A.; Nørskov, J. K. Catalyst Design by Interpolation in the Periodic Table: Bimetallic Ammonia Synthesis Catalysts [2]. *Journal of the American Chemical Society*. 2001, pp 8404–8405. https://doi.org/10.1021/ja010963d.

(69) Sato, K.; Nagaoka, K. Boosting Ammonia Synthesis under Mild Reaction Conditions by Precise Control of the Basic Oxide–Ru Interface. *https://doi.org/10.1246/cl.200855* **2021**, *50* (4), 687–696. https://doi.org/10.1246/CL.200855.

(70) Yan, H.; Gao, W.; Cui, J.; Zhang, W.; Pei, Q.; Wang, Q.; Guan, Y.; Feng, S.; Wu, H.; Cao, H.; Guo, J.; Chen, P. Dinitrogen Fixation Mediated by Lanthanum Hydride. *Journal of Energy Chemistry* **2022**, *72*, 1–7. https://doi.org/10.1016/j.jechem.2022.04.011.

(71) Ooya, K.; Li, J.; Fukui, K.; Iimura, S.; Nakao, T.; Ogasawara, K.; Sasase, M.; Abe, H.; Niwa, Y.; Kitano, M.; Hosono, H. Ruthenium Catalysts Promoted by Lanthanide Oxyhydrides with High Hydride-Ion Mobility for Low-Temperature Ammonia Synthesis. *Adv Energy Mater* **2021**, *11* (4). https://doi.org/10.1002/aenm.202003723.

(72) Fukui, K.; Iimura, S.; Iskandarov, A.; Tada, T.; Hosono, H. Room-Temperature Fast H-Conduction in Oxygen-Substituted Lanthanum Hydride. *J Am Chem Soc* **2022**, *144* (4), 1523–1527. https://doi.org/10.1021/jacs.1c11353.

(73) Ye, T. N.; Lu, Y.; Kobayashi, Y.; Li, J.; Park, S. W.; Sasase, M.; Kitano, M.; Hosono, H. Efficient Ammonia Synthesis over Phase-Separated Nickel-Based Intermetallic Catalysts. *Journal of Physical Chemistry C* **2020**, *124* (52), 28589–28595. https://doi.org/10.1021/ACS.JPCC.0C09590/SUPPL_FILE/JP0C09590_SI_001.PDF.

(74) Miyahara, S. I.; Sato, K.; Tsujimaru, K.; Wada, Y.; Ogura, Y.; Toriyama, T.; Yamamoto, T.; Matsumura, S.; Inazu, K.; Nagaoka, K. Co Nanoparticle Catalysts Encapsulated by BaO-La2O3Nanofractions for Efficient Ammonia Synthesis Under Mild Reaction Conditions. *ACS Omega* **2022**, *7* (28), 24452–24460. https://doi.org/10.1021/ACSOMEGA.2C01973/SUPPL_FILE/AO2C01973_SI_001.PDF.

(75) Che, M. Nobel Prize in Chemistry 1912 to Sabatier: Organic Chemistry or Catalysis? *Catal Today* **2013**, *218–219*, 162–171. https://doi.org/10.1016/j.cattod.2013.07.006.

(76) Vojvodic, A.; Medford, A. J.; Studt, F.; Abild-Pedersen, F.; Khan, T. S.; Bligaard, T.; Nørskov, J. K. Exploring the Limits: A Low-Pressure, Low-Temperature Haber-Bosch Process. *Chem Phys Lett* **2014**, *598*, 108–112. https://doi.org/10.1016/j.cplett.2014.03.003.

(77) Nakao, T.; Tada, T.; Hosono, H. First-Principles and Microkinetic Study on the Mechanism for Ammonia Synthesis Using Ru-Loaded Hydride Catalyst. *Journal of Physical Chemistry C* **2020**, *124* (3), 2070–2078. https://doi.org/10.1021/acs.jpcc.9b10850.

(78) Kitano, M.; Kujirai, J.; Ogasawara, K.; Matsuishi, S.; Tada, T.; Abe, H.; Niwa, Y.; Hosono, H. Low-Temperature Synthesis of Perovskite Oxynitride-Hydrides as Ammonia Synthesis Catalysts. *J Am Chem Soc* **2019**, *141* (51), 20344–20353. https://doi.org/10.1021/jacs.9b10726.

(79) Hosono, H.; Kitano, M. Advances in Materials and Applications of Inorganic Electrides. *Chemical Reviews*. American Chemical Society March 10, 2021, pp 3121–3185. https://doi.org/10.1021/acs.chemrev.0c01071.

(80) Tang, Y.; Kobayashi, Y.; Masuda, N.; Uchida, Y.; Okamoto, H.; Kageyama, T.; Hosokawa, S.; Loyer, F.; Mitsuhara, K.; Yamanaka, K.; Tamenori, Y.; Tassel, C.; Yamamoto, T.; Tanaka, T.; Kageyama, H. Metal-Dependent Support Effects of

Oxyhydride-Supported Ru, Fe, Co Catalysts for Ammonia Synthesis. *Adv Energy Mater* **2018**, *8* (36). https://doi.org/10.1002/aenm.201801772.

(81) Gao, W.; Feng, S.; Yan, H.; Wang, Q.; Xie, H.; Jiang, L.; Zhang, W.; Guan, Y.; Wu, H.; Cao, H.; Guo, J.; Chen, P. In Situ Formed Co from a Co-Mg-O Solid Solution Synergizing with LiH for Efficient Ammonia Synthesis. *Chemical Communications* **2021**, *57* (69), 8576–8579. https://doi.org/10.1039/d1cc03063a.

(82) Hu, Z.; Mahin, J.; Datta, S.; Bell, T. E.; Torrente-Murciano, L. Ru-Based Catalysts for H2 Production from Ammonia: Effect of 1D Support. *Top Catal* **2019**, *62* (17–20), 1169–1177. https://doi.org/10.1007/s11244-018-1058-3.

(83) Zhu, L.; Cadigan, C.; Duan, C.; Huang, J.; Bian, L.; Le, L.; Hernandez, C. H.; Avance, V.; O'Hayre, R.; Sullivan, N. P. Ammonia-Fed Reversible Protonic Ceramic Fuel Cells with Ru-Based Catalyst. *Communications Chemistry 2021 4:1* **2021**, *4* (1), 1–10. https://doi.org/10.1038/s42004-021-00559-2.

(84) López-Rodríguez, S.; Davó-Quiñonero, A.; Bailón-García, E.; Lozano-Castelló, D.; Bueno-López, A. Effect of Ru Loading on Ru/CeO2 Catalysts for CO2 Methanation. *Molecular Catalysis* **2021**, *515*, 111911. https://doi.org/10.1016/J.MCAT.2021.111911.

(85) Kobayashi, Y.; Kitano, M.; Kawamura, S.; Yokoyama, T.; Hosono, H. Kinetic Evidence: The Rate-Determining Step for Ammonia Synthesis over Electride-Supported Ru Catalysts Is No Longer the Nitrogen Dissociation Step. *Catal Sci Technol* **2017**, *7* (1), 47–50. https://doi.org/10.1039/c6cy01962e.

(86) Hosono, H. Electron Transfer from Support/Promotor to Metal Catalyst: Requirements for Effective Support. *Catal Letters* **2022**, *152* (2), 307–314. https://doi.org/10.1007/s10562-021-03648-y.

(87) Kitano, M.; Yamagata, K.; Hosono, H. Why Ca2NH Works as an Efficient and Stable Support of Ru Catalyst in Ammonia Synthesis. *Research on Chemical Intermediates* **2021**, *47* (1), 235–248. https://doi.org/10.1007/s11164-020-04332-3.

(88) Kishida, K.; Kitano, M.; Sasase, M.; Sushko, P. v.; Abe, H.; Niwa, Y.; Ogasawara, K.; Yokoyama, T.; Hosono, H. Air-Stable Calcium Cyanamide-Supported Ruthenium Catalyst for Ammonia Synthesis and Decomposition. *ACS Appl Energy Mater* **2020**, *3* (7), 6573–6582. https://doi.org/10.1021/acsaem.0c00754.

(89) Mizoguchi, H.; Okunaka, M.; Kitano, M.; Matsuishi, S.; Yokoyama, T.; Hosono, H. Hydride-Based Electride Material, LnH2 (Ln = La, Ce, or Y). *Inorganic Chemistry*. American Chemical Society September 6, 2016, pp 8833–8838. https://doi.org/10.1021/acs.inorgchem.6b01369.

(90) Sato, K.; Imamura, K.; Kawano, Y.; Miyahara, S. ichiro; Yamamoto, T.; Matsumura, S.; Nagaoka, K. A Low-Crystalline Ruthenium Nano-Layer Supported on Praseodymium Oxide as an Active Catalyst for Ammonia Synthesis. *Chem Sci* **2016**, *8* (1), 674–679. https://doi.org/10.1039/C6SC02382G.

(91) Hargreaves, J. S. J. Nitrides as Ammonia Synthesis Catalysts and as Potential Nitrogen Transfer Reagents. *Appl Petrochem Res* **2014**, *4* (1), 3–10. https://doi.org/10.1007/s13203-014-0049-y.

(92) Gong, Y.; Wu, J.; Kitano, M.; Wang, J.; Ye, T. N.; Li, J.; Kobayashi, Y.; Kishida, K.; Abe, H.; Niwa, Y.; Yang, H.; Tada, T.; Hosono, H. Ternary Intermetallic LaCoSi as a Catalyst for N2 Activation. *Nature Catalysis 2018 1:3* **2018**, *1* (3), 178–185. https://doi.org/10.1038/s41929-017-0022-0.

Chapter 2

(1) Food and Agriculture Organization of the United Nations. *World Fertilizer Trends and Outlook to 2022*; Rome, 2019.

(2) Smith, C.; Hill, A. K.; Torrente-Murciano, L. Current and Future Role of Haber-Bosch Ammonia in a Carbon-Free Energy Landscape. *Energy Environ Sci* **2020**, *13* (2), 331–344. https://doi.org/10.1039/c9ee02873k.

(3) Wang, Q.; Guo, J.; Chen, P. Recent Progress towards Mild-Condition Ammonia Synthesis. *Journal of Energy Chemistry*. Elsevier B.V. September 1, 2019, pp 25–36. https://doi.org/10.1016/j.jechem.2019.01.027.

(4) Rouwenhorst, K. H. R.; Van der Ham, A. G. J.; Lefferts, L. Beyond Haber-Bosch: The Renaissance of the Claude Process. *Int J Hydrogen Energy* **2021**, *46* (41), 21566–21579. https://doi.org/10.1016/j.ijhydene.2021.04.014.

(5) *2020 Ammonfuel Report an industrial view of ammonia as a marine fuel*. https://www.ocimf.org/?view=article&id=1289:2020-ammonfuel-report-an-industrial-view-of-ammonia-as-a-marine-fuel&catid=160 (accessed 2023-06-30).

(6) Ojelade, O. A.; Zaman, S. F. Ammonia Decomposition for Hydrogen Production: A Thermodynamic Study. *Chemical Papers* **2021**, *75* (1), 57–65. https://doi.org/10.1007/s11696-020-01278-z.

(7) Marakatti, V. S.; Gaigneaux, E. M. Recent Advances in Heterogeneous Catalysis for Ammonia Synthesis. *ChemCatChem*. Wiley Blackwell December 4, 2020, pp 5838–5857. https://doi.org/10.1002/cctc.202001141.

(8) Humphreys, J.; Lan, R.; Tao, S. Development and Recent Progress on Ammonia Synthesis Catalysts for Haber–Bosch Process. *Advanced Energy and Sustainability Research* **2021**, *2* (1), 2000043. https://doi.org/10.1002/aesr.202000043.

(9) Li, L.; Zhang, T.; Zhou, Y.; Wang, X.; Au, C. tong; Jiang, L. Review on Catalytic Roles of Rare Earth Elements in Ammonia Synthesis: Development and Perspective. *Journal of Rare Earths*. Editorial Office of Chinese Rare Earths January 1, 2022, pp 1–10. https://doi.org/10.1016/j.jre.2021.06.014.

(10) Chang, F.; Gao, W.; Guo, J.; Chen, P. Emerging Materials and Methods toward Ammonia-Based Energy Storage and Conversion. *Advanced Materials*. John Wiley and Sons Inc December 1, 2021. https://doi.org/10.1002/adma.202005721.

(11) Hosono, H.; Kitano, M. Advances in Materials and Applications of Inorganic Electrides. *Chemical Reviews*. American Chemical Society March 10, 2021, pp 3121–3185. https://doi.org/10.1021/acs.chemrev.0c01071.

(12) Reese, M.; Marquart, C.; Malmali, M.; Wagner, K.; Buchanan, E.; McCormick, A.; Cussler, E. L. Performance of a Small-Scale Haber Process. *Ind Eng Chem Res* **2016**, *55* (13), 3742–3750. https://doi.org/10.1021/acs.iecr.5b04909.

(13) Jacobsen, C. J. H.; Dahl, S.; Clausen, B. G. S.; Bahn, S.; Logadottir, A.; Nørskov, J. K. Catalyst Design by Interpolation in the Periodic Table: Bimetallic Ammonia Synthesis Catalysts [2]. *Journal of the American Chemical Society*. 2001, pp 8404–8405. https://doi.org/10.1021/ja010963d.

(14) Vojvodic, A.; Medford, A. J.; Studt, F.; Abild-Pedersen, F.; Khan, T. S.; Bligaard, T.; Nørskov, J. K. Exploring the Limits: A Low-Pressure, Low-Temperature Haber-Bosch Process. *Chem Phys Lett* **2014**, *598*, 108–112. https://doi.org/10.1016/j.cplett.2014.03.003.

(15) Wang, P.; Chang, F.; Gao, W.; Guo, J.; Wu, G.; He, T.; Chen, P. Breaking Scaling Relations to Achieve Low-Temperature Ammonia Synthesis through LiH-Mediated Nitrogen Transfer and Hydrogenation. *Nat Chem* **2017**, *9* (1), 64–70. https://doi.org/10.1038/nchem.2595.

(16) Ye, T. N.; Park, S. W.; Lu, Y.; Li, J.; Sasase, M.; Kitano, M.; Hosono, H. Contribution of Nitrogen Vacancies to Ammonia Synthesis over Metal Nitride Catalysts. *J Am Chem Soc* **2020**, *142* (33), 14374–14383. https://doi.org/10.1021/jacs.0c06624.

(17) Gong, Y.; Li, H.; Li, C.; Bao, X.; Hosono, H.; Wang, J. Insight into Rare-Earth-Incorporated Catalysts: The Chance for a More Efficient Ammonia Synthesis.

Journal of Advanced Ceramics 2022 11:10 **2022**, *11* (10), 1499–1529. https://doi.org/10.1007/S40145-022-0633-Z.

(18) Lin, B.; Liu, Y.; Heng, L.; Wang, X.; Ni, J.; Lin, J.; Jiang, L. Morphology Effect of Ceria on the Catalytic Performances of Ru/CeO2 Catalysts for Ammonia Synthesis. *Ind Eng Chem Res* **2018**, *57* (28), 9127–9135. https://doi.org/10.1021/acs.iecr.8b02126.

(19) Sato, K.; Nagaoka, K. Boosting Ammonia Synthesis under Mild Reaction Conditions by Precise Control of the Basic Oxide–Ru Interface. *https://doi.org/10.1246/cl.200855* **2021**, *50* (4), 687–696. https://doi.org/10.1246/CL.200855.

(20) Ma, Z.; Zhao, S.; Pei, X.; Xiong, X.; Hu, B. New Insights into the Support Morphology-Dependent Ammonia Synthesis Activity of Ru/CeO2 Catalysts. *Catal Sci Technol* **2017**, *7* (1), 191–199. https://doi.org/10.1039/C6CY02089E.

(21) Wang, X.; Li, L.; Zhang, T.; Lin, B.; Ni, J.; Au, C. T.; Jiang, L. Strong Metal–Support Interactions of Co-Based Catalysts Facilitated by Dopamine for Highly Efficient Ammonia Synthesis: In Situ XPS and XAFS Spectroscopy Coupled with TPD Studies. *Chemical Communications* **2019**, *55* (4), 474–477. https://doi.org/10.1039/C8CC07130F.

(22) Mizoguchi, H.; Okunaka, M.; Kitano, M.; Matsuishi, S.; Yokoyama, T.; Hosono, H. Hydride-Based Electride Material, LnH2 (Ln = La, Ce, or Y). *Inorganic Chemistry*. American Chemical Society September 6, 2016, pp 8833–8838. https://doi.org/10.1021/acs.inorgchem.6b01369.

(23) Ooya, K.; Li, J.; Fukui, K.; Iimura, S.; Nakao, T.; Ogasawara, K.; Sasase, M.; Abe, H.; Niwa, Y.; Kitano, M.; Hosono, H. Ruthenium Catalysts Promoted by Lanthanide Oxyhydrides with High Hydride-Ion Mobility for Low-Temperature Ammonia Synthesis. *Adv Energy Mater* **2021**, *11* (4). https://doi.org/10.1002/aenm.202003723.

(24) Nakaya, Y.; Furukawa, S. Catalysis of Alloys: Classification, Principles, and Design for a Variety of Materials and Reactions. *Chem Rev* **2022**. https://doi.org/10.1021/ACS.CHEMREV.2C00356/ASSET/IMAGES/MEDIUM/CR2C00356_0069.GIF.

(25) Croisé, C.; Alabd, K.; Tencé, S.; Gaudin, E.; Villesuzanne, A.; Courtois, X.; Bion, N.; Can, F. Influence of the Rare Earth (R) Element in Ru-Supported RScSi Electride-like Intermetallic Catalysts for Ammonia Synthesis at Low Pressure:

Insight into NH3 Formation Mechanism. *ChemCatChem* **2023**, *15* (3). https://doi.org/10.1002/CCTC.202201172.

(26) Croisé, C.; Alabd, K.; Villesuzanne, A.; Can, F.; Courtois, X.; Gaudin, E.; Tencé, S.; Bion, N. Role of Hydride Ion within Ru/LaScSi and Ru/CeTiGe Catalysts for NH3 Synthesis: A Combination of DFT and Experimental Nitrogen Isotopic Exchange Studies. *Catal Commun* **2023**, *179*, 106689. https://doi.org/10.1016/J.CATCOM.2023.106689.

(27) Wu, J.; Li, J.; Gong, Y.; Kitano, M.; Inoshita, T.; Hosono, H. Intermetallic Electride Catalyst as a Platform for Ammonia Synthesis. *Angewandte Chemie International Edition* **2019**, *58* (3), 825–829. https://doi.org/10.1002/ANIE.201812131.

(28) Li, J.; Wu, J.; Wang, H.; Lu, Y.; Ye, T.; Sasase, M.; Wu, X.; Kitano, M.; Inoshita, T.; Hosono, H. Acid-Durable Electride with Layered Ruthenium for Ammonia Synthesis: Boosting the Activity via Selective Etching. *Chem Sci* **2019**, *10* (22), 5712–5718. https://doi.org/10.1039/C9SC01539F.

(29) Gong, Y.; Wu, J.; Kitano, M.; Wang, J.; Ye, T. N.; Li, J.; Kobayashi, Y.; Kishida, K.; Abe, H.; Niwa, Y.; Yang, H.; Tada, T.; Hosono, H. Ternary Intermetallic LaCoSi as a Catalyst for N2 Activation. *Nature Catalysis 2018 1:3* **2018**, *1* (3), 178–185. https://doi.org/10.1038/s41929-017-0022-0.

(30) Latroche, M.; Percheron-Guégan, A. Structural and Thermodynamic Studies of Some Hydride Forming RM3-Type Compounds (R=lanthanide, M=transition Metal). *J Alloys Compd* **2003**, *356–357*, 461–468. https://doi.org/10.1016/S0925-8388(03)00116-6.

(31) Joubert, J. M.; Paul-Boncour, V.; Cuevas, F.; Zhang, J.; Latroche, M. LaNi5 Related AB5 Compounds: Structure, Properties and Applications. *J Alloys Compd* **2021**, *862*, 158163. https://doi.org/10.1016/J.JALLCOM.2020.158163.

(32) Santos, D. M. F.; Šljukić, B.; Amaral, L.; Macciò, D.; Saccone, A.; Sequeira, C. Nickel-Cerium Alloys for Borohydride Oxidation. *ECS Trans* **2013**, *58* (1), 1893–1901. https://doi.org/10.1149/05801.1893ECST/XML.

(33) Tsukuda, R.; Ohhashi, S.; Xu, Y.; Nishimura, C.; Kameoka, S. Catalytic Hydrogenation of C2H2 over Amorphous CeNi2Hx and Crystalline CeNi2: Effects of Hydrogen-Induced Amorphization and Oxidation. *Mater Trans* **2022**, *63* (3), 343–350. https://doi.org/10.2320/MATERTRANS.MT-M2021202.

(34) Lushnikov, S. A. Desorption of Hydrogen from CeNi3 Intermetallic Hydrides. *Defect and Diffusion Forum* **2010**, *297–301*, 35–39. https://doi.org/10.4028/WWW.SCIENTIFIC.NET/DDF.297-301.35.

(35) Jiang, Y. F.; Liu, J. C.; Xu, C. Q.; Li, J.; Xiao, H. Breaking the Scaling Relations for Efficient N2-to-NH3 Conversion by a Bowl Active Site Design: Insight from LaRuSi and Isostructural Electrides. *Chinese Journal of Catalysis* **2022**, *43* (8), 2183–2192. https://doi.org/10.1016/S1872-2067(22)64129-9.

(36) Ye, T. N.; Lu, Y.; Kobayashi, Y.; Li, J.; Park, S. W.; Sasase, M.; Kitano, M.; Hosono, H. Efficient Ammonia Synthesis over Phase-Separated Nickel-Based Intermetallic Catalysts. *Journal of Physical Chemistry C* **2020**, *124* (52), 28589–28595. https://doi.org/10.1021/ACS.JPCC.0C09590/SUPPL_FILE/JP0C09590_SI_001.PDF.

(37) Miyahara, S. I.; Sato, K.; Tsujimaru, K.; Wada, Y.; Ogura, Y.; Toriyama, T.; Yamamoto, T.; Matsumura, S.; Inazu, K.; Nagaoka, K. Co Nanoparticle Catalysts Encapsulated by BaO-La2O3Nanofractions for Efficient Ammonia Synthesis Under Mild Reaction Conditions. *ACS Omega* **2022**, *7* (28), 24452–24460. https://doi.org/10.1021/ACSOMEGA.2C01973/SUPPL_FILE/AO2C01973_SI_001.PDF.

(38) Kobayashi, Y.; Kitano, M.; Kawamura, S.; Yokoyama, T.; Hosono, H. Kinetic Evidence: The Rate-Determining Step for Ammonia Synthesis over Electride-Supported Ru Catalysts Is No Longer the Nitrogen Dissociation Step. *Catal Sci Technol* **2017**, *7* (1), 47–50. https://doi.org/10.1039/c6cy01962e.

(39) Kitano, M.; Inoue, Y.; Yamazaki, Y.; Hayashi, F.; Kanbara, S.; Matsuishi, S.; Yokoyama, T.; Kim, S. W.; Hara, M.; Hosono, H. Ammonia Synthesis Using a Stable Electride as an Electron Donor and Reversible Hydrogen Store. *Nat Chem* **2012**, *4* (11), 934–940. https://doi.org/10.1038/nchem.1476.

(40) Gong, Y.; Li, H.; Wu, J.; Song, X.; Yang, X.; Bao, X.; Han, X.; Kitano, M.; Wang, J.; Hosono, H. Unique Catalytic Mechanism for Ru-Loaded Ternary Intermetallic Electrides for Ammonia Synthesis. *J Am Chem Soc* **2022**. https://doi.org/10.1021/jacs.2c01899.

(41) Zheng, J.; Liao, F.; Wu, S.; Jones, G.; Chen, T.; Fellowes, J.; Sudmeier, T.; McPherson, I. J.; Wilkinson, I.; Tsang, S. C. E. Efficient Non-dissociative Activation of Dinitrogen to Ammonia over Lithium-Promoted Ruthenium Nanoparticles at Low Pressure. *Angewandte Chemie* **2019**, *131* (48), 17496–17502. https://doi.org/10.1002/ange.201907171.

(42) Miyahara, S. ichiro; Sato, K.; Kawano, Y.; Imamura, K.; Ogura, Y.; Tsujimaru, K.; Nagaoka, K. Ammonia Synthesis over Lanthanoid Oxide–Supported Ruthenium

Catalysts. *Catal Today* **2021**, *376*, 36–40. https://doi.org/10.1016/J.CATTOD.2020.08.031.

(43) Hiromoto, S.; Kano, K.; Suzuki, Y.; Asami, K.; Chiba, A.; Hanawa, T. Surface Characterization and Anodic Polarization of Nitrogen-Ion-Implanted Nickel-Free Co-Cr-Mo Alloy. *Mater Trans* **2005**, *46* (7), 1627–1632. https://doi.org/10.2320/MATERTRANS.46.1627.

(44) Kitano, M.; Inoue, Y.; Ishikawa, H.; Yamagata, K.; Nakao, T.; Tada, T.; Matsuishi, S.; Yokoyama, T.; Hara, M.; Hosono, H. Essential Role of Hydride Ion in Ruthenium-Based Ammonia Synthesis Catalysts. *Chem Sci* **2016**, *7* (7), 4036–4043. https://doi.org/10.1039/c6sc00767h.

(45) Ye, T. N.; Park, S. W.; Lu, Y.; Li, J.; Sasase, M.; Kitano, M.; Tada, T.; Hosono, H. Vacancy-Enabled N2 Activation for Ammonia Synthesis on an Ni-Loaded Catalyst. *Nature* **2020**, *583* (7816), 391–395. https://doi.org/10.1038/s41586-020-2464-9.

(46) Li, C.; Shi, Y.; Zhang, Z.; Ni, J.; Wang, X.; Lin, J.; Lin, B.; Jiang, L. Improving the Ammonia Synthesis Activity of Ru/CeO2 through Enhancement of the Metal–Support Interaction. *Journal of Energy Chemistry* **2021**, *60*, 403–409. https://doi.org/10.1016/J.JECHEM.2021.01.031.

Chapter 3

(1) Reese, M.; Marquart, C.; Malmali, M.; Wagner, K.; Buchanan, E.; McCormick, A.; Cussler, E. L. Performance of a Small-Scale Haber Process. *Ind Eng Chem Res* **2016**, *55* (13), 3742–3750. https://doi.org/10.1021/acs.iecr.5b04909.

(2) Alfa Laval, H. H. T. V. S. G. *Ammonfuel. An Industrial View of Ammonia as a Marine Fuel*; 2020.

(3) Rouwenhorst, K. H. R.; Van der Ham, A. G. J.; Lefferts, L. Beyond Haber-Bosch: The Renaissance of the Claude Process. *Int J Hydrogen Energy* **2021**, *46* (41), 21566–21579. https://doi.org/10.1016/j.ijhydene.2021.04.014.

(4) Smith, C.; Hill, A. K.; Torrente-Murciano, L. Current and Future Role of Haber-Bosch Ammonia in a Carbon-Free Energy Landscape. *Energy Environ Sci* **2020**, *13* (2), 331–344. https://doi.org/10.1039/c9ee02873k.

(5) Ojelade, O. A.; Zaman, S. F. Ammonia Decomposition for Hydrogen Production: A Thermodynamic Study. *Chemical Papers* **2021**, *75* (1), 57–65. https://doi.org/10.1007/s11696-020-01278-z.

(6) Wang, Q.; Guo, J.; Chen, P. Recent Progress towards Mild-Condition Ammonia Synthesis. *Journal of Energy Chemistry*. Elsevier B.V. September 1, 2019, pp 25–36. https://doi.org/10.1016/j.jechem.2019.01.027.

(7) Chang, F.; Gao, W.; Guo, J.; Chen, P. Emerging Materials and Methods toward Ammonia-Based Energy Storage and Conversion. *Advanced Materials*. John Wiley and Sons Inc December 1, 2021. https://doi.org/10.1002/adma.202005721.

(8) Carreon, M. L. Plasma Catalytic Ammonia Synthesis: State of the Art and Future Directions. *J Phys D Appl Phys* **2019**, *52* (48), 483001. https://doi.org/10.1088/1361-6463/AB3B2C.

(9) Hong, J.; Prawer, S.; Murphy, A. B. Plasma Catalysis as an Alternative Route for Ammonia Production: Status, Mechanisms, and Prospects for Progress. *ACS Sustain Chem Eng* **2018**, *6* (1), 15–31. https://doi.org/10.1021/ACSSUSCHEMENG.7B02381/ASSET/IMAGES/MEDIUM/SC-2017-02381B_0021.GIF.

(10) Reichle, S.; Felderhoff, M.; Schüth, F. Mechanocatalytic Room-Temperature Synthesis of Ammonia from Its Elements Down to Atmospheric Pressure. *Angewandte Chemie - International Edition* **2021**, *60* (50), 26385–26389. https://doi.org/10.1002/anie.202112095.

(11) Li, L.; Zhang, T.; Cai, J.; Cai, H.; Ni, J.; Lin, B.; Lin, J.; Wang, X.; Zheng, L.; Au, C. T.; Jiang, L. Operando Spectroscopic and Isotopic-Label-Directed Observation of LaN-Promoted Ru/ZrH2 Catalyst for Ammonia Synthesis via Associative and Chemical Looping Route. *J Catal* **2020**, *389*, 218–228. https://doi.org/10.1016/j.jcat.2020.05.039.

(12) Moon, J.; Cheng, Y.; Daemen, L.; Novak, E.; Ramirez-Cuesta, A. J.; Wu, Z. On the Structural Transformation of Ni/BaH2 During a N2-H2 Chemical Looping Process for Ammonia Synthesis: A Joint In Situ Inelastic Neutron Scattering and First-Principles Simulation Study. *Top Catal* **2021**, *64* (9–12), 685–692. https://doi.org/10.1007/s11244-021-01445-w.

(13) Yan, H.; Gao, W.; Wang, Q.; Guan, Y.; Feng, S.; Wu, H.; Guo, Q.; Cao, H.; Guo, J.; Chen, P. Lithium Palladium Hydride Promotes Chemical Looping Ammonia Synthesis Mediated by Lithium Imide and Hydride. *Journal of Physical Chemistry C* **2021**, *125* (12), 6716–6722. https://doi.org/10.1021/acs.jpcc.1c01230.

(14) Wang, S.; Yu, W.; Xu, S.; Han, K.; Wang, F. Ammonia from Photothermal N2Hydrogenation over Ni/TiO2Catalysts under Mild Conditions. *ACS Sustain Chem Eng* **2022**, *10* (1), 115–123.

https://doi.org/10.1021/ACSSUSCHEMENG.1C04931/SUPPL_FILE/SC1C04931_SI_001.PDF.

(15) Li, Y.; Wang, H.; Priest, C.; Li, S.; Xu, P.; Wu, G. Advanced Electrocatalysis for Energy and Environmental Sustainability via Water and Nitrogen Reactions. *Advanced Materials* **2021**, *33* (6). https://doi.org/10.1002/ADMA.202000381.

(16) McEnaney, J. M.; Singh, A. R.; Schwalbe, J. A.; Kibsgaard, J.; Lin, J. C.; Cargnello, M.; Jaramillo, T. F.; Nørskov, J. K. Ammonia Synthesis from N2 and H2O Using a Lithium Cycling Electrification Strategy at Atmospheric Pressure. *Energy Environ Sci* **2017**, *10* (7), 1621–1630. https://doi.org/10.1039/c7ee01126a.

(17) Humphreys, J.; Lan, R.; Tao, S. Development and Recent Progress on Ammonia Synthesis Catalysts for Haber–Bosch Process. *Advanced Energy and Sustainability Research* **2021**, *2* (1), 2000043. https://doi.org/10.1002/aesr.202000043.

(18) Marakatti, V. S.; Gaigneaux, E. M. Recent Advances in Heterogeneous Catalysis for Ammonia Synthesis. *ChemCatChem*. Wiley Blackwell December 4, 2020, pp 5838–5857. https://doi.org/10.1002/cctc.202001141.

(19) Arroyo-Caire, J.; Diaz-Perez, M. A.; Lara-Angulo, M. A.; Serrano-Ruiz, J. C. A Conceptual Approach for the Design of New Catalysts for Ammonia Synthesis: A Metal—Support Interactions Review. *Nanomaterials 2023, Vol. 13, Page 2914* **2023**, *13* (22), 2914. https://doi.org/10.3390/NANO13222914.

(20) Smith, C.; Torrente-Murciano, L. Guidance for Targeted Development of Ammonia Synthesis Catalysts from a Holistic Process Approach. *Chem Catalysis*. Cell Press November 18, 2021, pp 1163–1172. https://doi.org/10.1016/j.checat.2021.09.015.

(21) Hosono, H.; Kitano, M. Advances in Materials and Applications of Inorganic Electrides. *Chemical Reviews*. American Chemical Society March 10, 2021, pp 3121–3185. https://doi.org/10.1021/acs.chemrev.0c01071.

(22) Saadatjou, N.; Jafari, A.; Sahebdelfar, S. Ruthenium Nanocatalysts for Ammonia Synthesis: A Review. *Chemical Engineering Communications*. Taylor and Francis Ltd. May 1, 2015, pp 420–448. https://doi.org/10.1080/00986445.2014.923995.

(23) Li, L.; Zhang, T.; Zhou, Y.; Wang, X.; Au, C. tong; Jiang, L. Review on Catalytic Roles of Rare Earth Elements in Ammonia Synthesis: Development and Perspective. *Journal of Rare Earths*. Editorial Office of Chinese Rare Earths January 1, 2022, pp 1–10. https://doi.org/10.1016/j.jre.2021.06.014.

(24) Nakaya, Y.; Furukawa, S. Catalysis of Alloys: Classification, Principles, and Design for a Variety of Materials and Reactions. *Chem Rev* **2022**.

https://doi.org/10.1021/ACS.CHEMREV.2C00356/ASSET/IMAGES/MEDIUM/CR2C00356_0069.GIF.

(25) Guo, J.; Chen, P. Interplay of Alkali, Transition Metals, Nitrogen, and Hydrogen in Ammonia Synthesis and Decomposition Reactions. *Acc Chem Res* **2021**, *54* (10), 2434–2444. https://doi.org/10.1021/acs.accounts.1c00076.

(26) Sato, K.; Nagaoka, K. Boosting Ammonia Synthesis under Mild Reaction Conditions by Precise Control of the Basic Oxide–Ru Interface. *https://doi.org/10.1246/cl.200855* **2021**, *50* (4), 687–696. https://doi.org/10.1246/CL.200855.

(27) Gong, Y.; Li, H.; Li, C.; Bao, X.; Hosono, H.; Wang, J. Insight into Rare-Earth-Incorporated Catalysts: The Chance for a More Efficient Ammonia Synthesis. *Journal of Advanced Ceramics 2022 11:10* **2022**, *11* (10), 1499–1529. https://doi.org/10.1007/S40145-022-0633-Z.

(28) Miyahara, S. ichiro; Sato, K.; Kawano, Y.; Imamura, K.; Ogura, Y.; Tsujimaru, K.; Nagaoka, K. Ammonia Synthesis over Lanthanoid Oxide–Supported Ruthenium Catalysts. *Catal Today* **2021**, *376*, 36–40. https://doi.org/10.1016/J.CATTOD.2020.08.031.

(29) Ma, Z.; Zhao, S.; Pei, X.; Xiong, X.; Hu, B. New Insights into the Support Morphology-Dependent Ammonia Synthesis Activity of Ru/CeO2 Catalysts. *Catal Sci Technol* **2017**, *7* (1), 191–199. https://doi.org/10.1039/C6CY02089E.

(30) Kitano, M.; Inoue, Y.; Sasase, M.; Kishida, K.; Kobayashi, Y.; Nishiyama, K.; Tada, T.; Kawamura, S.; Yokoyama, T.; Hara, M.; Hosono, H. Self-Organized Ruthenium-Barium Core-Shell Nanoparticles on a Mesoporous Calcium Amide Matrix for Efficient Low-Temperature Ammonia Synthesis. *Angewandte Chemie* **2018**, *130* (10), 2678–2682. https://doi.org/10.1002/ange.201712398.

(31) Fernández, C.; Sassoye, C.; Debecker, D. P.; Sanchez, C.; Ruiz, P. Effect of the Size and Distribution of Supported Ru Nanoparticles on Their Activity in Ammonia Synthesis under Mild Reaction Conditions. *Appl Catal A Gen* **2014**, *474*, 194–202. https://doi.org/10.1016/J.APCATA.2013.09.039.

(32) Song, Z.; Cai, T.; Hanson, J. C.; Rodriguez, J. A.; Hrbek, J. Structure and Reactivity of Ru Nanoparticles Supported on Modified Graphite Surfaces: A Study of the Model Catalysts for Ammonia Synthesis. *J Am Chem Soc* **2004**, *126* (27), 8576–8584.
https://doi.org/10.1021/JA031718S/ASSET/IMAGES/MEDIUM/JA031718SN00001.GIF.

(33) Wang, P.; Chang, F.; Gao, W.; Guo, J.; Wu, G.; He, T.; Chen, P. Breaking Scaling Relations to Achieve Low-Temperature Ammonia Synthesis through LiH-Mediated Nitrogen Transfer and Hydrogenation. *Nat Chem* **2017**, *9* (1), 64–70. https://doi.org/10.1038/nchem.2595.

(34) Hosono, H. Electron Transfer from Support/Promotor to Metal Catalyst: Requirements for Effective Support. *Catal Letters* **2022**, *152* (2), 307–314. https://doi.org/10.1007/s10562-021-03648-y.

(35) Ooya, K.; Li, J.; Fukui, K.; Iimura, S.; Nakao, T.; Ogasawara, K.; Sasase, M.; Abe, H.; Niwa, Y.; Kitano, M.; Hosono, H. Ruthenium Catalysts Promoted by Lanthanide Oxyhydrides with High Hydride-Ion Mobility for Low-Temperature Ammonia Synthesis. *Adv Energy Mater* **2021**, *11* (4). https://doi.org/10.1002/aenm.202003723.

(36) Kitano, M.; Inoue, Y.; Yamazaki, Y.; Hayashi, F.; Kanbara, S.; Matsuishi, S.; Yokoyama, T.; Kim, S. W.; Hara, M.; Hosono, H. Ammonia Synthesis Using a Stable Electride as an Electron Donor and Reversible Hydrogen Store. *Nat Chem* **2012**, *4* (11), 934–940. https://doi.org/10.1038/nchem.1476.

(37) Gong, Y.; Li, H.; Wu, J.; Song, X.; Yang, X.; Bao, X.; Han, X.; Kitano, M.; Wang, J.; Hosono, H. Unique Catalytic Mechanism for Ru-Loaded Ternary Intermetallic Electrides for Ammonia Synthesis. *J Am Chem Soc* **2022**. https://doi.org/10.1021/jacs.2c01899.

(38) Kobayashi, Y.; Kitano, M.; Kawamura, S.; Yokoyama, T.; Hosono, H. Kinetic Evidence: The Rate-Determining Step for Ammonia Synthesis over Electride-Supported Ru Catalysts Is No Longer the Nitrogen Dissociation Step. *Catal Sci Technol* **2017**, *7* (1), 47–50. https://doi.org/10.1039/c6cy01962e.

(39) Li, W.; Liu, P.; Niu, R.; Li, J.; Wang, S. Influence of CeO2 Supports Prepared with Different Precipitants over Ru/CeO2 Catalysts for Ammonia Synthesis. *Solid State Sci* **2020**, *99*, 105983. https://doi.org/10.1016/J.SOLIDSTATESCIENCES.2019.105983.

(40) Sato, K.; Imamura, K.; Kawano, Y.; Miyahara, S. ichiro; Yamamoto, T.; Matsumura, S.; Nagaoka, K. A Low-Crystalline Ruthenium Nano-Layer Supported on Praseodymium Oxide as an Active Catalyst for Ammonia Synthesis. *Chem Sci* **2016**, *8* (1), 674–679. https://doi.org/10.1039/C6SC02382G.

(41) Wang, X.; Peng, X.; Zhang, Y.; Ni, J.; Au, C. T.; Jiang, L. Efficient Ammonia Synthesis over a Core–Shell Ru/CeO2 Catalyst with a Tunable CeO2 Size: DFT

Calculations and XAS Spectroscopy Studies. *Inorg Chem Front* **2019**, *6* (2), 396–406. https://doi.org/10.1039/C8QI01244J.

(42) Feng, Z.; Guo, F.; Zhang, Y.; Ichikawa, T.; Zheng, J. Oxygen Vacancies Rich CeO2 Supported Ru Catalyst for Efficient Hydrogenation of N-Ethylcarbazole at Mild Temperature. *Applied Catalysis B: Environment and Energy* **2025**, 125059. https://doi.org/10.1016/J.APCATB.2025.125059.

(43) Folkesson, B.; Bjorøy, M.; Pappas, J.; Skaarup, S.; Aaltonen, R.; Swahn, C.-G. ESCA Studies on the Charge Distribution in Some Dinitrogen Complexes of Rhenium, Iridium, Ruthenium, and Osmium. *Acta Chem Scand* **1973**, *27*, 287–302. https://doi.org/10.3891/ACTA.CHEM.SCAND.27-0287.

(44) Khan, M. M. T.; Srivastava, S. Some New Ruthenium(III) Schiff Base Complexes: A Photoelectron Spectroscopic Study. *Polyhedron* **1988**, *7* (12), 1063–1065. https://doi.org/10.1016/S0277-5387(00)86396-2.

(45) Kim, H. B.; Park, E. D. Ammonia Decomposition over Ru Catalysts Supported on Alumina with Different Crystalline Phases. *Catal Today* **2023**, *411–412*, 113817. https://doi.org/10.1016/J.CATTOD.2022.06.032.

(46) Osozawa, M.; Hori, A.; Fukai, K.; Honma, T.; Oshima, K.; Satokawa, S. Improvement in Ammonia Synthesis Activity on Ruthenium Catalyst Using Ceria Support Modified a Large Amount of Cesium Promoter. *Int J Hydrogen Energy* **2022**, *47* (4), 2433–2441. https://doi.org/10.1016/J.IJHYDENE.2021.10.204.

(47) Silvestre-Albero, J.; Rodríguez-Reinoso, F.; Sepúlveda-Escribano, A. Improved Metal-Support Interaction in Pt/CeO2/SiO2 Catalysts after Zinc Addition. *J Catal* **2002**, *210* (1), 127–136. https://doi.org/10.1006/JCAT.2002.3670.

(48) Peng, Z.; Wang, Y.; Yin, C.; Qiu, S.; Xia, Y.; Zou, Y.; Xu, F.; Sun, L.; Chu, H. Uniform Dispersion of Ultrafine Ruthenium Nanoparticles on Nano-Cube Ceria as Efficient Catalysts for Hydrogen Production from Ammonia-Borane Hydrolysis. *Sustain Energy Fuels* **2023**, *7* (3), 821–831. https://doi.org/10.1039/D2SE01542K.

(49) Hao, Y. juan; Ma, Y. guang; Zhang, X.; Li, J.; Wang, S.; Chen, X.; Li, F. tang. Unraveling the Importance between Electronic Intensity and Oxygen Vacancy on Photothermocatalytic Toluene Oxidation over CeO2. *Chemical Engineering Journal* **2022**, *433*, 134619. https://doi.org/10.1016/J.CEJ.2022.134619.

(50) Balcerzak, M. Analytical Methods for the Determination of Ruthenium: The State of the Art. *Crit Rev Anal Chem* **2002**, *32* (3), 181–226. https://doi.org/10.1080/10408340290765524.

(51) Suoranta, T.; Niemelä, M.; Perämäki, P. Comparison of Digestion Methods for the Determination of Ruthenium in Catalyst Materials. *Talanta* **2014**, *119*, 425–429. https://doi.org/10.1016/J.TALANTA.2013.11.043.

Annex II. Communications presented in international conferences

Title: Efficient ruthenium over ceria catalysts for ammonia synthesis at mild conditions as a chemical platform for green hydrogen storage.

Speaker: Javier Arroyo−Caire.

Communication type: *Oral presentation*

Conference: *European Hydrogen Energy Conference*

Conference dates: March 6th-8th 2023.

Conference place: Bilbao, Spain

Category: International

THE FAST TRACK TO THE HYDROGEN ECONOMY

EUROPEAN HYDROGEN ENERGY CONFERENCE

EHEC 2024

European Hydrogen Energy Conference 2024

CERTIFICATE OF PARTICIPATION

This is to certify that

JAVIER ARROYO-CAIRE

from Universidad Loyola Andalucía

attended the European Hydrogen Energy Conference 2024 with an oral communication entitled:

Efficient ruthenium over ceria catalysts for ammonia synthesis at mild conditions as a chemical platform for green hydrogen storage

The Conference took place at Bilbao Exhibition Centre (Bilbao, Spain) from 6th to 8th of March 2024.

Organizer:

AeH2

Title: Ru/CeO_2-Al_2O_3 Based Materials as Efficient Catalysts for Ammonia Synthesis: a Kinetic Analysis.

Speaker: Javier Arroyo−Caire.

Communication type: *Oral presentation*

Conference: *Global Research Conference on Catalysis and Chemical Engineering Technology*

Conference dates: September 23rd-25th 2024.

Conference place: Munich, Germany

Category: International

Global Research Conference on
Catalysis and Chemical
Engineering Technology

September 23-25, 2024
Munich, Germany

CERTIFICATE OF PARTICIPATION

This certificate is presented to

Prof./ Dr./ Mrs/ Ms. Javier Arroyo-Caire

Universidad Loyola Andalucia, Spain

for their excellent Invited Presentation on "Ru/CeO_2-Al_2O_3 Based Materials as Efficient Catalysts for Ammonia Synthesis: A Kinetic Analysis"

at CATCHEM2024 in Munich, Germany on September 23-25, 2024.

FOSTER RESEARCH CONFERENCES

Gartzen Lopez
University of the Basque, Spain

Biz Kwun Nam Hui
University of Macau, China

Abdeltif Amrane
Université de Rennes, France

Maria C. Iliuta
Laval University, Canada

FOSTER RESEARCH
Innovate. Explore. Collaborate

Annex III. Methodology

The methodology followed in the compendium of publications described in the Section 2 of this thesis is specified in each chapter. Nevertheless, some specific aspects about the materials and methods are clarified in order to make the analysis of this document more friendly for the reader, as follows:

1. **Analysis of the state-of-the-art**. An initial screening of reviews and small number of references were provided to the author. The platform *Researchgate* was used as a dynamic platform to the development of a more complete analysis of the state-of-the-art. A deep research was conducted by selecting the most relevant (i.e., most cited) references in which the initial reviews provided were cited and/or referenced. As a result, a scientific publication was achieved, as shown in the Chapter 1. As long as this paper was published in 2023, some of the most recent advances found in the state-of-the-art (i.e., 2023-2025) are covered in the Introduction of this thesis.
2. **Statistical analysis of the experimental results**. The analysis of the results used to obtain the reaction orders was similar in all the Chapters of this thesis and it is specifically shown in the Section 4.2.2 of this document. To obtain the apparent activation energies, an Arrhenius analysis was conducted: the dependence of the reaction rate with the reaction temperature was obtained, while keeping constant the rest of the parameters. As a result, the ammonia synthesis rate can be expressed as a function of the reaction temperature, as expressed in Eq. 9:

   $$R=k'\cdot e^{-\frac{E_A}{R\cdot T}} \qquad \text{Eq. 3}$$

   Where k' is the apparent frequency factor, R is the ideal gases constant, T is the reaction temperature and E_A is the apparent activation energy.

   In order to ensure the reproducibility of the results shown in the Chapters 3 and 4 of this thesis, the analysis of the kinetic parameters was carried out in duplicate. The criteria followed, as aforementioned, was to achieve standard deviations below 10 % in the apparent activation energies and the ammonia synthesis rates at 400 ºC and 0.1 MPa. With the exception of the samples S2, S7 and S8 from the Chapter 3 and the sample A1 from the Chapter 4, duplicate experiments led to achieve the reproducibility restrictions. For the exceptions specifically mentioned, triplicate experiments were conducted.

TESIS DOCTORAL DEPOSITADA EN LA UNIVERSIDAD LOYOLA
SEVILLA, 2025